



The Use of Steelmaking Slags in Land and Marine
Applications

Lucy Victoria Fisher

Submitted to Swansea University in fulfilment of the
requirements for the Degree of
Doctor of Philosophy

Swansea University
December 2022

Summary

Iron and steel are essential components of the world's infrastructure and have applications across all industries. Demand for steel across the world has led to 1900 million tons being produced annually, with this number expected to keep increasing. This means that the waste coming from the steelmaking process will most likely also keep increasing. Basic oxygen steelmaking (BOS) slag is a waste product from the secondary steelmaking process. However much of the BOS slag goes to landfill and does not get utilised as well as it could be.

This thesis explores several different ways BOS slag can be utilised and looks at how effective it is in each application. The first application tested is the ability for the BOS slag to capture CO₂ and how this then makes it suitable for applications within the concrete industry. The slag's reaction to sea water was then assessed and what harmful effects it could possibly have on the environment. Slag is well known for being a good fertiliser for plants due to its desirable composition made up of Calcium, Silicon, Iron and others. The slag was tested to see if this specific kind of slag could provide fertiliser properties. It was also explored if the slag could be functionalised with carboxylic acids in order to become hydrophobic or hydrophilic meaning that when the slag is used as fertiliser for plants, water can be channelled towards the seed and not be absorbed before it reaches the seed.

Declarations

This work has not previously been accepted in substance for any degree and is not being concurrently submitted in candidature for any degree.

Signed..........

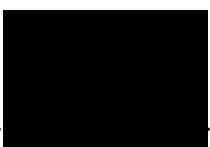
Date.....19.12.22.....

This thesis is the result of my own investigations, except where otherwise stated. Other sources are acknowledged by footnotes giving explicit references. A bibliography is appended.

Signed..........

Date.....19.12.22.....

I hereby give consent for my thesis, if accepted, to be available for electronic sharing

Signed..........

Date.....19.12.22.....

The University's ethical procedures have been followed and, where appropriate, that ethical approval has been granted.

Signed..........

Date.....19.12.22.....

Everything will be ok in the end, and if its not ok, it's not the end.

The sky's no limit.

Table of Contents

Acknowledgements.....	1
List of Figures.....	2
List of Tables.....	7
Abbreviations.....	9
Glossary.....	10
Chapter 1: Introduction and Literature Review.....	11
1.1: Thesis Structure.....	12
1.2: Thesis Aims and Objectives.....	13
1.3: Recent Applications.....	15
1.3.1: Leaching Behaviour of Steelmaking Slag.....	15
1.3.2: Construction Applications.....	18
1.3.3: Geopolymers.....	22
1.3.5: Slag use in Road surfaces and Pavements.....	23
1.3.6: Slag use as Railway Ballast.....	28
1.3.7: Fertiliser.....	28
1.3.8: Slag use as a catalyst.....	30
1.3.9: Metal Recovery from Slag.....	30
1.3.10: The Regeneration of Seaweed and Microalgae.....	32
1.3.11: Phytoplankton Applications.....	33
1.3.12: Adsorbent Properties.....	34
1.3.13: Arsenic Removal by Steelmaking Slag.....	35
Chapter 2: Experimental Materials and Methods.....	36
2.1: Chemicals.....	37
2.2: Techniques.....	39
2.2.1: Microwave Plasma Atomic Emission Spectroscopy (MP-AES).....	39

2.2.2: Contact Angle	41
2.2.3: Thermogravimetric analysis (TGA).....	43
2.2.4: Fourier-transform infrared spectroscopy (FTIR).....	44
2.2.5: Brunauer–Emmett–Teller (BET) Gas Sorption	45
Chapter 3: Experimental CO ₂ Sequestration Trials using Basic Oxygen Steelmaking Slag ...	49
3.1: Introduction.....	50
3.2: Materials and Methods.....	51
3.2.1: Slag	51
3.2.2: Slag sample crushing	51
3.2.3: Characterization	52
3.3: Results and Discussion	52
3.4: Conclusions.....	55
Chapter 4: Nutrient Leaching Experiment.....	56
4.1: Introduction.....	57
4.2: Methodology and Materials	58
4.2.1: Methodology to produce model seawater	59
4.2.2: Methodology for Nutrient Leaching Experiments.....	59
4.2.3: Slag sample crushing	60
4.2.4: Accelerated Nutrient Leaching	61
4.3: Results from Jar 1-5-10mm LF BOS Slag (C)	62
4.3.1: Weight Change of Slag	64
4.3.2: Microwave Plasma Atomic Emission Spectroscopy (MP-AES) of Model Sea Water	65
4.3.3: pH Change of Model Sea Water in Jar 1	65
4.4: Results from Jar 2- 45mm HF BOS Slag (A)	66
4.4.1: Weight Change of Slag	68

4.4.2: Microwave Plasma Atomic Emission Spectroscopy (MP-AES) of Model Sea Water	68
4.4.3: pH Change of Model Sea Water in Jar 2	70
4.5: Results from Jar 3- 45mm LF BOS Slag (B).....	70
4.5.1: Weight Change of Slag	72
4.5.2: Microwave Plasma Atomic Emission Spectroscopy (MP-AES) of Model Sea Water	72
4.5.3: pH Change of Model Sea Water in Jar 3	74
4.6: Results from Jar 4-0-10mm LF BOS Slag.....	74
4.6.1: Surface area change of slag	75
4.6.2: Microwave Plasma Atomic Emission Spectroscopy (MP-AES) of Model Sea Water	76
4.6.3: pH Change of Model Sea Water in Jar 4	77
4.7: Results from Accelerated Leaching Experiment	78
4.7.1: Weight Change and Surface area change of Slag in Accelerated Leaching Experiments	78
4.7.2: Microwave Plasma Atomic Emission Spectroscopy (MP-AES) of Model Sea Water in Accelerated Leaching Experiment.....	80
4.7.3: pH Change of Model Sea Water in Accelerated Leaching Experiments.....	81
4.8: Discussion.....	81
4.9: Conclusion	82
Chapter 5: Functionalization of Basic Oxygen Steelmaking Slag.....	84
5.1: Introduction.....	86
5.2: Experimental Methods.....	87
5.2.1: Synthesis of Functionalized Slag.....	87
5.2.2: Characterisation	88
5.3: Results and Discussion	89

5.4: Conclusion	96
Chapter 6: Effect of Functionalized and Unfunctionalized Basic Oxygen Steelmaking Slag on the Growth of Cereal Wheat (<i>Triticum aestivum</i>).....	97
6.1: Introduction.....	99
6.2: Methods	100
6.2.1: Chemicals and Materials.....	100
6.2.2: Functionalized BOS slag synthesis and characterization	100
6.2.3: Plant growth.....	101
6.3: Results and Discussion	103
6.3.1: Optical Microscopy.....	103
6.3.2: Plant growth.....	104
6.3.3: Mass gain from plants.....	106
6.3.4: Average height of plants	107
6.3.5: Germination rate	109
6.3.6: Composite visual score graphs (CVS).....	110
6.3.7: Microwave plasma atomic emission spectroscopy (MP-AES).....	112
6.3.8: Functionality versus growth.....	115
6.3.9: Distilled water versus rainwater	116
6.4: Conclusions.....	122
Chapter 7: Conclusions and Further Work	124
7.1: Conclusions.....	125
7.2: Further work	127
Appendix A: Additional Tables for Chapter 4: Nutrient Leaching Experiment with Model Sea Water.....	129
Appendix B: Additional Figures for Chapter 5: Functionalization of Basic Oxygen Steelmaking Slag	133
Bibliography	147

Acknowledgements

I would like to thank Professor Andrew R Barron for his guidance and support throughout the duration of this thesis. I would like to thank him for his funding of the project as well as the wonderful lab facilities provided. The guidance and help navigating the world of publishing scientific papers was also invaluable. I would also like to thank all of the Energy Safety Research Institute (ESRI) faculty for their investments made in the purchase and maintenance of lab equipment throughout my time in the research group. I would also like to thank Professor Enrico Andreoli and Dr James Courtney for their assistance with my thesis.

Thanks also go to my friends and colleagues who I worked alongside in ESRI. Your support and lab guidance was wonderful. The kindness and support as we navigated the tricky and unpredictable time of the COVID 19 pandemic was also truly invaluable, it will never be forgotten. A personal thank you goes to Dr Kat Glover, Dr Daniel Stewart, Henry Apsey, Dr Wafaa Al-Shatty, Dr Stephen Shearan, Dr Louise Hamdy, Odin Bain, Dr Michael Warwick, Dr Dan Jones, Dr Don Hill and Max Newberry.

My thanks also go to my friends for their unwavering support and understanding of the struggles associated with undertaking a PhD. It has really helped me through some very tough times.

Finally I would like to thank my parents for their wonderful support and kind words in moments of struggle. Thanks also go to my family for providing wonderful distractions when needed.

List of Figures

Figure 1. 1: Image showing an example of the aquarium tanks used in the slag leaching experiment (Kato et al., 2020).	16
Figure 1. 2: Circular vehicle simulator (L. Hu et al., 2021)	25
Figure 2. 1: Schematic diagram of a microwave plasma atomic emission spectrometer (Agilent, 2021)	39
Figure 2. 2: The Agilent Technologies 4200 MP-AES used in experiments.....	41
Figure 2. 3: Figure showing the contact angle criteria for a sample to be hydrophilic or hydrophobic (Lerman, 2017).	42
Figure 2. 4: Image showing a Krüss DSA25 Expert Drop shape analyser.	43
Figure 2. 5: Image showing the TA instruments SDT Q600.	44
Figure 2. 6: Image showing the Thermo Scientific Nicolet iS10 FT-IR-ATR Spectrometer used for all samples.	45
Figure 2. 7: Image showing how the adsorbate forms a monolayer on the sample surface (Anton Paar, 2021).	46
Figure 2. 8: Image showing a typical BET plot to work out the specific surface area of a sample.	46
Figure 2. 9: Image showing the Quantachrome Nova 2000e Surface Area and Pore Size Analyser.	48
Figure 3. 1: iSorb plot of dry CO ₂ adsorption capacity (mmolCO ₂ /g) of sample C as a function of CO ₂ pressure (atmosphere).	53
Figure 3. 2: TGA plot showing mass loss (%) as a function of temperature (°C) plotted against time (minutes) in sample C.	53
Figure 3. 3: plot of log(Q _e) versus log(P _{CO₂}) for dry CO ₂ adsorption by sample C (R ² = 0.991).	54
Figure 4. 1: Example of accelerated leaching experiment set up with overhead mechanical stirrer.	62
Figure 4. 2: Photographic images of Jar 1 from 25/06/19-29/04/2020.....	64
Figure 4. 3: Graph showing the weight of a solid slag sample from Jar 1 during the duration of	

the experiment with a trendline.....	64
Figure 4. 4: Graph showing the change in Calcium (Ca), Potassium (K) and Magnesium (Mg) concentration in model sea water solution measured over 12 months in Jar 1.....	65
Figure 4. 5: Graph showing the pH change over 12 months for Jar 1: 5-10mm LF BOS slag.	66
Figure 4. 6: Photographic images of Jar 2 from 25/06/19-29/04/2020.....	67
Figure 4. 7: Graph showing the weight of a solid slag sample from Jar 2 during the duration of the experiment with a trendline.....	68
Figure 4. 8: Graph showing the change in Calcium (Ca), Potassium (K) and Magnesium (Mg) concentration in model sea water measured over 12 months in Jar 2.....	69
Figure 4. 9: Graph showing the pH change over 12 months for Jar 2: 45mm HF BOS slag. .	70
Figure 4. 10: Photographic images of Jar 3 from 25/06/19-29/04/2020.....	71
Figure 4. 11: Graph showing the weight of a solid slag sample from Jar 3 during the duration of the experiment with a trendline.	72
Figure 4. 12: Graph showing the change in Calcium (Ca), Potassium (K) and Magnesium (Mg) concentration in model sea water measured over 12 months in Jar 3.....	73
Figure 4. 13: Graph showing the pH change over 12 months for Jar 3: 45mm LF BOS slag.	74
Figure 4. 14: Photographic images of Jar 4 from 25/06/19-29/04/2020.....	75
Figure 4. 15: Graph showing the change in the slag surface area from Jar 4 over the 12-month duration of the experiment. The standard deviation is shown by the error bars.....	76
Figure 4. 16: Graph showing the change in Calcium (Ca), Potassium (K) and Magnesium (Mg) concentration in model sea water measured over 12 months in Jar 4.....	77
Figure 4. 17: Graph showing the pH change over 12 months for Jar 4: 0-10mm LF BOS slag.	78
Figure 4. 18: Bar chart comparing the average percentage weight loss in the accelerated leaching experiment after 24 hours. The error bars show the standard deviation of the 3 measurements.....	79
Figure 5. 1: A photograph showing the placement of a water droplet on a pressed pellet of BOS slag functionalised with lauric acid in a 1:1 ratio.	89
Figure 5. 2: Contact angle measurement of the lauric acid functionalized BOS slag (BOS slag:lauric acid = 1:1).....	90
Figure 5. 3: TGA plots under air of (a) BOS slag, lauric acid-BOS slag, and lanolin-BOS slag, and (b) BOS slag and cysteic acid-BOS slag.....	92

Figure 5. 4: TGA plot under air for 45mm HF BOS slag functionalised with Isostearic acid in a 1:1 ratio with derivative plots.	93
Figure 5. 6: TGA Plot under air of Isostearic acid with derivative plot of isostearic acid.	93
Figure 5. 7: FTIR spectra of the Isostearic acid functionalized BOS slag (BOS slag: Isostearic acid = 1:1)	94
Figure 5. 8: FTIR spectra of the Lauric acid functionalized BOS slag (BOS slag: Lauric acid = 1:1).	95
Figure 5. 9: FTIR spectra of the Lanolin functionalized BOS slag (BOS slag: Lanolin = 1:2).	95
Figure 5. 10: FTIR spectra of the Cysteic acid functionalized BOS slag (BOS slag: Cysteic Acid = 1:1).	96
Figure 6. 1: Optical microscopy image of BOS slag used in the study ($\times 200$).	104
Figure 6. 2: Photographic images of the plant growth are shown on days 1, 4 and 8. The sample numbers correspond to those in Table 1.	106
Figure 6. 3: Plots of seed mass gain as a function of time (days) for samples dispersed in DI water. Error bars represent one standard deviation.	107
Figure 6. 4: Plot of average plant height after 8 days for all samples studied. Error bars represent one standard deviation.	109
Figure 6. 5: Plot of mean germination rate (GR) for samples studied. Error bar represents one standard deviation.	110
Figure 6. 6: Plot of mean germination time (MGT) for samples studied. Error bar represents one standard deviation.	110
Figure 6. 7: Plots (a-n) of composite visual growth scores (CVS) for samples studied. Error bars represent one standard deviation.	112
Figure 6. 8: Optical microscopy image of sample 2 plant root ($\times 200$).	115
Figure 6. 9: Photographic images of the plant growth shown on days 1, 4 and 8 for Sample 1 (no slag), sample 2 (unfunctionalized slag with DI water), and sample 3 (unfunctionalized slag with rainwater).	116
Figure 6. 10: Plots of seed mass gain as a function of time (days). Error bars represent one standard deviation.	118
Figure 6. 11: Plot of average plant height after 8 days for all samples studied. Error bars represent one standard deviation.	118

Figure 6. 12: Plot of mean germination rate (GR) for samples studied. Error bar represents one standard deviation.	119
Figure 6. 13: Plot of mean germination time (MGT) for samples studied. Error bar represents one standard deviation.	119
Figure 6. 14: Plots of composite visual growth scores (CVS) for samples studied for (a) no slag, (b) unfunctionalized slag with DI water, and (c) unfunctionalized slag with rainwater. Error bars represent one standard deviation.....	120
Figure B. 1: Contact angle measurement of isosteric acid functionalised BOS slag (1:1)....	134
Figure B. 2: Contact angle measurement of isosteric acid functionalised BOS slag (1:1.25)	134
Figure B. 3: Contact angle measurement of isosteric acid functionalised BOS slag (1:1.5).134	
Figure B. 4: Contact angle measurement of Lauric acid functionalised BOS slag (1:1).....	135
Figure B. 5: Contact angle measurement of Lauric acid functionalised BOS slag (1:1.25)..	135
Figure B. 6: Contact angle measurement of Lauric acid functionalised BOS slag (1:1.5)....	135
Figure B. 7: Contact angle measurement of Lanolin functionalised BOS slag (1:2)	136
Figure B. 8: Contact angle measurement of Lanolin functionalised BOS slag (1:3)	136
Figure B. 9: Contact angle measurement of isosteric acid functionalised BOS slag (1:5)....	136
Figure B. 10: TGA plot used to calculate grafting density of BOS slag: Isosteric acid in a 1:1 ratio.	137
Figure B. 11: TGA plot used to calculate grafting density of BOS slag: Isosteric acid in a 1:1.25 ratio.	137
Figure B. 12: TGA plot used to calculate grafting density of BOS slag: Isosteric acid in a 1:1.5 ratio.	138
Figure B. 13: TGA plot used to calculate grafting density of BOS slag: Lauric acid in a 1:1 ratio.	138
Figure B. 14: TGA plot used to calculate grafting density of BOS slag: Lauric acid in a 1:1.25 ratio.	139
Figure B. 15: TGA plot used to calculate grafting density of BOS slag: Lauric acid in a 1:1.5 ratio.	139
Figure B. 16: TGA plot used to calculate grafting density of BOS slag: Lanolin in a 1:2 ratio.	140
Figure B. 17: TGA plot used to calculate grafting density of BOS slag: Lanolin in a 1:3 ratio.	140

Figure B. 18: TGA plot used to calculate grafting density of BOS slag: Lanolin in a 1:5 ratio.	141
Figure B. 19: TGA plot used to calculate grafting density of BOS slag: Cysteic Acid in a 1:1 ratio.	141
Figure B. 20: TGA plot used to calculate grafting density of BOS slag: Cysteic Acid in a 1:1.25 ratio.	142
Figure B. 21: TGA plot used to calculate grafting density of BOS slag: Cysteic Acid in a 1:1.5 ratio.	142
Figure B. 22: FTIR spectra of isosteric acid functionalised BOS slag (1:1)	143
Figure B. 23: FTIR spectra of isosteric acid functionalised BOS slag (1:1.25)	143
Figure B. 24: FTIR spectra of isosteric acid functionalised BOS slag (1:1.5)	143
Figure B. 25: FTIR spectra of Lauric acid functionalised BOS slag (1:1)	144
Figure B. 26: FTIR spectra of Lauric acid functionalised BOS slag (1:1.25)	144
Figure B. 27: FTIR spectra of Lauric acid functionalised BOS slag (1:1.5)	144
Figure B. 28: FTIR spectra of Lanolin functionalised BOS slag (1:2)	145
Figure B. 29: FTIR spectra of Lanolin functionalised BOS slag (1:3)	145
Figure B. 30: FTIR spectra of Lanolin functionalised BOS slag (1:5)	145
Figure B. 31: FTIR spectra of Cysteic acid functionalised BOS slag (1:1)	146
Figure B. 32: FTIR spectra of Cysteic acid functionalised BOS slag (1:1.25)	146
Figure B. 33: FTIR spectra of Cysteic acid functionalised BOS slag (1:1.5)	146

List of Tables

Table 2. 1: Table of chemicals, suppliers, and associated CAS number.	37
Table 3. 1: The CO ₂ adsorption capacity (mmol/g) of basic oxygen steelmaking (BOS) slag determined by thermogravimetric analysis (TGA) and gas adsorption using iSorb.....	52
Table 3. 2: Calculated Freundlich isotherm constant (K_f) and heterogeneity factor (n) for dry CO ₂ adsorption of basic oxygen steelmaking (BOS) slag determined by gas adsorption.	54
Table 4. 1: Table of the concentration of salts used in the production of model sea water (ASTM International, 2003).....	59
Table 4. 2: Table showing the average weight of Samples A, B and C at the start of the experiment.....	60
Table 4. 3: Table showing the average weight of Samples A, B, C and D at the start of the experiment.....	61
Table 4. 4: Table showing the average BET surface area change after 24 hours in the accelerated leaching experiment.	79
Table 4. 5: Table showing the Ca concentration after 24 hours of accelerated leaching in model seawater. The measurement is the average of the 3 experimental repeats completed, with the standard deviation also shown.	80
Table 4. 6: Table showing the K concentration after 24 hours of accelerated leaching in model seawater. The measurement is the average of the 3 experimental repeats completed, with the standard deviation also shown.	80
Table 4. 7: Table showing the Mg concentration after 24 hours of accelerated leaching in model seawater. The measurement is the average of the 3 experimental repeats completed, with the standard deviation also shown.	80
Table 4. 8: Table showing the pH change before and after 24 hours of the accelerated leaching experiment for all 4 jars. The measurement is the average of the 3 experimental repeats completed, with the standard deviation also shown.....	81
Table 5. 1: The ratio of slag:reagent used in functionalization experiments.	87
Table 5. 2: Table showing the molecular weight of each carboxylic acid used to calculate grafting density.	89

Table 5. 3: Contact angle and grafting density for BOS slag functionalized with isostearic acid, lauric acid and lanolin.	90
Table 5. 4: Time for water droplet adsorption and calculated grafting density for cysteic acid-functionalized BOS slag.	91
Table 6. 1: Summary of samples and BOS slag dosage used.	102
Table 6. 2: Qualitative Visual Growth Rating System (S. M. Lee et al., 2018).	102
Table 6. 3: ANOVA variance table for all samples.	108
Table 6. 4: ANOVA summary table of calculated values for all samples.	108
Table 6. 5: MP-AES data for all samples. The error represents one standard deviation.	114
Table 6. 6: ANOVA variance table for no slag, unfunctionalized slag and unfunctionalized slag with rainwater.	117
Table 6. 7: ANOVA summary table of calculated values for no slag, unfunctionalized slag and unfunctionalized slag with rainwater.	117
Table 6. 8: MP-AES data for all samples. The error represents one standard deviation.	121
Table A. 1: Table showing the amounts of Zn, Fe, Cu, Mn, Al and Si found in trace amounts in Jar 1: 5-10mm LF BOS slag over the 12 month duration of the nutrient leaching experiment.	130
Table A. 2: Table showing the amounts of Zn, Fe, Cu, Mn, Al and Si found in trace amounts in Jar 2: 45 mm HF BOS slag over the 12 month duration of the nutrient leaching experiment.	130
Table A. 3: Table showing the amounts of Zn, Fe, Cu, Mn, Al and Si found in trace amounts in Jar 3: 45 mm LF BOS slag over the 12 month duration of the nutrient leaching experiment.	131
Table A. 4: Table showing the amounts of Zn, Fe, Cu, Mn, Al and Si found in trace amounts in Jar 4: 0-10 mm LF BOS slag over the 12 month duration of the nutrient leaching experiment.	131

Abbreviations

BET	Brunauer-Emmett-Teller
BF	Blast Furnace
BOS	Basic Oxygen Steelmaking
EAF	Electric Arc Furnace
EDS	Energy-Dispersive X-ray Spectroscopy
FTIR	Fourier Transform Infrared Spectroscopy
ICP	Inductively Coupled Plasma Optical Emission Spectroscopy
MP-AES	Microwave Plasma Atomic Emission Spectroscopy
SEM	Scanning Electron Microscopy
TGA	Thermogravimetric Analysis
XRD	X-Ray Powder Diffraction
XRF	X-ray Fluorescence

Glossary

Anoxic	Greatly deficient in oxygen.
Anthropogenic	(chiefly of environmental pollution and pollutants) originating in human activity.
Biota	The animal and plant life of a particular region, habitat, or geological period.
Crystalline	A Crystalline material is one in which the atoms are situated in a repeating or periodic array over large atomic distances. Meaning long range order exists such that upon solidification the atoms will position themselves in a repetitive three dimensional pattern in which each atom is bonded to its nearest neighbour atoms.
Eutrophic	(of a lake or other body of water) rich in nutrients and so supporting a dense plant population, the decomposition of which kills animal life by depriving it of oxygen.
Ferromagnetic	having a high susceptibility to magnetization, the strength of which depends on that of the applied magnetizing field, and which may persist after removal of the applied field. This is the kind of magnetism displayed by iron, and is associated with parallel magnetic alignment of neighbouring atoms.
Homologous	Having the same relation, relative position or structure.
Hydrolyzed	Breakdown by chemical reaction with water
Immiscible	Not forming a homogeneous mixture when mixed.
Microbial	Relating to or characteristic of a microorganism, especially a bacterium causing disease or fermentation.
Mesocosm	An outdoor experimental system which examines the natural environment under controlled conditions.
Mesotrophic	Containing a medium level of nutrients
Oligotrophic	Relatively poor in plant nutrients and containing abundant oxygen in the deeper parts.
Paramagnetic	Very weakly attracted by the poles of a magnet, but not retaining any permanent magnetism.
Stochastic	Having a random probability distribution or pattern that may be analysed statistically but may not be predicted precisely.
Wettability	The ability of a liquid to maintain contact with a solid surface and it is controlled by the balance between intermolecular interactions of the adhesive type (liquid to surface) and cohesive type (liquid to liquid)

Chapter 1: Introduction and Literature Review

1.1: Thesis Structure

Chapter 1 begins by stating the aims and objectives of the research project as well as providing reasoning behind carrying out the project. The chapter will then examine some of the more recent applications and literature available in the area. This provides an idea of the valuable properties that can be used to exploit steelmaking slags and allows the reader to look at what makes them an attractive product to be used in the circular economy. Further information on the steelmaking process and production of steelmaking slag, as well as further applications, can be found in my MSc thesis entitled "The Use of Steelmaking Slags in Marine Applications" (Fisher, 2018).

Chapter 2 explains the chemicals and methods used through this body of work. Further information on the collection of the slag samples can be found in my MSc thesis, "The Use of Steelmaking Slags in Marine Applications" (Fisher, 2018). This thesis also includes a complete characterisation study of the slag material. Chapter 2 first talks about the various chemicals used and which experiments they were used in, and finally, the theory behind how each analytical technique used throughout the body of work functions.

Chapter 3 is the first experimental chapter of the thesis, which presents work previously published in a peer-reviewed journal called 'Recent Progress in Materials'. Lidsen Publishing published this. The work characterises the CO₂ sequestration ability of 3 different types of steelmaking slag collected from Tata Steel and assesses their suitability to alleviate steel industry emissions.

Chapter 4 evaluates the interaction of BOS slag and model seawater. Examples were taken from all 4 grades of BOS slag that were supplied for the research. Two main experimental parts make up this chapter, one of which looks at the interaction over 12 months with the slag in static seawater in a dark environment in order to simulate undersea conditions. The other looks at what happens when the water is agitated using a mechanical stirrer and what effect this causes.

Chapter 5 takes a new direction, assessing what happens when the BOS slag is modified, and the material's surface properties are changed. The BOS slag is modified with several carboxylic

acids in different ratios to find the optimum conditions to create a hydrophobic and hydrophilic slag. This chapter is written in the format of a conference paper, as the work was presented at an online conference. The work was introduced in an online Zoom conference format. The online conference was the 8th Brunei International Conference on Engineering and Technology 2021. The conference was from the 8th-10th November 2021.

Chapter 6 evolves the ideas spoken about in Chapter 5 and looks at using both the hydrophobic and hydrophilic slag as fertiliser to enhance the growth of wheatgrass plants. This chapter was previously published in a peer-reviewed journal, 'Resources, Conservation and Recycling Advances' published by Elsevier Publishing. It has been inserted into this thesis with permission from the original publisher.

Chapter 7 draws all of the work from the PhD together and is a chapter of reflection and discussions of the future work that could lead on and be completed from the work completed in this thesis.

1.2: Thesis Aims and Objectives

The steelmaking industry produces 20 million tons of waste slag annually in Europe. Around half of this waste is basic oxygen steelmaking slag (BOS slag). BOS slag is a by-product of a secondary steelmaking process in which pig iron from the blast furnace primary steelmaking step is refined into steel using basic oxygen steelmaking. BOS slag is mainly a non-metallic by-product of silicates, alumina silicates, calcium aluminium silicates, iron oxides and other crystalline compounds (Fisher & Barron, 2019, 2021; C. Liu et al., 2016; Shen & Forssberg, 2003). BOS slag is also not as heavily recycled as other types of slag; therefore, much of it is not utilised. It is harder to reuse BOS slag than other slag types, such as blast furnace slag, due to the high calcium carbonate content (Fisher & Barron, 2019).

BOS slag contains many valuable components; recycling the BOS slag is a more favourable option than letting it sit in a landfill, where it is a financial liability to the operator. There are also considerable amounts of BOS slag classed as legacy slag sitting in landfills in the UK. This is an untapped resource of valuable material that could be utilised (Riley et al., 2020). Therefore, there is a growing need within the UK steel industry to use this resource, which

yielded this project's aims and objectives. As is highlighted throughout the literature, there are many different applications that BOS slag can be applied in (Fisher & Barron, 2019). However, when designing and scoping out the experiments in this thesis, there was very little information surrounding how UK steelmaking slags may perform in specific applications. It cannot be assumed that UK-produced BOS slag will yield the same results in a specific application as BOS slag produced in Japan, for example. This is due to the fact that BOS slag produced in different countries can be inherently different due to its chemical composition. The chemical composition is influenced by the grade of steel that was being made when the slag was being produced. Grades of steel worldwide will be very different due to market factors and the applications it is being used for in each region. Therefore, the overarching aim of this study is to determine if UK BOS slag is suitable for reuse applications and, if yes, what applications it would have the most impact in. The scope of this study will only assess BOS slag.

The first aim of this work is to quantify the amount of CO₂ sequestration that could be achieved using UK BOS slag, as this was one of the applications reported on the most in the literature. Experiments were therefore designed to quantify the amount of CO₂ UK BOS slag could sequester and store. In the literature, there were examples of sequestration being completed in a moist environment and an un-moist environment, as well as variations in pressures (Chang et al., 2012; Sipilä et al., 2008). The experiments herein test the UK BOS with differing variables in line with this.

At the time of designing the experiments in this thesis, there was a promising project happening in the Swansea Bay, South Wales area known as the Swansea Tidal Lagoon Project. More information about this can be found in Chapter 4. Therefore, it was pertinent to assess UK BOS slag for use in a marine environment to look into whether the slag would be useful to the developers as a construction material or lagoon defence material, for example. Herein, the experiments in this thesis can be used to assess the effects between model sea water and BOS slag. This forms the second aim of this body of work.

There is considerable work available in the literature on the functionalisation of alumina oxides and iron oxides, as well as others. In this subject area, the raw starting materials can be functionalised to become hydrophobic or hydrophilic, yielding applications in areas such as water purification (Hill et al., 2019, 2020; Maguire-Boyle et al., 2012; Maguire-Boyle & Barron, 2011). Therefore, the third aim of the thesis was to look into whether BOS slag could

be used as a raw starting material for functionalisation as well as to quantify the performance of the material that is produced.

As mentioned in Section 1.3.7, steelmaking slag has been reported to do well at being used as a raw material for fertiliser; therefore, the fourth aim of this body of work is first to assess UK BOS slag's ability to aid plant growth and secondly to assess how various materials conditions can aid or hinder plant growth. By testing unfunctionalised, hydrophobic and hydrophilic variants of BOS slag, This work is aimed at alleviating water scarcity pressures in arid regions, where it would be helpful to have a hydrophobic material that can channel water towards a seed/roots and aid in irrigation (Karanisa et al., 2021). The growth of the Cereal Wheat (*Triticum aestivum*) plant was assessed as this has previously responded well and displayed enhanced growing characteristics in the presence of iron oxides (S. M. Lee et al., 2018).

1.3: Recent Applications

1.3.1: Leaching Behaviour of Steelmaking Slag

Several researchers have assessed the leaching behaviour of steelmaking slag and if it elutes any hazardous chemicals. In testing completed by Li et al. in 2018, four different size fractions of crushed BOS slag were placed into a glass bottle and agitated in deionized water for 8 hours. The pH was then measured after the experiment. It was found that the pH increased more when the size fraction of the slag was smaller; this was because the smaller particle size allowed the CaO in the BOS slag to leach out, raising the pH of the water and making it more alkaline. It was also observed that under lower temperature conditions, the pH value of the slag was greater. The pH value caused by the smaller size fraction of steelmaking slag rose above safe levels which meant it could be considered hazardous waste. However the pH produced by the larger size fraction did not rise above hazardous levels. Therefore, it can be said that the slag should be used in the original form it comes in if it is to be used for a marine application (Y. Li et al., 2019).

Kashiyawa et al., found similar results when they completed a batch leaching test in which 4 different types of slag of different particle sizes were mixed with distilled water for 3 hours at a constant temperature. The pH of the solution was then measured. The solution was then

filtered, and the liquid was analysed using inductively coupled plasma optical emission spectroscopy (ICP-OES). A kinetic model was then applied to the data from the batch-leaching experiments. In samples with smaller particle diameter, calcium elution tendency was found to be higher due to the smaller surface area. It was also observed that the amount of calcium elution is not particularly affected by the Fe_2O_3 content (Kashiwaya et al., 2020).

Kato et al. set up an experiment in Japan that assessed the effect steelmaking slag had on marine life over 5 years. The experiment was done in 2 aquarium tanks that were both agitated using a wave-making device with controlled high and low tides. Lighting was used to simulate seasonal fluctuations in light. Both tanks had dredged soil from the Japanese ocean spread along the bottom, except one had been enhanced with steelmaking slag to be used as a soil stabilisation medium.

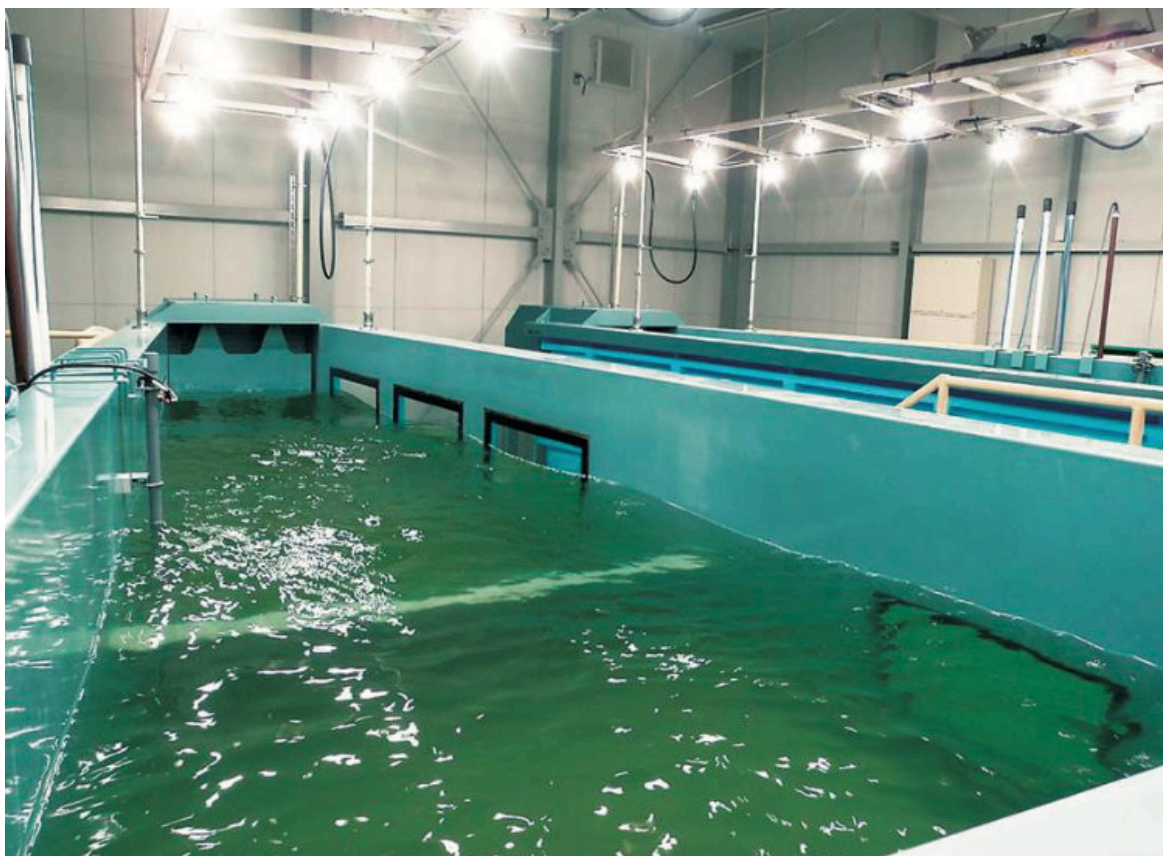


Figure 1. 1: Image showing an example of the aquarium tanks used in the slag leaching experiment (Kato et al., 2020).

In both tanks, plants native to Matoya Bay, Japan, were planted. Seawater from Tokyo Bay was used as the example seawater in the experiment. The water was replenished and changed

throughout the duration of the experiment. The effects on 3 separate marine species were assessed, including bioluminescent bacteria, microalgae and copepod crustaceans. It was found that the slag-modified soil was stabilised and not affected by the wave-making. When compared to the other tank with the non-slag-modified soil the soil moved around much more. It was found that over the 5 years, the 3 marine species were not affected by the slag and potential toxic effects (Kato et al., 2020).

Foekema et al. did a study in which the effect of BOS slag on marine ecosystems was analysed over 12 weeks. During the experiment, 3 different test materials were used, e.g. BOS slag, natural quarry rock and pebbles. Each of these was added to mesocosm systems containing live organisms that had been set up to simulate the environment found in nature. One mesocosm system simulated the environment found at the Oosterschelde estuary in the Netherlands, where BOS slag had been previously applied to the estuary in order to act as an erosion defence on the river bank. The effects of the water replenishment rate on the mesocosms were also assessed. The BOS slag was found to have no detrimental effect on the mesocosm ecosystem. It was also observed that vanadium was the most reliable element that could be traced in the mesocosms, meaning the BOS slag concentration could be reliably traced. However, it should be noted that vanadium was only observed in low background concentrations. The mesocosm data helped to interpret field data taken over 4 years at the Oosterschelde estuary, which has shown that the BOS slag has had no detrimental ecological effect on the ecosystem at the estuary (Foekema et al., 2021).

The recycling of steelmaking slag is currently very low in Vietnam due to a lack of consistent and reliable recycling processes that would lead to suitable quality steelmaking slag being recycled. In 2021 a paper was published that assessed if it would be suitable to reuse steelmaking slag produced in Vietnam for road construction material. Both BOS and EAF slag were tested during the experiment. The material was evaluated using two methods, which assessed the material's leachability potential, US-EPA 1311 and JIS K 0058. US-EPA 1311 is a US standard that is the 'Toxicity Characteristic Leaching Procedure'. So it measures how likely it is hazardous chemicals will leach out of slag. JIS K 0058 is a Japanese standard for measuring the amount and type of chemicals in slags. Both methods had different parameters. JIS K 0058 used deionised water as the leachant and mixed the slag at 200 rpm for 6 hours. Whereas EPA 1311 used acetic acid as the leachant and mixed the slag for 18 hours at 30 rpm. The pH of both the solutions was measured, and the concentration of elements was measured

using ICP-OES. The results of the two test methods yielded different results. When the leachate solution had a lower pH, a higher amount of elements were leached out. The lower pH during this test method was caused by using acetic acid during the test method. The test method JIS K 0058 that used deionised water as the leachate had higher pH results, but the elements leached out were below detectable levels for the ICP. The author suggests that the BOS and EAF slag are suitable for roadbed material (Huong Nguyen et al., 2021).

The effect of natural weathering on steelmaking slag has also been evaluated by assessing slag that has been exposed to a forest environment for 35 years. Ladle and EAF slag were used to repair 2 forest tracks 35 and 19 years ago, respectively. Researchers then sampled the slag from these 2 tracks to assess how its composition had changed and its effect on the environment around it. The samples were analysed using Raman Spectroscopy, SEM/EDS and XRD. It was found that in both slag samples, CO₂ had been absorbed, as the presence of CaCO₃ had been observed. Hashemite (Ba(S,Cr)O₄) and Crocoite (PbCrO₄) were both found to be present in the slag. These are both Cr(VI) containing minerals. Cr (VI) can be harmful if it leaches out to the environment around it, so the author suggests that these slags be reused with caution. Brucite (Mg(OH)₂) and Portlandite (Ca(OH)₂) were also found in the slag suggesting that overtime the slag had absorbed water. This also suggests that the slag had expanded over time, which led to the broken footpath surface that was observed (Gómez-Nubla et al., 2018).

1.3.2: Construction Applications

In 2019 Lin et al., found that optimal mechanical properties can be achieved when a BOS slag in a very fine powder form is used. They found that when coarser aggregate was used, there was a reduction in mechanical properties. The optimum BOS slag aggregate ratio was a 10 wt.% replacement for traditional aggregate. They found that the more BOS slag was used, the more the concrete suffered from expansion and cracking problems. It is unclear whether the slag underwent any pre-treatment, e.g., a weathering treatment to stop the expansion effects. The concrete also set faster the more slag was used (W. T. Lin et al., 2019).

Andrade et al., explored this concept further. They found that the BOS slag caused better compressive strength than the other concretes made with natural aggregates. The interface transition zone (ITZ) is the transition zone between the aggregate and cement. It was found

that the ITZ in the natural aggregate concretes was not uniform and was also very porous. The ITZ was less porous and more uniform in the BOS slag concrete, which is highly desirable in strong concrete (Andrade et al., 2021).

A review study on steel slag as aggregate by Chandru et al. concluded that the rough and porous texture of BOS slag contributes to a more bonded ITZ zone. In turn, increasing the mechanical properties of the concrete. They found that the presence of β -C₂S in BOS slag improved the long-term compressive strength of the concrete due to its slow hydration nature. The authors found the concrete to be stronger when it was used as coarse aggregate rather than fine aggregate or a combination of both fine and coarse (Chandru et al., 2020).

In similar studies, Jexembayeva et al., and Chen et al., found that 5%-15% BOS slag was the optimal proportion to add to a cement mix (Y. L. Chen & Lin, 2020; Jexembayeva et al., 2020).

In light of the issue, Lin et al., found that a more significant proportion of BOS slag being used caused the concrete to crack. Research by Zareei et al., states that nano-silica particles in combination with BOS slag should be added to the concrete to prevent this cracking phenomenon. If a crack forms, they found that the nano-silica suppresses the crack propagation, and the crack does not become as wide. This is because the nano-silica particles react with the slag to form additional calcium silicate hydrate (CSH), which is a critical component in the strength development of concrete. This results in a denser concrete matrix and a less porous structure. However, the modifications do lessen the workability of the concrete, meaning it does not flow well, and if it is to be used, the appropriate compaction method must be used (Zareei et al., 2019).

Raw materials, *e.g.* limestone and clay, are customarily used to create cement clinker, but when supplemented with steelmaking slag, the sintering temperature can be significantly reduced. Using the steel slag as clinker in cement plants would also improve their carbon emission outputs. Gao et al., calculated that the emissions could be reduced dramatically since less power is needed for clinker production. The purchase of steel slag is also cheaper for the cement production facility than purchasing limestone (Gao et al., 2021).

Leading on from this, Cao et al., completed a study in which heat treatment was used to modify the properties of BOS slag. The slag was heated to between 1300-1450 °C in different variants

of the experiment, held at this temperature for 30 minutes and then rapidly cooled back down to room temperature. The slag was then ground into a powder using a ball mill. This was done for different time durations, *e.g.* 15 minutes, 25 minutes, 35 minutes, 45 minutes and 55 minutes. The slag samples were mixed with traditional clinker materials such as limestone, sandstone and shale. The mixtures then underwent a clinker sintering procedure in which they were held in a furnace for 30 minutes at 850 °C and then rapidly cooled back to room temperature. This process improved the grindability and hydration activity of the steel slag, making it more suitable for use in the steel industry. They found that the iron and calcium ferrite phases were reduced, which have both been known to make the slag harder to grind. The experiments found that the sintered product containing 16.86 % slag was sintered at 1400 °C performed the best (Cao et al., 2019).

In some cases, however, the iron content can pose a problem in the cement clinker as it can cause a problem with the durability of the matrices. This could mean limiting the amount of steel slag used as a clinker. The iron content increases the material's ductility, meaning it is harder to grind the material into the desired shape. However, this can be easily remedied by the slag undergoing crushing and magnetic iron removal. In a review conducted in 2021 of all available technologies, it was concluded that in most cases, steel slag typically has high angularity and a rough surface texture which both can contribute to the higher performance of the cementitious matrices. It was found that when ground into a powder, steel slag can improve the overall mechanical properties and increase compressive strength by up to 20% when the steel slag is evenly distributed throughout the cement. During testing, the addition of steelmaking slag initially increases the porosity of the cement, so during chloride and carbonation tests, the performance is terrible. However, when the slag concrete is allowed to cure for around 90 days, the test performance is equal to portland cement clinker and, in some cases, superior (Martins et al., 2021; Pan et al., 2019).

Unfortunately, the fire resistance of concrete created using steelmaking slag has not been overly researched. In the little research, researchers compared traditional and slag-based concrete that had both been exposed to an elevated temperature of 300 °C. They concluded there was no noticeable change to the properties of both the concrete. Nevertheless, when the concretes were exposed to a temperature of 400 °C upwards, there was a noticeable decrease in the indentation hardness of the material, suggesting that the mechanical strength of the concrete had decreased (Sandanyake et al., 2020).

Other kinds of steelmaking waste, *e.g.* stainless steel slag and blast furnace slag, have also been shown to be suitable replacements for natural aggregates. In a study done in 2021, it was shown that both could enhance concrete properties. For example, the slump and flow characteristics of the concrete were both high, meaning the concrete would be easily workable in a real-world scenario. The compressive and tensile strength increased with a higher proportion of blast furnace slag. The stainless steel slag did not cause as much of an increase in tensile strength. The paper found the optimum amount of replacement to be a combination of the two types of slag, with the optimum combination being 20 % blast furnace slag and 10 % stainless steel slag (H. Y. Wang et al., 2021).

In specific applications, such as concrete structures with complex geometries, more substantial, more ductile concrete is required, known as steel fibre-reinforced concrete (SFRC) (Neves & Fernandes de Almeida, 2004). This concrete can also undergo natural aggregate replacement and still have the same properties. Kim et al., explored whether blast furnace slag could be used in this type of concrete and how it would react in a marine environment. They tested the concrete using two different replacement ratios for the blast furnace slag, 30 % and 50 %. The NT build 492 test was used to determine the level of chloride ion migration into the samples (Nordtest, 1999). The samples were also immersed in seawater in South Korea. The research found that the rate at which the chloride ions can penetrate the concrete decreased with a higher proportion of blast furnace slag. This is due to the concrete being denser. The service life of the concrete was predicted through Life 365 software, where it was predicted it would take more than 100 years for the chloride ions to penetrate 50 mm into the sample. These results were reflected in the samples immersed in the sea; however, the author mentions that more prolonged testing needs to occur in this experiment. The authors conclude that by including blast furnace slag in SFRC, the service life of the concrete structure would be extended (S. Kim et al., 2021). A similar study was completed by Ouda in which BOS slag concrete's reaction to water was assessed, and similar results were found (Ouda, 2019).

Another application BOS slag concrete has been tested for is its use in concrete paving blocks. Researchers found that paving blocks can be made of portland cement using up to 70 % BOS slag aggregate in the mixture. The concrete paving slabs passed all tests associated with BS EN 1338:2003, which is the standard for creating paving blocks (Jalull & Ganjian, 2019).

In an actual world application study on the use of steelmaking slag concrete as a building material in a residential home in a tropical location, it was found to be suitable. Thermal simulations were conducted between 3 homes one built with EAF slag concrete, one built with BOS slag concrete, and one built with natural aggregate concrete. It was found that the homes with steelmaking slag had a lower thermal conductivity than the aggregate natural homes, meaning they were generally cooler in the summer simulation. In the winter simulation, the natural aggregate homes were 1°C warmer. Both results are very positive results as it shows that steelmaking slag-based homes would save on the cost of air conditioning and heating throughout the year (Franco et al., 2019).

Another positive aspect of the application is that the slag can be multi-use. In section 1.8.9.4, it is mentioned that slag has good phosphorus adsorption capacity, Roychand et al., experimented with slag that had previously been used for phosphorus capture and then used it as a coarse aggregate in a cement application. This shows how the use of BOS slag can be used to encourage a more circular economy (Roychand et al., 2020).

1.3.3: Geopolymers

Mine tailings are a waste solid rock material that is a by-product of mining minerals from the ground. They are mainly composed of aluminium and silicon. Geopolymers are made when aluminium/silicon-rich materials are combined with alkali and cured at an elevated temperature. Therefore mine tailings can make excellent starting materials for geopolymers; however, they are highly crystalline, requiring further additions to enhance their activities. BOS slag and fly ash are suitable for this application because they contain CaO, SiO and Al₂O₃. BOS slag and the mine tailings are combined with potassium hydroxide (KOH) and then cured at elevated temperatures for some time to form the geopolymer. When tested, the BOS slag geopolymer was found to have a higher compressive strength of 21.44 Mpa than the fly ash geopolymer. The tests were conducted on a stress controlled compressive strength machine with a stress rate of 0.25 MPa/s. This was due to the formation of calcium silicate hydrate phases. These phases also served another purpose and immobilised any Fe and heavy metals in the geopolymer that the mine tailings may have introduced. A 12-month static leaching test on the geopolymer found that neither the BOS nor fly ash geopolymer allowed any harmful elements to leach out. This is a promising application for waste materials in green construction

materials (Falayi, 2020). Sithole et al., also found BOS slag geopolymers to have a similar metal removal effect on acid mine drainage that contained high levels of Fe, Al, Mn, Zn, Ni and Cu (Sithole et al., 2020).

In an alternative application, BOS slag can be made into a geopolymer coating and applied to the surface of the concrete. Due to the coatings high emissivity value, it has the effect of being able to reflect heat and provide cooling properties to what it is coating. Wu et al., recorded a temperature drop of 5.9 °C due to the coating in a simulated sunlight experiment. The coating bonded as well as a commercial paint coating due to the BOS slag reacting with $\text{Ca}(\text{OH})_2$ on the surface of the concrete (Wu et al., 2020).

1.3.5: Slag use in Road surfaces and Pavements

In recent years, steel slag usage in road surfaces and pavements has become popular in Japan and Australia; it can create road shoulders and the hot asphalt mixture used to create road surfaces. Its application in this field has become so popular due to its properties, such as being a tough and dense material which allows a thinner layer of asphalt to be paved. The angular slag particles interlock very well together, therefore increasing the asphalt's resistance to tyre track marks and resistance to skidding (Kehagia, 2009). The durability and anti-peel resistance of the surface is excellent also. The slag-asphalt mixture retains its heat for a long time, meaning the road surface or pavement surface is easier to put down. Slag does however have a very high specific gravity making transport costs 20 % more expensive. However, these transport costs can be tolerated due to the slags other desirable properties (Gencel et al., 2021). In order to overcome the volume expansion problems previously seen by several researchers of road surfaces, including Gauthier et al., the road surface can undergo a weathering process to prevent expansion caused by hydration (Gautier et al., 2013). This weathering process is around 6 months long; however, steam weathering can be used for faster production (Gencel et al., 2021).

The top layer of aggregate applied on a road surface is an open-graded asphalt friction course (OGAFC). OGAFC is usually a layer around 25-50mm thick. This layer leads to the road surface not facilitating the quick runoff of stormwater. OGAFCs provide good skid resistance, reduced spray, and less chance of hydroplaning. One of the significant problems with using

traditional aggregate to create this layer is moisture damage traditional aggregate allows. Causing deterioration in the adhesive bond between the asphalt cement and the aggregate surface. Acidic and more neutral rainwater pHs can also affect the longevity of OGAFc. Pathak et al., looked at how suitable BOS slag would be as an aggregate in this application and how it would be affected by different pH values. Natural aggregate and BOS slag were trialled together in different ratios and with two different asphalt binders. These were polymer-modified bitumen (PMB) of grade 40 and crumb rubber-modified bitumen (CRMB) of grade 60. The different combinations of samples were each tested using a modified boiling water test, tensile strength ratio test and wet abrasion loss test. The modified boiling water test tested the durability of the bond between the aggregate and the binder to find out how durable the bond was. This testing found that there was a much lower stripping index in the samples with more BOS slag, meaning that the binder did not come off the aggregate as quickly or as easily. This was true even in the much harsher acidic environment. The rough morphology of the BOS slag allowed a much thicker asphalt film to be created, allowing a better bond. This provides more evidence as to why BOS slag is suitable for use in aggregate for road surfaces (Pathak et al., 2020).

Skid resistance can be analysed using a circular vehicle simulator consisting of four car tyres that rotate over different asphalt samples for a prolonged time. Each tyre provides 40KN of force which is about the same as a normal passenger car. The simulator can be seen in Figure 1.2. This test simulates how long the anti-skid resistance of a road may last. The researchers tested the simulator using different asphalts made up using different BOS slag and granite ratios. The ratios were 0 % BOS slag replacement, 25 % replacement, 50 % replacement, 75 % replacement and 100 % BOS slag replacement. At the end of the experiment, it was found that the samples with 50 % BOS slag replacement provided the highest anti-skid resistance. The 75 % and 100 % ratios did not achieve the same performance as they polished too fast and did not provide a surface with friction. BOS slag can be said to be less wear-resistant and softer than granite. The two differing hardness profiles of the aggregates meant that one wore faster than the other creating an uneven, rougher surface, which in turn provided a surface with more friction, increasing the antiskid resistance. It would seem that the 50 % replacement ratio provided the optimum balance of the two aggregates (L. Hu et al., 2021).



Figure 1. 2: Circular vehicle simulator (L. Hu et al., 2021)

The amount of free lime present in steelmaking slag can effect the volume expansion properties of it e.g. if the slag is used in a road surface it can lead to issues with the road surface cracking (Fisher & Barron, 2019). Therefore it can be useful to measure the amount of free lime present before the slag is utilised. Imashuku et al., performed experiments in which cathodoluminescence (CL) was used to determine the percentage of free lime. In the method, the BOS slag is bombarded with electrons, and the spectra produced can be used to determine the amount of free lime present. The free lime emits an orange spectrum. This is due to the dissolved manganese (II) ions in the free lime. The method suggests using X-ray excited optical luminescence (XEOL) to gain a quick analysis of the amount of free lime present in the slag, which could be used on-site at the steel plant (Imashuku & Wagatsuma, 2020). This method can help decide if the slag would be helpful for road building.

With this idea, if a situation arose in which only some of the slag a plant was producing was suitable for road construction, it could be mixed with another material to create the road, so it does not go to waste. Harbour sediment is often dredged to alter the depth of docks where ships may be docking. This harbour sediment is often dumped back into ocean disposal areas, where it is wasted and not used at all. BOS slag can be mixed with this dredged harbour sediment to

create a road surface. Researchers found that the appropriate strength for a road surface can be reached with a ratio of 50 % BOS slag to 50 % harbour sediment (Lim et al., 2021).

As previously mentioned Another big concern in recycling BOS slag is its leaching effect, as many of the elements in the composition of the slag are soluble in water and can leach out and harm the environment around it. Cui et al., have explored the microstructure BOS slag creates in the asphalt, and if the leaching behaviour of the slag is enhanced or suppressed. The BOS slag underwent hydrodynamic testing. It was found that the release of heavy metals was inhibited by the encapsulation effect of the asphalt, reducing the leaching concerns. The slag was also found to reinforce asphalt and enhance the strength of the microstructure (Cui et al., 2021). Hu et al., found that the adhesive strength of the BOS slag to the asphalt was extremely good, even better than traditional asphalts such as andesite and limestone. This was tested using a moisture stripping test. They found this was due to the rough surface texture and alkaline nature of the BOS slag (R. Hu et al., 2020). This suggests that the BOS slag would stay encapsulated in asphalt infinitely, and the leaching of harmful heavy metals would not be a concern.

Whereas Xie et al., found the leaching effect to be a concern in a slag aggregate asphalt-based pavement system after 15 years. They found that high concentrations of Cr, Pb, Ni, Cu, Zn, Cd and As in the soil under the pavement. They analysed the weathered BOS slag from the pavement and found the weathered BOS slag had a lower concentration of these elements suggesting the elements had leached out into the soil (Xie et al., 2020).

Li et al., also observed the excellent adhesion of BOS slag to asphalt when the two are combined in a pavement application. The researchers performed experiments to assess the radiation-cooling effects of the BOS slag on the surrounding environment and measured how much heat energy could be absorbed. This was done using emissivity measurements, thermal conductivity, and indoor and outdoor temperature measurements. Three different proportions of BOS slag replacement were tested, e.g. 45 wt.%, 55 wt.% and 75 wt.%. They found that the most heat was absorbed 3 cm below the surface with the asphalt with 75 wt.% BOS slag replacement, absorbing the most heat at the end of the experiment. With the world's rising temperature due to climate change, BOS slag pavements that provide a radiation-cooling effect would be very useful in areas that suffer from the urban heat island effect. The urban heat island effect is when cities are built out of materials that retain and absorb heat, creating a warmer

environment (Y. F. Li et al., 2021; Rosenzweig et al., 2006). Researchers in Egypt showed that BOS slag was suitable for concrete pavements. They used it to replace natural aggregate traditionally used in concrete pavements (Tahwia et al., 2020).

In order to achieve the highest strength of the road surface, steel slag aggregate and bitumen can be heated together, resulting in a pavement where 90-95 wt % is composed of aggregates. A pavement with a thickness of around ~5cm can withstand 90-140 tons of heavy equipment passing over it without deformation (Gencel et al., 2021).

Liu et al., points out that there is little research on using slag asphalt in roads in colder climates, *e.g.*, places where the ground frequently goes through freeze-thaw cycles. In 2019 research was conducted on how steel slag reacted when going through freeze-thaw cycles, as well as the mechanical properties and if the slag would crack under low temperatures. Slag replaced traditional basalt aggregate in five different ratios (0 %, 25 %, 50 %, 75 % and 100 %) in order to find the optimum ratio. Marshall stability is a test in which the stability of the mixture is measured in order to predict how it would react to multiple compressive stresses from vehicles going over its surface of it. They found that the marshall stability increased linearly with the added slag. The indirect tensile strength of the mixtures was found to decrease with more slag added. However, the mixture could withstand more stress before fracturing and failing. This indicated that the addition of slag had a positive effect on the low-temperature cracking resistance of the material. The sample tested with 100 % slag had the best water stability and highest indirect tensile strength even after 15 freeze-thaw cycles. Meaning the sample had the best freeze-thaw resistance. The authors concluded that a 100 % slag asphalt material would be suitable for road building in colder regions and fulfil the need for more sustainable road materials (H. Liu et al., 2019).

Even though BOS slag has many impressive properties, as discussed above, it is essential to remember that the material's life cycle analysis can also impact if it would be suitable to use on road surfaces or pavements. Pavements made using ordinary stone were used as a comparison. The study was assessed using Simapro using an uncertainty analysis methodology. It was found that using BOS slag for pavements can lead to a 12 % reduction in emissions compared to using ordinary stone. This reduction in emissions can be attributed to the fact that BOS slag is produced as a by-product of steel production, and no energy has been consumed in producing it. Whereas with ordinary stone, much energy goes into the mining of the stone

as well as energy going into transporting it to its final destination. The distances from BOS slag to be transported before it is added to the asphalt are also significant. Suppose the BOS slag is transported more than 430 km, then it becomes non-cost efficient and produces more emissions than natural stone production. This suggests that if BOS slag is to be used in pavements and road surfaces, then the asphalt production facility should be set up in the same area as a steel production plant, for example, as this would eliminate the emissions from transport (Xie et al., 2021).

1.3.6: Slag use as Railway Ballast

Several researchers have previously commented on the suitability of steelmaking slag as railway ballast due to its similarity in shape and properties to traditional limestone ballast underneath the tracks. A comparison experiment conducted in 2017 by Esmaili et al., found that the slag provided 27 % more lateral resistance than limestone ballast (Esmaili et al., 2017; Gencel et al., 2021). A study done in 2021 by Jia et al., showed similar results, with the slag's resistance to shear breakage being found to be 16.46 %-19.48 % higher than traditional railway ballast materials (Jia et al., 2021).

1.3.7: Fertiliser

In 2020 Wen et al., studied the effect that modified BOS slag and unmodified BOS slag may have on the nitrogen concentration in soil and the effect on the microbial community contained within the soil. Quite often, nitrogen can leach out of soil too fast for plant growth. This is caused by it leaching out when the groundwater level is high, for example, in farmland. Raw BOS slag waste was collected from a steel plant in China. The waste was then crushed and sieved. Then it was washed using deionised water, dried at 105 °C for 4 hours, and cooled back to room temperature in a desiccator. Some of this slag was then used in a modification process in which it was mixed with aluminium hydroxide ($\text{Al}(\text{OH})_3$) and deionised water. It was then aged at room temperature for 10 hours, calcinated and heated to 800 °C for 2 hours, and cooled back down (Yang et al., 2017). Soil leaching experiments were conducted on the raw BOS slag and modified raw BOS slag. The slag was mixed with the soil in a leaching column with water periodically to simulate a leaching cycle. The leachate was collected at the bottom of the column to measure the soil's nitrogen concentration. It was found that the column with

modified BOS slag had a lower nitrate concentration in the leachate, suggesting that the nitrogen was being released in a controlled way. The addition of both kinds of slags raised the pH of the soil, but the modified BOS slag had less of an effect than the other slag. The modified slag's effect on the microbial community was also very good, with a broader range of bacteria in the soil (Wen, Yang, Dang, Yang, et al., 2020).

In coastal areas, excess sodium is often found in the soil due to its proximity to seawater. This poses a significant problem for farmers who farm there. In Italy, BOS slag was applied to the soil over a 3-year Lysimeter trial on wheat and tomato plants. A lysimeter is a device that can measure the amount of precipitation an area receives as well as the amount of precipitation lost to soil (Howell, 2005). At the end of the trial, it was found that the BOS slag had lowered the sodium level in the soil and increased the tomato yield available to the farmers. This was because the soil contained Ca^{2+} and Mg^{2+} bivalent cations, which competed with the sodium for sorption sites and prevented the sodium from staying in the soil. The durum wheat did not manage to grow as well, which could be caused by the higher levels of V and Cr that were found in the soil. V and Cr are known to cause toxicity to plants. The author suggests that if the BOS slag is used as a fertiliser, the V and Cr concentrations should be assessed before use to prevent crop harm (Pistocchi et al., 2017).

However, even though BOS slag is helpful as a fertilizer, it must also be noted that due to its unpredictable composition, there is a risk that it may contain heavy metals, which can have an adverse effect on the crops it was meant to fertilise. A recent study was completed in Havana in which plant grown on land contaminated by slag was analysed. The slag was from a nearby abandoned steel plant. The concentrations of Cadmium (Cd), Chromium (Cr), Nickel (Ni) and Lead (Pb) were assessed using ICP-OES. The crops tested were all crops that were available for human consumption. It was found that Cd, Cr and Pb were all present in the soil at higher levels than is safe for human consumption. Cd was found in the highest numbers, mainly in the edible part of the plant, for example, the leaf of a vegetable. The main human exposure route for Cr, Cd and Ni was if the consumer were to ingest the vegetable, they would have 70 % of the allowable daily dose in that one vegetable. In comparison, the main digestion route for Pb was through contaminated soil particles that may still be on the vegetable (Alfaro et al., 2021).

1.3.8: Slag use as a catalyst

The composition of steelmaking slag generally contains many catalytically active components, making it suitable for reuse in catalytic applications. Slag can undergo different treatments such as acid modification, alkali modification, high-temperature modification and mechanical modification. These can all be used to increase the slag's surface area and pore size, creating more catalytic sites. Most studies found that the best catalysis results come from using a combination of these methods. Some applications slag can be used for include catalytic pyrolysis, organic degradation, electrocatalysis, photocatalysis, transesterification and carbon capture and storage (F. P. Wang et al., 2021).

For example, in a study done in South Korea on the CO₂ pyrolysis of waste tyres to produce H₂, steel slag was used as a catalyst. With the addition of the catalysis, the pyrolysis was enhanced by 400 % when performed at 400 °C (Cho et al., 2020). In a similar pyrolysis process, steelmaking slag was used as a catalyst in the CO₂ pyrolysis of pine sawdust to produce syngas. The syngas can produce other fuels, such as methanol and diesel (Capodaglio & Bolognesi, 2019; S. Lee et al., 2020). Similar research on pine sawdust pyrolysis found that the catalytic ability is enhanced even more if the steel slag is combined with nickel through a mixing process. Researchers found that a higher yield of syngas could be achieved (Guo et al., 2019). In a similar application, steel slag can also be used to prepare electrodes in the form of Sn/Mn-loaded steel slag zeolite particles. These particles can then be used to degrade rhodamine B, a common pollutant in water. Rhodamine B is used in manufacturing as a dye (Kaur et al., 2014; Z. Zhang et al., 2020).

1.3.9: Metal Recovery from Slag

In the Panzhihua-Xichang areas of China, vast amounts of vanadium-bearing steel slag (VBSS) are produced yearly during the steelmaking process. Vanadium titanium magnetite ore goes through a mineral separation process to refine what is to go into the blast furnace. This produces some tailings. Tailings are then refined to recover TiO₂ using a sulfuric acid (H₂SO₄) decomposition process, which results in titanium dioxide waste acid. The process from the blast furnace produces VBSS, which has a high vanadium concentration. Zhang et al., proposed an idea in which the titanium dioxide waste acid could be used as a leaching agent for the

vanadium steelmaking slag. It was found that the titanium dioxide waste effectively allowed vanadium recovery from the slag. H_2SO_4 concentration in the acid played a prominent role in the leaching process, with a concentration of 300 g/L being the optimum concentration. This concentration effectively recovered 95 % of the vanadium from the slag. The leach residue contained traces of V at 0.06 % and some Fe, Ti, P, and Mg impurities. The residue can be further filtered to allow the further recovery of V (W. Zhang et al., 2021).

In a similar acid-leaching process, Siedlecka found that Fe could be recovered from basic oxygen furnace (BOF) sludge. BOF sludge is similar to BOS slag but contains significantly higher amounts of Fe. BOF sludge is a by-product of the flue gas produced during the basic oxygen steelmaking process. Scrubbers purify the flue gas before it is released into the atmosphere. This causes the transfer of pollutants from the gas into the water used to scrub. This results in a solution with suspended solids known as BOF sludge. 1M hydrochloric acid and 2.5M sulfuric acid were mixed in a reactor with several different experimental conditions, *e.g.*, different temperatures, time duration, solid-to-liquid ratio and stirrer speed. The remaining sludge was then filtered and separated into two separate waste streams. An Fe oxide sludge is left after the reaction, which can be dried and sent for a magnetic separation process to recover a concentration of Fe_2O_3 and Fe_3O_4 . The Fe oxides can then be reused in the steelmaking process. The other waste stream is a leachate of FeSO_4 which can be further processed by washing with ethyl alcohol to obtain $\text{FeSO}_4 \cdot 7\text{H}_2\text{O}$, which can be used as a coagulant in the sewage treatment process or as an additive in fertilizer mixes (Siedlecka, 2020).

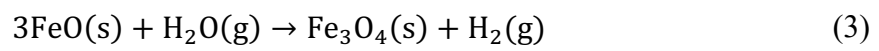
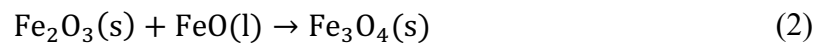
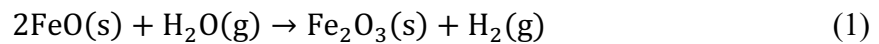
Electric arc furnace slag is similar to BOS slag and can undergo a two-stage pyro-hydrometallurgical process in which valuable slag components can be recovered. The first stage is a carbothermic reduction stage in which Fe, Mn and Nb can be recovered. The second stage, which involves acid baking and then water leaching, recovers elements from the Fe-depleted stage, such as Al, Ti and Mg (J. Kim & Azimi, 2021).

A reduction reaction can also be performed with BOS slag. BOS slag can be crushed and mixed with stone coal and held in an Argon atmosphere furnace for a period of time. This can then be quenched using cold water. The remaining product is a foaming slag interspersed with metal droplets. The metal droplets can be easily separated from the slag product for chemical analysis. The metal droplets consisted of Fe, Mn, P and V. These metal droplets can either be returned to the steelmaking process or can be further processed to recover the elements

contained in the droplets. The remaining slag product is rich in CaO, SiO₂, MgO and Al₂O₃ etc. This can be recycled to produce a glass ceramic product with a maximum bending strength of 95.83 Mpa. This property would make it suitable for use as a building decoration material (Y. Lin et al., 2021).

A similar application known as InduRed also exists in which slag is carbothermally reduced, which separates the phosphorus from the slag in a gaseous form. This then leads to an iron-rich alloy being left behind as well as the remaining components of the slag mixture. The phosphorus gas can then be used as input for the fertiliser production industry, and the liquid iron can be recycled in the steelmaking process (Breuer, 2021).

BOS slag can also be used in hydrogen production due to the reaction between steam and the iron oxides in the slag. This reaction can be seen below in equations 1-3.



Li et al., completed experiments on this in which slag was placed in a furnace with an argon atmosphere. Steam produced from deionised water was passed through the furnace for 5 hours at various temperatures. The output gases were measured using gas chromatography. It was found that the optimum temperature for H₂ generation was under 2000 °C. It was also found that the slag became more magnetic after the steam treatment, meaning that Fe recovery from the slag would be easier. This is a promising application as much research is currently being done into steelmaking that uses H₂ as the fuel source (P. Li et al., 2020).

1.3.10: The Regeneration of Seaweed and Microalgae

Batch leaching experiments were conducted on slag samples in which 1 g of slag (carbonated or non-carbonated) was placed into 100 ml artificial seawater. Furthermore, the addition of gluconic acid was added to some batch experiments. The batch experiments were then shaken for 192 hours, with sampling conducted at 12, 24, 48, 72, 96, 144 and 192 hours. The pH and redox potential was measured immediately after the aliquot was taken. The aliquot was then filtered to remove any solid residue. The Ca, Mg, and Si concentration was analysed using ICP-

OES, and the total Fe concentration was analysed using mass spectroscopy. It was found that the carbonated slag suppressed the pH rise of the seawater due to the CaO present in the slag being stabilised into an insoluble carbonate. The presence of gluconic acid induced the formation of stable chelated complexes of Fe. The combination of carbonating the slag and adding gluconic acid significantly increases the amount of Fe in the seawater and showing that steelmaking slag would be suitable for the application of restoration of seaweed populations (Sakurai et al., 2020).

Microalgae plays a significant role in several industries, such as medicine, food, renewable energy and wastewater purification. Microalgae plants are generally present throughout the oceans and lakes. Their characteristics include fast growth, a short reproduction cycle and rich nutrition. Steel slag, as previously mentioned, can provide valuable nutrients for the microalgae such as Fe, Ca, Mg, P and Si. Generally, steelmaking slag contains oxides which can cause an increase in the pH of the water the microalgae is being grown in, so the pH must be adjusted to ensure it is optimum for the microalgae. It has been found that citric acid and gluconic acid are beneficial in adjusting the pH value. Gluconic acid is also known to increase iron solubility in the aqueous solution as previously mentioned. Another use for microalgae is in producing biodiesel, which is a sustainable kind of fuel that can be used to replace traditional fossil fuels. Steel slag had a beneficial effect on the production of biodiesel in relation to this in that it does not provide nitrogen to the microalgae. This results in the microalgae having reduced protein synthesis, which results in a large amount of the carbon that should be used in proteins being instead converted into energy storage molecules, e.g. lipids. This forces the lipid content of the microalgae to be very high, which means a lot more oil can be produced from the microalgae. The authors also state that lipid content can increase in a phosphorus or sulphur-deficient environment (Mata et al., 2010; Yu et al., 2021; L. Zhang et al., 2019).

1.3.11: Phytoplankton Applications

Traditionally microalgae are cultivated in a free cell suspension system in an open pond or a closed photobioreactor. However, it has been previously shown that a biofilm harvesting method can lead to higher productivity. For example, *Chorella Vulgaris*, when grown as a biofilm, has been found to have a 30.4% increase in yield. The biofilm format increases the light that can get to the microalgae and makes a more straightforward gas exchange pathway. All of this means that the photosynthesis efficiency of the microalgae increases. With the

research that has previously been done into the effect that steel slag has on the growth of microalgae, Chen et al., studied if a biofilm of algae could be created around samples of BOS slag. They also assessed the feasibility of using the BOS slag and microalgae hybrid material to create an artificial reef structure. Three separate microalgal strains were examined: *Chlorella sorokiniana* PTC13, *Tetraselmis suecica* SC5 and *Nannochloropsis oceanica* DG. The common application for these strains is aquaculture feed. *T. suecica* SC5 achieved the largest biomass. The researchers believe this was down to the strain having a larger size and being able to adhere to the BOS slag surface more effortlessly. The *T. suecica* SC5 were harvested and found to be composed of 36.2% protein, 27.8% carbohydrate and 16.2 % lipid. These properties make the algae grown suitable for use as aquaculture feed. The researchers observed that the BOS slag surface, with its many nutrients, accelerated the alga's growth. So therefore, it concluded that if the slag were to be used as the starting block for an artificial reef structure, much marine life would be attracted to it. It is cheaper than using other materials, such as shipwrecks, to create artificial reefs (C. Y. Chen et al., 2021).

1.3.12: Adsorbent Properties

A study done in South Africa showed that BOS and BF slag could be used to treat acidic wastewater from an aluminium coating process in order not to pollute the municipal water it runs into. The slag can be used to raise the wastewater's pH level to a safer alkaline pH. For BOS slag, the pH was raised to 12, and for BF slag was raised to 6. They found that the slag can remove sulphates from the solution and BOS slag was superior at this as the higher pH meant that more sulphate was removed from the solution. 80 % of the sulphates were removed from the solution (Vessal, 2019).

However, the performance of BOS slag absorption varies across different elements. For example, it was found that if Pb, Cd, Zn and Cu are in a solution together, BOS slag has more of an affinity to absorb Pb before absorbing the other heavy metals mentioned. This absorption performance is affected by several factors, such as the heavy metal concentration, pH and solid-to-liquid ratio (Xue et al., 2020).

In another similar study, BOS slag was first thermally activated at 1000 °C for 24 hours to improve its surface area and porosity. 0.5 g of BOS slag was then used in batch experiments to assess its F removal capacity. It was found that F was successfully removed from the solution,

with uptake being rapid at the start and reaching equilibrium after 35 minutes. The optimum pH for F removal was around 6-10 (Islam & Patel, 2011).

When these findings are applied to a real-world application, such as restoring acid-contaminated soil and water near a mine, the results are promising. When applied to soil, the slag increased the pH, improved the diversity of the bacterial communities in the soil and plant growth and immobilised the heavy metal ions in the soil such as Pb, Zn, Cu, Cd and Cr. In the case of the acid mine water treatment, the results are similar, with 99 % of all trace metals, e.g. Pb, Cr, Cu, Cd, Co, Fe, Mn, Ni, Zn and Al, being removed (Saha et al., 2019; Wen, Yang, Dang, Miki, et al., 2020).

1.3.13: Arsenic Removal by Steelmaking Slag

Li et al., mentions how steelmaking slag can be used to detoxify wastewater from the copper smelting process. It is not specified in the study whether the slag was BF or BOS slag. They mention how normally, steelmaking slag has a low As removal rate and removal capacity, so they experimented with adding permanganate (KMnO_4). The experiments were conducted by adding 5 g of steelmaking slag to 100 ml of copper smelting wastewater with differing amounts of KMnO_4 . The steelmaking slag released Fe, Ca and Si ions and caused an increase in the pH levels of the solution. During the reaction, As(III) is oxidised to As (V) and Fe(II) is oxidised to Fe(III). This creates an amorphous FeAsO_4 precipitate and As-adsorbing $\text{Fe}(\text{OH})_3$ floc. This causes an As removal rate of 91.37 %. The released Fe ions were also further hydrolysed to $\text{Fe}(\text{OH})_3$ floc meaning more As was absorbed (Y. Li et al., 2021).

In other batch experiments done using BOS slag without KMnO_4 , the removal mechanism of As was found to be adsorption at pH 8-11 and at pH 11-13, amorphous calcium arsenate precipitation. The researchers found that at a higher pH value, the formation of $\text{Ca}(\text{OH})_2$ and CaCO_3 on the surface hindered the removal process of As. They also found that slag was suitable for removing Pb. Pb was removed from the solution by forming a Pb-OH precipitate (S. H. Kim et al., 2021).

Chapter 2: Experimental Materials and Methods

2.1: Chemicals

The chemicals used in the experimental work, their supplier, and the Chemical Abstracts Service (CAS) number are listed in Table 2.1 below.

Table 2. 1: Table of chemicals, suppliers, and associated CAS number.

Chemical name	Supplier	CAS No:	Experimental use
Sodium chloride (NaCl)	Sigma-Aldrich Company Ltd.	7647-14-5	Model seawater production
Magnesium chloride hexahydrate (MgCl ₂ •6H ₂ O)	Sigma-Aldrich Company Ltd.	7791-18-6	Model seawater production
Sodium sulphate (Na ₂ SO ₄)	Sigma-Aldrich Company Ltd.	7757-82-6	Model seawater production
Calcium chloride dihydrate (CaCl ₂ •2H ₂ O)	Sigma-Aldrich Company Ltd.	10035-04-8	Model seawater production
Potassium Chloride (KCl)	Sigma-Aldrich Company Ltd.	7447-40-7	Model seawater production
Sodium hydrogen carbonate (NaHCO ₃)	Merck Chemicals Ltd.	144-55-8	Model seawater production
Potassium Bromide (KBr)	Sigma-Aldrich Company Ltd.	7758-02-3	Model Sea Water Production
Strontium Chloride Hexahydrate (SrCl ₂ •6H ₂ O)	Fisher Scientific Ltd.	10025-70-4	Model Sea Water Production
Boric Acid (H ₃ BO ₃)	Fisher Scientific Ltd.	10043-35-3	Model Sea Water Production
Sodium Fluoride (NaF)	VWR International	7681-49-4	Model Sea Water Production

Sodium hydroxide (NaOH)	VWR International	1310-72-2	Model seawater production and phosphate removal
Potassium phosphate monobasic (KH ₂ PO ₄)	Sigma-Aldrich Company Ltd.	7778-77-0	Phosphate removal
Isostearic Acid	Tokyo Chemical Company	2724-58-5	Functionalisation of slag and the growth of wheatgrass
Lanolin	Sigma-Aldrich Ltd.	8006-54-0	Functionalisation of slag and the growth of wheatgrass
Lauric Acid	Sigma-Aldrich Ltd.	143-07-7	Functionalisation of slag and the growth of wheatgrass
Toulene	Sigma-Aldrich Ltd.	108-88-3	Functionalisation of slag and the growth of wheatgrass
Cysteic Acid	Sigma-Aldrich Ltd.	23537-25-9	Functionalisation of slag and the growth of wheatgrass
Nitric acid	Sigma-Aldrich Ltd.	7697-37-2	Functionalisation of slag and the growth of wheatgrass
ICP Multi-element	Sigma-Aldrich Ltd.	Several CAS	Nutrient leaching

standard solution VIII		numbers due to multi-element nature	experiments
Silicon Standard for ICP	Sigma-Aldrich Ltd.	7697-37-2 and 7664-39-3	Nutrient leaching experiments

2.2: Techniques

2.2.1: Microwave Plasma Atomic Emission Spectroscopy (MP-AES)

MP-AES is a powerful technique that can be used to measure the chemical composition of liquid samples. An industrial magnetron producing microwave energy forms microwave plasma. This microwave energy then passes through an axial magnetic field and an electrical field and is then combined with Nitrogen to create a plasma. The nitrogen source of the machine used had a nitrogen generator that pulled Nitrogen out of a compressed air stream (Agilent, 2021).

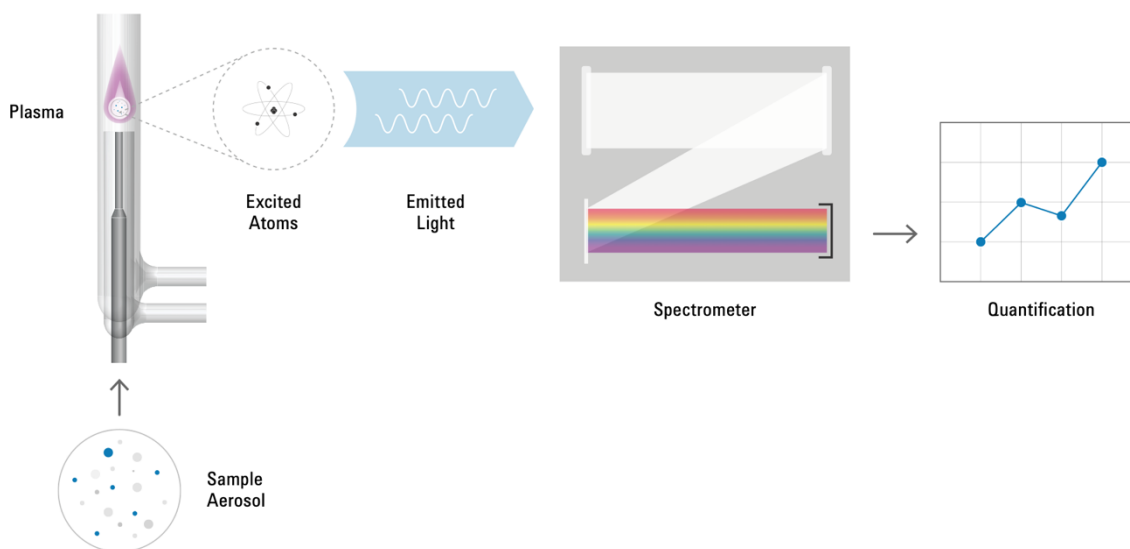


Figure 2. 1: Schematic diagram of a microwave plasma atomic emission spectrometer (Agilent, 2021)

Before testing any experimental samples, calibration standards are used to create concentration curves in the software so the wavelengths in the experimental standards can be quantified. The

equipment used for the analysis was an Agilent Technologies 4200 MP-AES with MP expert software. The machine used can be seen in Figure 2.2(Agilent, 2021).

Before MP-AES analysis, it was necessary to remove any solids from the samples, so each sample was centrifuged at 5000 rpm for 10 minutes. If any solids go into the MP-AES, it can cause damage. In order to quantify the amount of each element in the sample, it was necessary to quantify by making up calibration standards. Two standards were used during the experiments. One was a multi-element standard containing Al, B, Ba, Be, Bi, Ca, Cd, Co, Cr, Cu, Fe, Ga, K, Li, Mg, Mn, Na, Ni, Pb, Se, Sr, Te, Ti, and Zn. The other standard was a Si standard. These standards were used to make calibration solutions at the following ppm concentrations: 2, 4, 6, 8 and 10. These were always freshly made before any MP-AES analysis took place. If the machine did not calibrate appropriately, then analysis was not done. 50 μ l of each nutrient-leaching sample was diluted into 10 ml of lab-grade deionised water using a volumetric flask. This solution was then ready to be tested by the MP-AES.

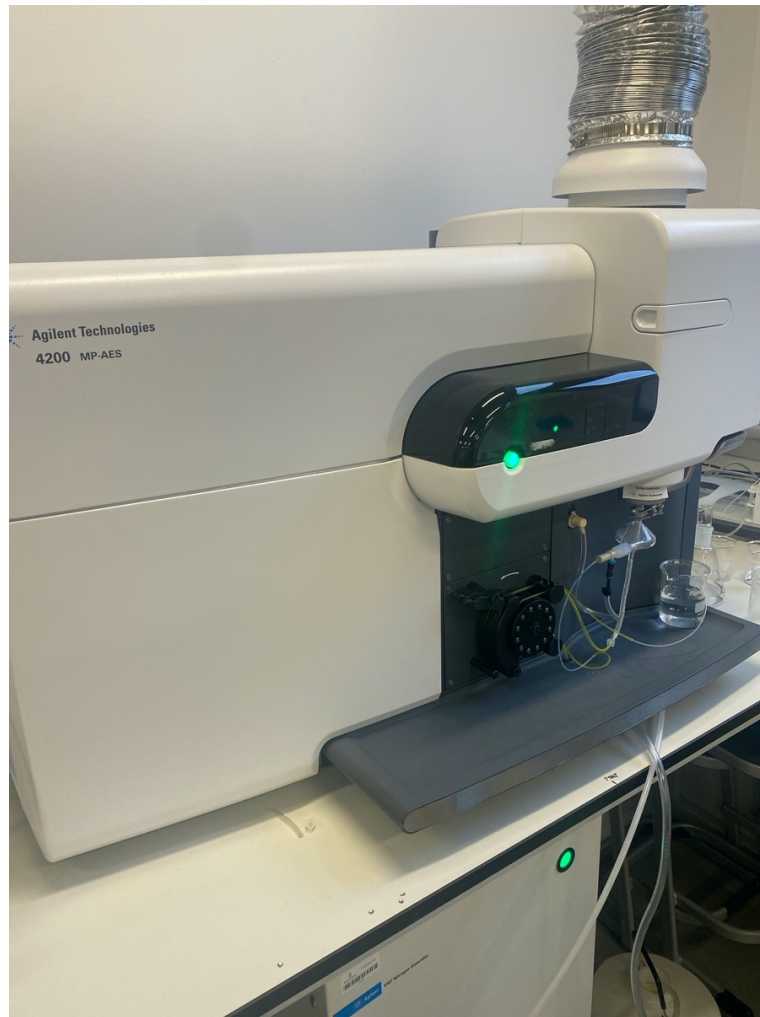


Figure 2. 2: The Agilent Technologies 4200 MP-AES used in experiments.

2.2.2: Contact Angle

The contact angle technique can be used to characterise the wettability of a surface by measuring the angle between the surface of a liquid droplet and the surface it is sitting on. It is a powerful technique to characterise a surface's properties, e.g., whether hydrophobic or hydrophilic. The criteria for whether a surface is hydrophobic or hydrophilic can be seen in Figure 2.3.

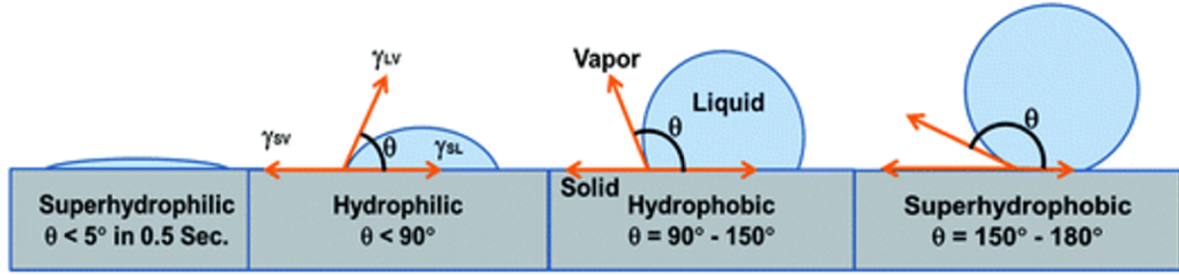


Figure 2. 3: Figure showing the contact angle criteria for a sample to be hydrophilic or hydrophobic (Lerman, 2017).

The contact angle can be used to calculate the surface free energy of a sample through the use of young's equation. Young's equation is equation 2.1. γ_{lv} is the surface tension of the liquid, γ_{sl} is the interfacial tension between the solid and liquid and γ_{sv} is the surface tension of the solid, i.e., surface free energy.

$$\gamma_{sv} = \gamma_{sl} + \gamma_{lv} \cos \theta_y \quad (2.1)$$

Young's equation assumes that the surface is flat with no surface roughness and that the chemical composition across the surface is the same. It also assumes there is no interaction between the surface and the liquid. Therefore, it is recommended that other types of contact angle measurement are performed, *e.g.*, static, or advanced and receding dynamic contact angle. Static contact angles are measured when a droplet is put onto a surface and measured. The droplet does not move; therefore, the solid-liquid boundary mentioned in Young's equation is non-moving. Dynamic contact angles are measured by advancing and reducing the volume of a droplet on the surface. The advancing angle is measured when the drop is at its maximum volume, and the receding angle is measured when the drop is at its minimum volume. The difference between these two angles is known as hysteresis. The hysteresis value is significantly influenced by the surface and can be used to determine how homogenous the surface is and how the surface's topography and chemical composition influences the droplet (Laurén, 2021). The contact angle used was a Krüss DSA25 Expert Drop shape analyser, shown in Figure 2.4.

The slag was compressed into a pellet using a pellet press with a 32mm die. The pellet was then placed onto the sample stage of the machine. A syringe was then filled with type 2, 15 MΩ.cm distilled water. The contact angle measurements were then controlled and measured through the software. The contact angle measured both the sessile drop and advanced and

receding contact angle. The measurements were completed in triplicate, so the value quoted is an average. The contact angle was used under standard conditions.



Figure 2. 4: Image showing a Krüss DSA25 Expert Drop shape analyser.

2.2.3: Thermogravimetric analysis (TGA)

Thermogravimetric analysis is a technique in which the mass of a sample is measured as it is heated up in a controlled atmosphere. The sample is put in a small pan that sits on a highly accurate balance inside a furnace. The furnace can be programmed to either cool or heat the sample at a specified rate. The mass of the sample information is then fed back into a computer, where it is plotted on a graph with the temperature information. An inert gas such as argon or a reactive gas can be used. The technique can quantify the loss of water or solvent, decarboxylation, pyrolysis, and many other applications (Perkin Elmer, 2015).

The TGA used for all experiments was a TA instrument SDT Q600, pictured in Figure 2.5.



Figure 2. 5: Image showing the TA instruments SDT Q600.

2.2.4: Fourier-transform infrared spectroscopy (FTIR)

Fourier Transform infrared spectroscopy is a fast and non-destructive characterisation technique that can identify different compounds, components, or a mixture. It is widely used for the identification of organics in organic synthesis or the identification of polymers. It uses the principle that when infrared (IR) radiation passes through a sample, some radiation is absorbed, and some interacts with the sample and is transmitted. This causes a unique infrared spectrum to be recorded, enabling the identification of the components of the sample.

The equipment used to analyse samples in the functionalisation experiments was a Thermo Scientific Nicolet iS10 FT-IR-ATR Spectrometer, pictured in Figure 2.6.

At the start of all testing with the FTIR, it was cleaned with isopropanol to ensure any previous samples were removed from the sample stage. A background scan was then taken to ensure that any spectra from the environment could be eliminated. The software was set to subtract the background spectrum from any measured spectrum automatically. All spectrums were recorded with a scan speed of 64 and a resolution of 4. All the spectrums were also recorded in transmittance mode. The spectrums and their components were then exported and identified using spectra from the literature (Merck, 2022).



Figure 2. 6: Image showing the Thermo Scientific Nicolet iS10 FT-IR-ATR Spectrometer used for all samples.

2.2.5: Brunauer–Emmett–Teller (BET) Gas Sorption

Brunauer–Emmett–Teller (BET) gas adsorption analysis can be used to measure the specific surface area of a sample and the pore size distribution of a powder sample. BET theory was first proposed in 1938 by Stephen Brunauer, Paul Hugh Emmett, and Edward Teller, who proposed equation 2.2, which can be used to determine the number of atoms of gas it would take to form a monolayer, X_m , of gas across the whole surface. The monolayer the adsorbate gas forms are well illustrated in Figure 2.7. P/P_0 is the relative pressure at the time of measurement, and C is related to the heat of adsorption. The equation describes the linear graph plot shown in Figure 2.8. As specific surface area is calculated from the first monolayer of gas, the first 5 points of a BET isotherm are typically used. From the linear plot of the first 5 data points, the slope and intercept can be calculated from this information and put into equation 2.3, which can be used to calculate the specific surface area of the sample. CSA is the cross-sectional area of the adsorbate, typically Nitrogen, in most experiments (Anton Paar, 2021; Brunauer et al., 1938).

$$\frac{1}{X[(P_0/P) - 1]} = \frac{1}{X_m C} + \frac{C - 1}{X_m C} \left(\frac{P}{P_0}\right) \quad (2.2)$$

$$SA = \frac{1}{\text{slope} + \text{intercept}} \cdot CSA \quad (2.3)$$

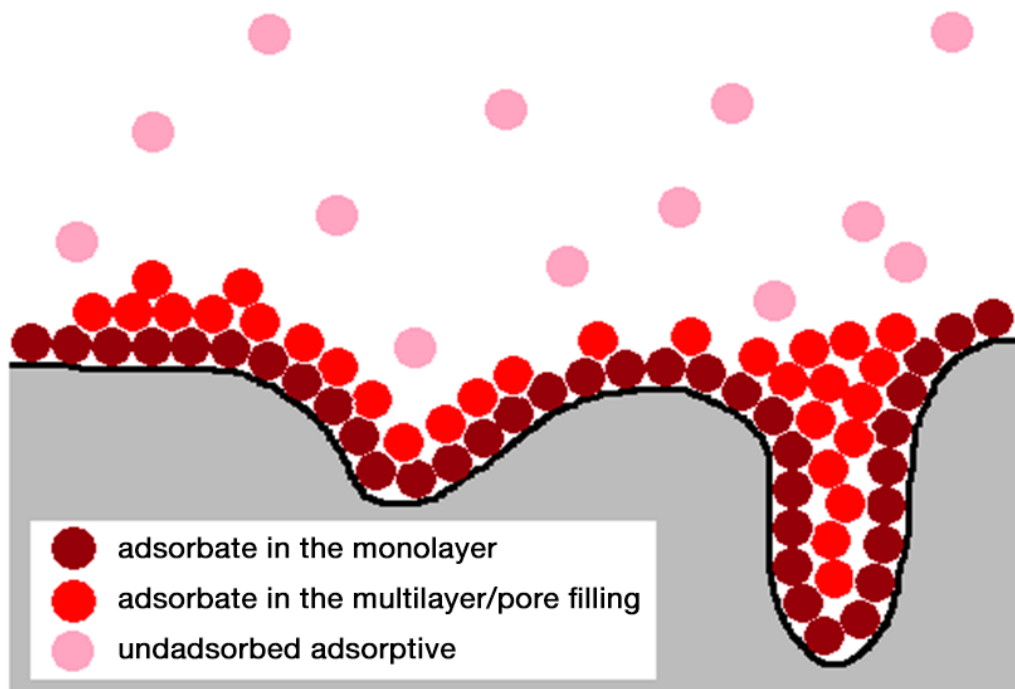


Figure 2. 7: Image showing how the adsorbate forms a monolayer on the sample surface (Anton Paar, 2021).

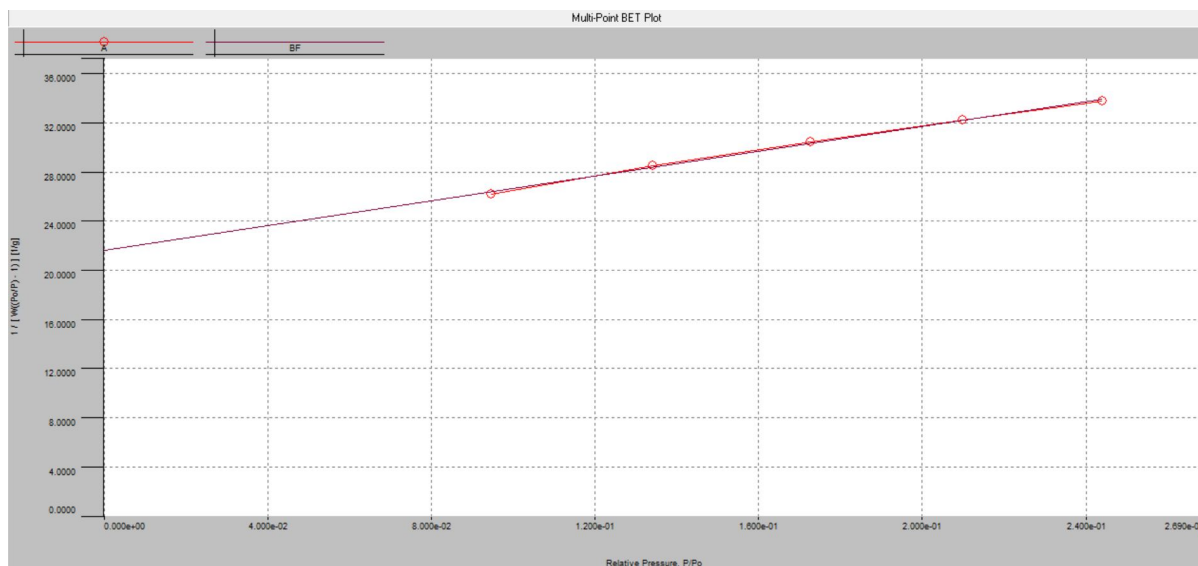


Figure 2. 8: Image showing a typical BET plot to work out the specific surface area of a sample.

The equipment used in my thesis was a Quantachrome NOVA 2000e Surface area and a Pore Size analyser. The equipment is pictured in Figure 2.9. It was used in helium mode, and Nitrogen was always used as the adsorbate gas. The analysis was always performed at 77 K.

The glass sample tube with a lid is first weighed, and the mass is noted down. The sample is then added to the sample tube, and the sample, sample tube and lid are weighed. As the samples were all steelmaking slag, around 22 g was always added to the sample tube for consistency. The amount of sample to add depends on the sample density, as the experiment can be hindered if too much or too little sample is added. The technique then works by first degassing a sample which is effectively a cleaning process for the sample, which can remove any dust, for example, or other contaminants that may cause a false surface area value to be given. The glass sample tubes are attached to the machine in the degassing side and put under a vacuum. Heating pockets are then added to aid the removal of contaminants. The samples were all degassed overnight at 120 °C. The criteria for choosing a temperature is to choose a temperature that the sample is stable at and will not alter anything about the sample. Once the degassing process is completed, the sample tube, sample, and lid are re-weighed to check that the degassing process has succeeded. Typically, the sample should decrease in mass due to the removal of contaminants. These weights can then be used to calculate the degassed sample weight. This information is put into the Quantachrome Novawin software. The sample tube can then be attached to the analysis side of the machine, and a dewar of liquid Nitrogen is added underneath. The liquid Nitrogen cools the sample down to the nitrogen boiling temperature of 77 K. If carbon dioxide is used as the adsorbate gas, then an ice bath is typically used. The analysis can then be started, and the sample tube is put under a vacuum. The first stage of the analysis involves helium gas going into the sample tube, which is used to measure the volume of the sample tube that does not have the sample in. After this stage, the sample tube is put back under vacuum, and the nitrogen adsorbate gas goes in to measure the specific surface area of the sample. The Novawin software has the BET equations built into the software, so it automatically calculates the specific surface area of the sample.



Figure 2. 9: Image showing the Quantachrome Nova 2000e Surface Area and Pore Size Analyser.

Chapter 3: Experimental CO₂
Sequestration Trials using Basic
Oxygen Steelmaking Slag

The work that follows has previously been published in a scientific paper that was published in the Lidsen publishing Journal 'Recent Progress in Materials'. The paper was published on 16th July 2021 (Fisher & Barron, 2021).

3.1: Introduction

The worst environmental consequences of the steelmaking industry are the CO₂ emissions from production. In 2020, for example, 1.89 tonnes of CO₂ was released into the atmosphere for every tonne of steel produced worldwide. This represents between 7-9 % of global anthropogenic CO₂ emissions. There is, therefore, a tremendous amount of pressure on the steelmaking industry to change its processes and lower its overall emissions. The two key ways that the steel industry can achieve this are to lower the overall emissions of steel production and to increase the amount of sinks they have for their emissions. In order to reach the targets set out by the Paris Agreement in 2015, both of these strategies must be adopted by the steel industry. The Paris Agreement is an international treaty set out by the United Nations to combat climate change. The treaty states that the global temperature must not exceed 2 °C above pre-industrial levels (World Steel Association, 2021). As of 2022, the UK was ranked the 27th most significant steel producer in the world and produced 6.1 Mt. This is a relatively small number compared to China's production, which produced 1013 Mt. Worldwide, 1878.5 Mt were produced in 2022 (World Steel Association, 2023).

One way sinks can be implemented into the steelmaking industry is through carbon capture technologies. As Fisher and Barron previously mentioned, much promising research surrounds how slag can be used to capture CO₂ due to its favourable calcium silicate composition. It is not just fresh slag that can be utilised for this purpose, legacy slag that has been landfilled can also alleviate carbon emissions (Fisher & Barron, 2019). Since 1875, between 490 and 640 million tonnes of slag have been generated within the UK. Much of this has been reused in applications such as roads and construction (Riley et al., 2020). However, Branca et al., estimates that 9% of these slags are internally stored, and around 14% are landfilled (T. A. Branca et al., 2020). Therefore, a large reserve of material can be utilised for carbon capture within different steel businesses. Riley et al., looked at the various slag landfill deposits throughout the UK. They estimated that through a direct carbonation method, there was the potential to sequester 296-337 kg CO₂/t of slag (Riley et al., 2020).

At the time of designing the experiments in this thesis, no experimental data could be found surrounding the CO₂ sequestration of slag produced by UK steel makers. As explained previously, CO₂ sequestration is a valuable strategy to combat the emissions that the UK steel industry produces; therefore, assessing the capacity of BOS slag to capture CO₂ is an important step. The following study aims to characterise 3 different samples of steelmaking slag from Tata Steel to assess if they would be suitable for further study in carbon sequestration applications.

3.2: Materials and Methods

3.2.1: Slag

Three different samples of basic oxygen steelmaking (BOS) slag were used in the study, and were collected from Tata Steel, Port Talbot, South Wales, SA13 2NG. On site BOS slag is sorted into two regimes using vibrating screens (45 mm and 5-10 mm) before being stored as piles. The measurement in the slag description refers to the average diameter of a piece of slag. Samples were taken from two piles of 45 mm slag (Samples A and B) and a sample was taken from the 5-10 mm pile (Sample C). The slag is officially designated as a waste product in the Tata Steel environmental permit (Natural Resources Wales, 2012).

3.2.2: Slag sample crushing

The slag sample to be crushed was placed into a low-density polyethylene (LDPE) plastic bag with a zip closure. The bag was then placed inside another LDPE bag, and this process was repeated 5 times. The bags were used to make sure that parts of the slag sample did not get propelled out of the crushing area. The bags were then placed on a piece of cardboard and then placed on a wooden workbench. The cardboard was used to prevent damage to the wooden workbench. A 0.45 kg hammer was then used to crush the slag sample. Once enough pieces of slag had been broken off in a smaller size fraction, they were placed into a pestle and mortar to be crushed into a powder suitable for CO₂ sequestration analysis.

3.2.3: Characterization

Thermogravimetric analysis (TGA) was performed using a TA Instruments SDT Q600. For each analysis, the sample was heated up to 700 °C to decompose the sample under argon and release any CO₂ that had previously been absorbed during storage. The TGA instrument was then allowed to cool to room temperature, and the sample was then exposed to wet CO₂ at a flow rate of 80 mL/min for 4 hours. Wet CO₂ has previously been observed to maximize CO₂ uptake for oxide mixtures (Lupu et al., 2006, 2007). Wet CO₂ was produced by bubbling CO₂ through a glass bubbler filled with distilled water. The sample was then heated to 100 °C and held for 5 minutes to remove any mass gain that may have been caused by water in the wet CO₂ flow. An accurate representation of the amount of CO₂ absorbed could be acquired. CO₂ gas sorption analysis was completed using a Quantachrome iSorb HP1 high-pressure gas sorption analyzer. Before analysis, each sample was degassed under vacuum for 4 hours at 180 °C. Each CO₂ isotherm was conducted at 83 °C to maximize CO₂ uptake (Polettini et al., 2016). For each CO₂ isotherm, 19 data points were collected from 0 to 10 bar.

3.3: Results and Discussion

Table 3. 1: The CO₂ adsorption capacity (mmol/g) of basic oxygen steelmaking (BOS) slag determined by thermogravimetric analysis (TGA) and gas adsorption using iSorb.

	CO ₂ Adsorption Capacity (mmol/g)		
	Sample A	Sample B	Sample C
TGA (1 bar)	0.077	0.139	0.264
iSorb (1 bar)	0.016	0.005	0.016
iSorb (10 bar)	0.041	0.034	0.034

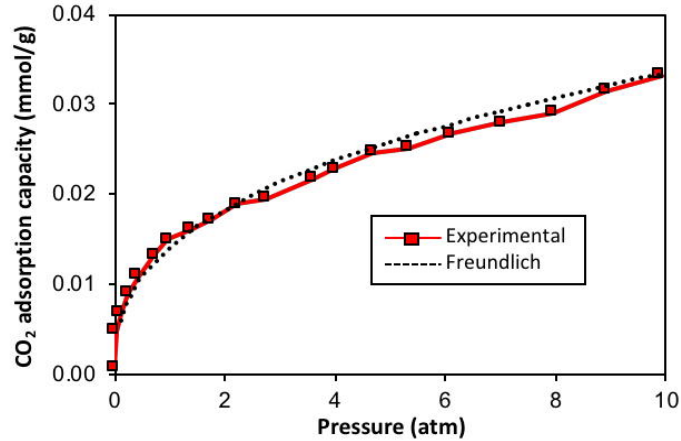


Figure 3. 1: iSorb plot of dry CO₂ adsorption capacity (mmol_{CO₂}/g) of sample C as a function of CO₂ pressure (atmosphere).

The resulting uptakes is summarized in Table 3.1 and representative plots are shown in Figure 3.1 and 3.2.

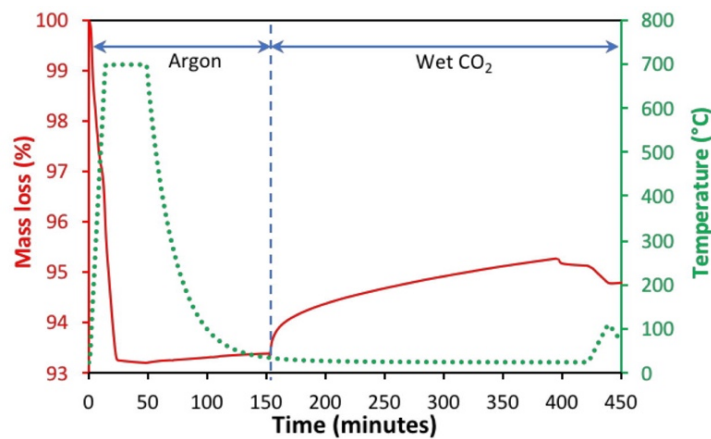


Figure 3. 2: TGA plot showing mass loss (%) as a function of temperature (°C) plotted against time (minutes) in sample C.

As noted above the presence of CaO and MgO in the slag samples offers potential of CO₂ capture/sequestration. The uptake measured with dry CO₂ on the as received slag samples are shown in Table 3.1. The data for the pressure dependent adsorption may be fitted successfully with the Freundlich isotherm as defined by Equation 1, where Q_e (mmol/g) is the capacity of adsorption of CO₂ by the adsorbents, K_f is the Freundlich isotherm constant (mmol/g.atm^{1/n}), and n is the heterogeneity factor that represents the deviation of the linearity of the adsorption.

$$Q_e = K_f (P_{CO_2})^{1/n} \quad (1)$$

Figure 3.3 shows an example of the plot of $\log(Q_e)$ versus $\log(P_{CO_2})$ from which the Freundlich isotherm constant (K_f) and heterogeneity factor (n) is obtained. A similar analysis of each of the data is summarized in Table 3.2. When the value of n is between 2 and 10 the adsorbent is considered to have a high adsorption capacity (Brdar et al., 2012). The Freundlich model is used for systems with a high degree of heterogeneity, where it is assumed that there is an exponential decrease in energy as the coverage of the surface occurs (Barka et al., 2013; Freundlich, 1907).

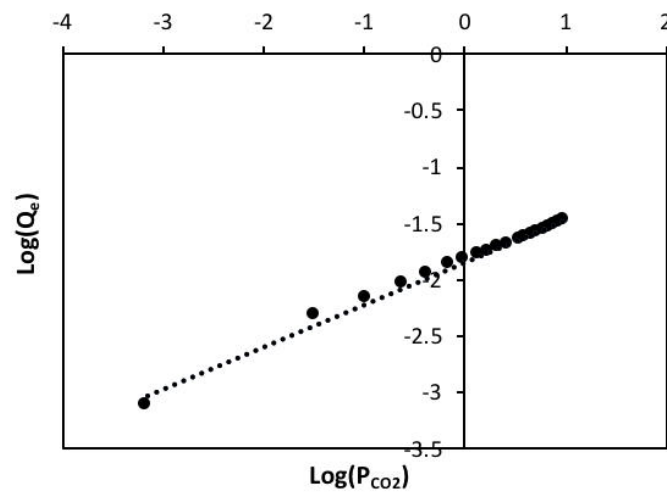


Figure 3. 3: plot of $\log(Q_e)$ versus $\log(P_{CO_2})$ for dry CO_2 adsorption by sample C ($R^2 = 0.991$).

Table 3. 2: Calculated Freundlich isotherm constant (K_f) and heterogeneity factor (n) for dry CO_2 adsorption of basic oxygen steelmaking (BOS) slag determined by gas adsorption.

	Sample A	Sample B	Sample C
K_f (mmol/g.atm ^{1/n})	0.0154	0.00367	0.0141
n	2.206	2.286	2.668
R^2	0.995	0.989	0.991

It has been shown in several previous studies that the amount of CO_2 captured when using wet CO_2 is significantly more than dry CO_2 (Lupu et al., 2006, 2007; Reddy et al., 2019; Sarperi et al., 2014). The moisture in the wet CO_2 gas stream allows soluble calcium from phases such as CaO , Ca_2SiO_4 , and Ca_3SiO_5 to dissolve and create calcium ions, which react with the

carbonate ions (formed upon CO₂ dissolution) to form CaCO₃ (Yilmaz et al., 2013). As such the uptake of wet CO₂ is significantly higher in all samples than dry CO₂ (Table 3.1). Therefore, as the iSorb analysis does not use wet CO₂ and instead uses dry CO₂ it did not perform as well as the TGA adsorption. Sample C was seen to absorb the most CO₂ during the wet CO₂ TGA experiment. When Sample C underwent ICP-OES and XRF compositional analysis previously it was found to have a higher concentration of Ca and Si than Samples A and B.

3.4: Conclusions

This chapter presents the CO₂ sequestration ability of BOS steelmaking slag produced at a UK steelmaking plant, Tata Steel. The experiments proved that BOS slag produced at UK steel plants would suit CO₂ sequestration applications. Sample C had the best performance in both the wet and dry CO₂ sequestration scenarios. When the dry CO₂ experiments data was fitted to the Freundlich isotherm model, all 3 samples obtained an n factor that reflected a high adsorption value, with Sample C achieving the highest value of 2.668. The CO₂ sequestration performance across all 3 samples, when wet CO₂ was utilised, was far superior to dry CO₂, with Sample C performing best.

Therefore, this suggests that the BOS slag from UK steel plants would be suitable to be reutilised in CO₂ sequestration applications, helping UK steel producers alleviate some of the environmental burdens they cause.

Chapter 4: Nutrient Leaching

Experiment

4.1: Introduction

As previously mentioned, there is immense pressure on the steel industry to reduce its emissions to alleviate climate change's effect. A simple way to categorise the emissions produced by the steel industry is to use the method of Scope 1,2 and 3 emissions set by the Greenhouse Gas Protocol (GHG). The greenhouse gas protocol is a standard that allows all businesses to categorise their emissions following a specific framework. Scope 1 emissions are described as direct emissions from sources owned or controlled by a company. Scope 2 emissions are described as indirect emissions from the company's operation, e.g., emissions from the production of electricity used within the business. Finally, scope 3 emissions are not produced by the company but by products or services in its value chain. For example, emissions from the purchasing, using and then disposing of specific products are accounted for in scope 3 emissions (Todeschini, 2017).

As mentioned in Chapter 3, the steelmaking process, including coal burning, releases many emissions into the atmosphere. These can be categorised as Scope 1 emissions under the Greenhouse gas protocol. Scope 2 emissions for the steelmaking industry will come from the energy it purchases to power all of the steelmaking processes, e.g. the heating of furnaces and operation of hot, cold and finishing lines. Scope 3 emissions can be categorised as any other emissions associated with the operation of the steelmaking plant, e.g. the production of raw materials and consumables.

The Swansea Tidal Lagoon project was a proposed tidal lagoon project in South Wales that would have been constructed in Swansea Bay. The lagoon was intended to house several water turbines that could produce between 0.25-3.1 GWh of electricity per day (Todeschini, 2017). If this project were to go ahead, it would greatly help to alleviate the scope 2 emissions from the Tata Steel steelmaking process in South Wales, as the tidal lagoon would be producing electricity with much lower emissions. However, many raw materials are required to produce the tidal lagoon, such as building and construction materials. As steelmaking slag is a waste material from the steelmaking process, it is valuable to assess the effect that steelmaking slag can have on a marine environment. So, to do this, an experiment was designed to look at what effect steelmaking slag would have on seawater and what effect the seawater would have on the steelmaking slag. As steelmaking slag contains potentially harmful metals, e.g., chromium

and nickel, the risk of these metals leaching out had to be assessed (D. Gao et al., 2020; Manso et al., 2006; Motz & Geiseler, 2001; Yi et al., 2012). If these metals were to leach out, there would be a high risk of environmental damage. As the ocean's tides can also be powerful and cause high amounts of erosion, an accelerated leaching experiment was performed in which the slag samples were agitated to assess their leaching potential when exposed to water motion.

4.2: Methodology and Materials

The methodology for the experiment was adapted from the British Standard BS EN 12457-1:2002, which outlines a leaching compliance test for granular waste materials and sludges (Technical Committee, 2002). The standard describes a one-stage batch test in which a liquid-to-solid ratio of 2 L/kg and the particle size is below 4 mm. However, the project aimed to investigate an application for steelmaking slag with minimal processing cost. The slag samples were larger than 4 mm as received, so the guidance that the slag samples should be smaller than 4 mm was not used as this would mean crushing them and adding to the processing cost. Which in the real world scenario at the steel plant it would not be feasible or cost effective to crush the samples so they were used as-received. On average, the samples received were 45 mm in diameter.

Two separate experiments were performed for the slag to assess its leaching behaviour. One experiment lasted 12 months, in which the slag was not agitated at all, as this was not feasible for 12 months. The other experiment was done over 24 hours in which the slag was agitated using a mechanical stirrer to simulate ocean conditions over 24 hours.

A model seawater solution was used so the experiments could be easily replicated. This was instead of collecting seawater from Swansea Bay, for example, where the seawater nutrient concentration could be highly variable. The standard ASTM D 1141 was chosen to make the model seawater, as this was used in a similar research paper (ASTM International, 2003; Shi et al., 2019).

The jars were numbered as follows:

1. 5-10mm LF BOS Slag (C)
2. 45mm HF BOS Slag (A)

3. 45mm LF BOS Slag (B)
4. 0-10mm LF BOS Slag (D)

4.2.1: Methodology to produce model seawater

All salts, in their quantities seen below in Table 4.1., were measured using an analytical balance.

Table 4. 1: Table of the concentration of salts used in the production of model sea water (ASTM International, 2003).

Compound	Concentration (g/L)
Sodium Chloride (NaCl)	24.53
Magnesium Chloride (MgCl ₂)	5.20
Sodium Sulfate (Na ₂ SO ₄)	4.09
Calcium Chloride (CaCl ₂)	1.16
Potassium Chloride (KCl)	0.695
Sodium Bicarbonate (NaHCO ₃)	0.201
Potassium Bromide (KBr)	0.101
Boric acid (H ₃ BO ₃)	0.027
Strontium Chloride (SrCl ₂)	0.025
Sodium Fluoride (NaF)	0.003

They were then all added into a beaker containing 1 litre of laboratory-grade distilled water (Type 2, 15 MΩ.cm). This was then magnetically stirred in a beaker in a fume hood with no heat applied until all salts had been dissolved. After the salts had been dissolved into the solution, the pH of the solution was measured using a Mettler Toledo FiveGo portable pH meter with a lab pH electrode LE438. The pH of the solution was then adjusted to pH 8.2 using a 0.1 M sodium hydroxide (NaOH) solution. The solution was then transferred into a glass storage bottle with a tight lid for future use.

4.2.2: Methodology for Nutrient Leaching Experiments

4 litres of model seawater were produced using the previously mentioned method. The 4 litres of model seawater were then distributed between 4 separate glass jars labelled 1, 2, 3, and 4,

each containing samples A, B, C, and D. 1 litre of seawater was placed in each jar. For Samples A, B, and C, 12 pieces of slag were randomly selected from the sample containers received from Tata Steel. 12 pieces of slag were selected from each category. Each piece of slag was weighed in order to find the average weight of the pieces for each category. Table 4.2 below lists the average weight of the samples.

Table 4. 2: Table showing the average weight of Samples A, B and C at the start of the experiment.

Sample	The average weight of the slag piece at T=0 (g)
A	30.23
B	72.74
C	20.75

As Sample D was a powder, it was not possible to collect individual pieces. So as Sample C was the most similar in composition, 20.75 g of Sample D was randomly selected for the experiment. Each jar was wrapped in tin foil and placed into a dark cupboard. This was done to simulate undersea conditions where there is no light. The experiment was run over 12 months. Each month the jars were unwrapped and photographed. The pH of the jar was measured. A 20 ml aliquot of water was removed each month, and this was diluted and analysed using microwave plasma atomic emission spectroscopy (MP-AES). As sample D could not be weighed due to the nature of the sample, surface area analysis was performed on the sample using Brunauer-Emmett-Teller (BET) surface area analysis.

4.2.3: Slag sample crushing

Due to the nature of BET analysis, the sample was required to be a homogenous powder. The method below details how this was carried out.

The slag sample to be crushed was placed inside several low-density polyethene (LDPE) plastic bags with zip closures. The bags were used to make sure the pieces of slag were contained when being crushed. The bags were placed onto a piece of cardboard to protect the surface below. A 16 oz hammer was used for crushing the slag in the bags. Once the sample was

suitably crushed, the sample was sieved using a 212 mm sieve to remove any large bits of slag that did not get crushed. The sample that remained after sieving was then crushed further into a homogenous powder using a pestle and mortar.

4.2.4: Accelerated Nutrient Leaching

One piece from samples A, B, C, and D was randomly selected. This experiment was completed in triplicate.

Table 4. 3: Table showing the average weight of Samples A, B, C and D at the start of the experiment.

Sample	The average weight of the slag piece at T=0 (g)		
	Trial 1	Trial 2	Trial 3
A	34.202	31.184	30.463
B	31.708	43.252	38.364
C	23.124	19.835	11.927
D	18.295	18.295	18.295

The 4 samples were weighed on an analytical balance before the experiment and then placed into a polypropylene beaker. The values are shown in Table 4.3 as sample D was the 0-10 mm LF BOS slag powder-like sample and most similar to Sample C. It was decided that the amount of sample used in the experiment was dictated by the average weight throughout the experiments of Sample C. A specified amount of model seawater was made using the aforementioned procedure in section 4.2.1 (ASTM International, 2003). This amount was calculated using the British standards publication PD CEN/TS 15862:2012, which suggests a liquid/ solid ratio of 12 cm³.cm⁻². A rough calculation was made of the sample volume so the correct ratio of model seawater to add could then be calculated (British Standards Institution, 2012). An overhead mechanical stirrer was used due to the magnetic nature of the samples. This was set to 400 rpm, and the experiment was left stirring for 24 hours. The experiment was also wrapped in tin foil to be compared to the year-long nutrient leaching experiment. The foil ensured that no light was allowed in. After 24 hours, the pH of the solution was measured.. A 20 ml aliquot of the model sea water was taken for analysis. This sample was centrifuged,

diluted, and then analysed using MP-AES.

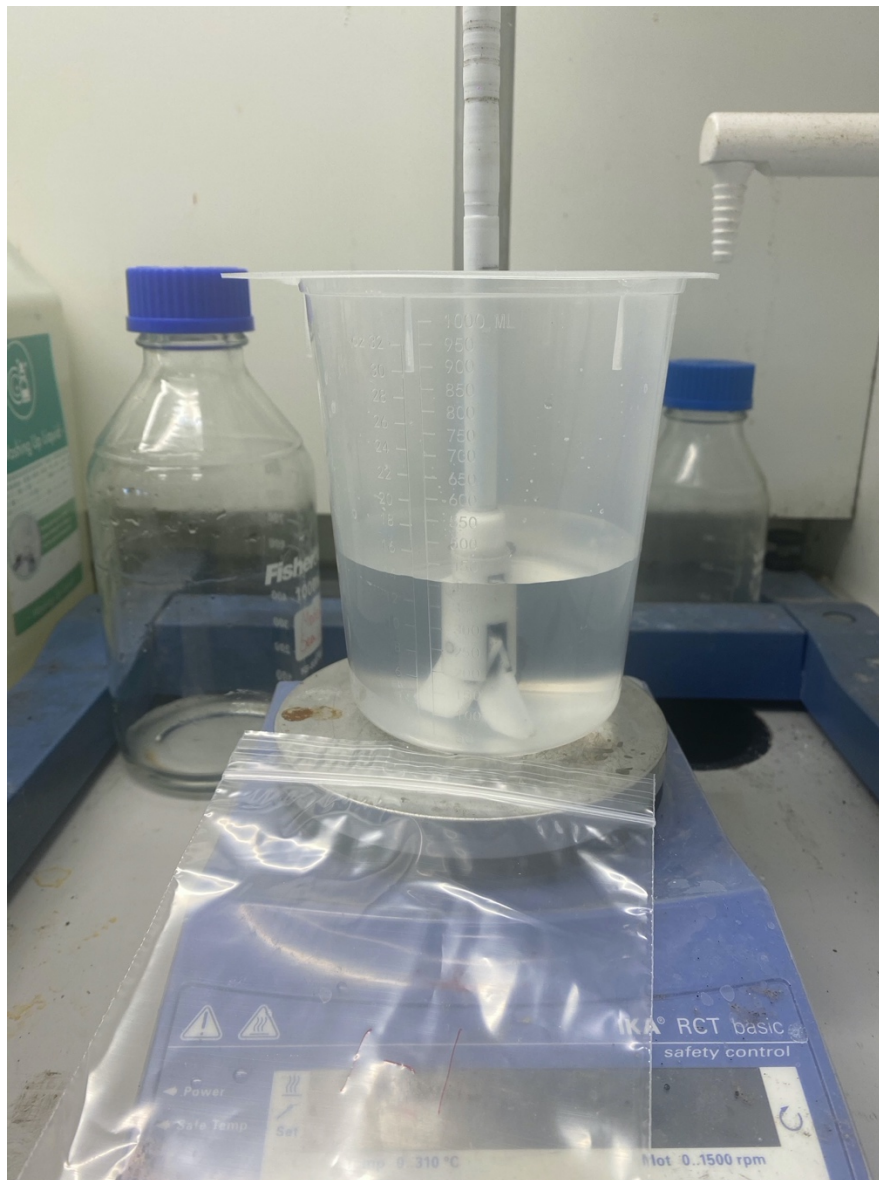
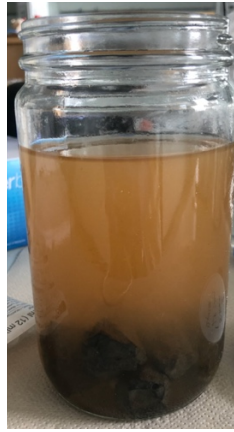


Figure 4. 1: Example of accelerated leaching experiment set up with overhead mechanical stirrer.

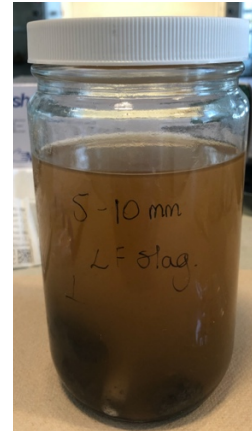
4.3: Results from Jar 1-5-10mm LF BOS Slag (C)



25/06/19



25/07/19



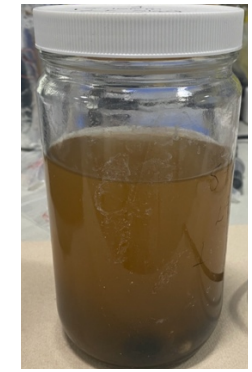
25/08/19



25/09/19



25/10/19



25/11/19



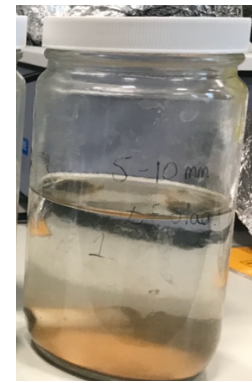
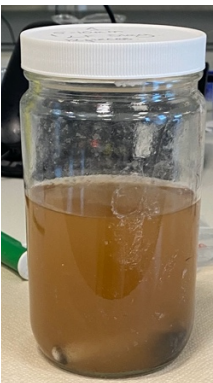
13/12/19



10/01/20



07/02/20



06/03/20

03/04/20

29/04/20

Figure 4. 2: Photographic images of Jar 1 from 25/06/19-29/04/2020

Figure 4.2 illustrates the colour change that occurred over the 12-month duration of the experiment. Over the first 3 months, the colour gets a deeper red/brown progressively. This suggests that the iron oxide, a known slag component, has leached out into the water. In the 2 images for the final 2 months of the experiment, the iron oxide appears to have settled on the bottom of the jar and is no longer suspended in the seawater solution.

4.3.1: Weight Change of Slag

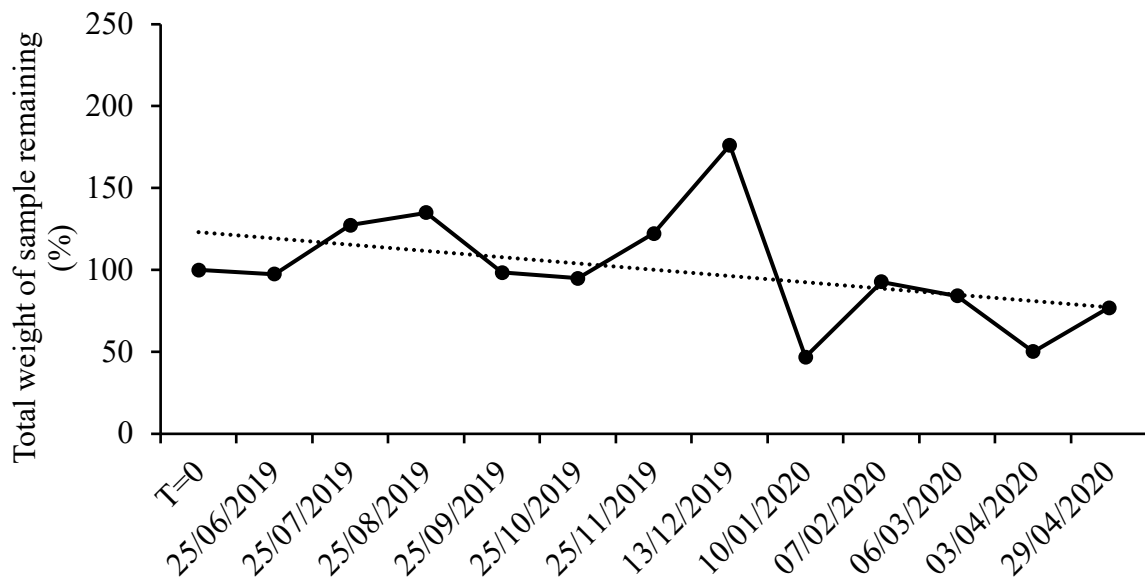


Figure 4. 3: Graph showing the weight of a solid slag sample from Jar 1 during the duration of the experiment with a trendline.

Figure 4.3 demonstrates the weight change by the slag throughout the experiment. The graph indicates the weight change, as each piece of slag had a different starting weight. The trendline in the graph shows that across the 12-month duration of the experiment, the weight showed a trend of decreasing. This suggests that the leaching of elements was occurring.

4.3.2: Microwave Plasma Atomic Emission Spectroscopy (MP-AES) of Model Sea Water

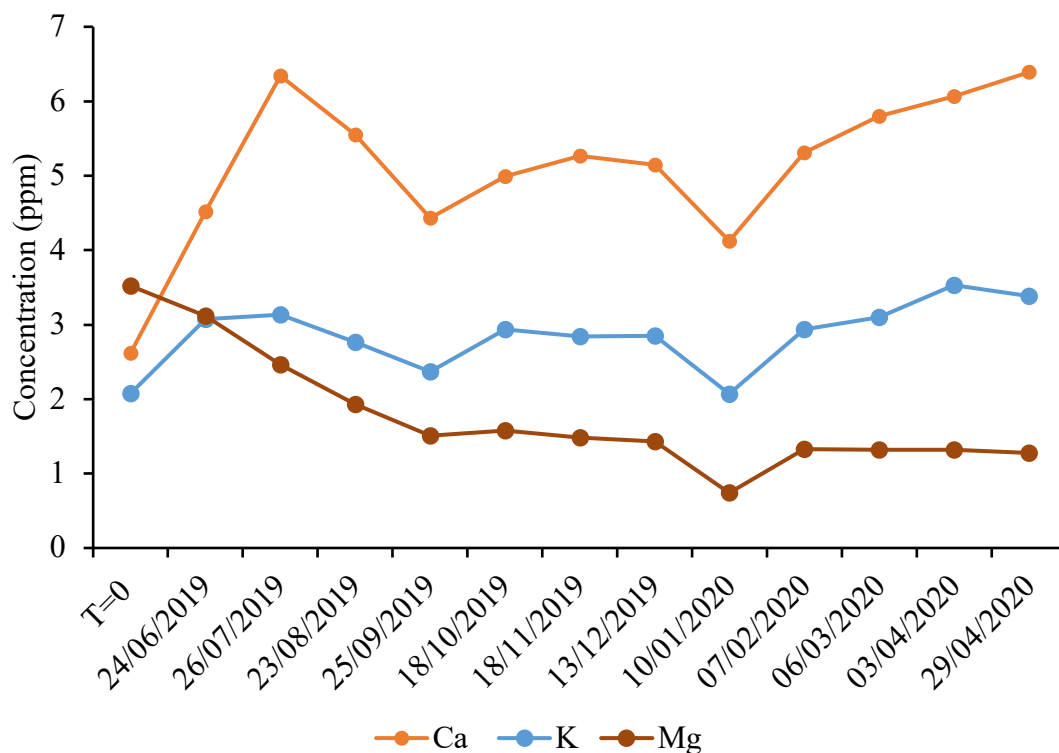


Figure 4. 4: Graph showing the change in Calcium (Ca), Potassium (K) and Magnesium (Mg) concentration in model sea water solution measured over 12 months in Jar 1.

Figure 4.4 shows how the concentration of Ca, K and Mg fluctuated over the 12 months of the experiment. Zinc (Zn), Iron (Fe), Copper (Cu), Manganese (Mn), Aluminium (Al) and Silicon (Si) concentrations were also measured over the 12 months; however, they were only present in trace amounts so that data appears in Appendix A in Table A.1. In Figure 4.2 it can be seen that the Ca concentration fluctuates, but overall it can be said that it increases over the 12 months. It increases from a starting value of 2.62 ppm to 6.39 ppm. K also acts similarly and increases from 2.08 ppm to 3.38 ppm, with some fluctuations. However, Mg decreased throughout the experiment from 3.52 ppm to 1.28 ppm.

4.3.3: pH Change of Model Sea Water in Jar 1

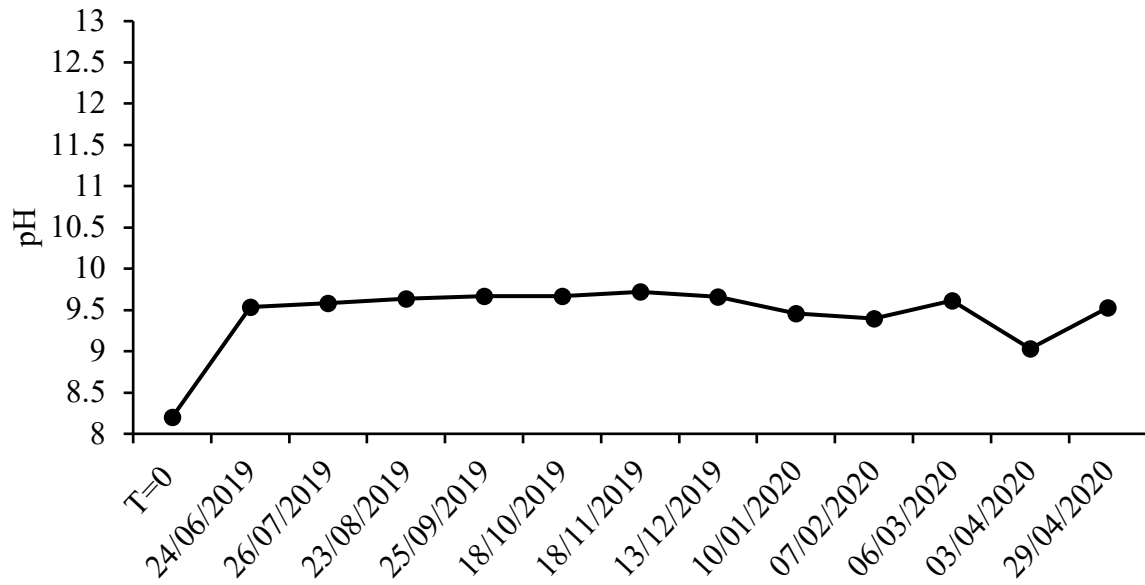
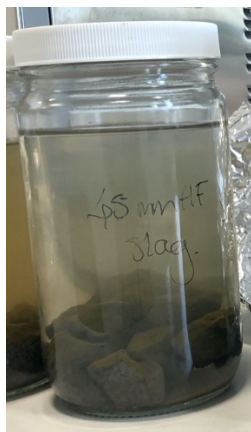


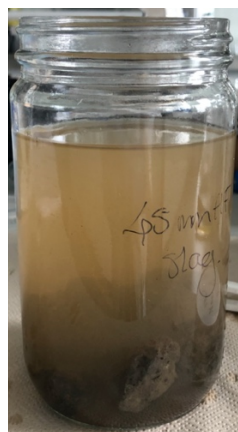
Figure 4. 5: Graph showing the pH change over 12 months for Jar 1: 5-10mm LF BOS slag.

There was an initial increase in pH from 8.2 to 9.54. The pH stayed around this level for 12 months with only slight fluctuations.

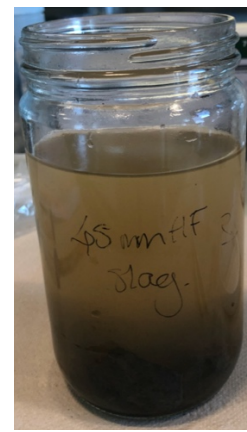
4.4: Results from Jar 2- 45mm HF BOS Slag (A)



25/06/19



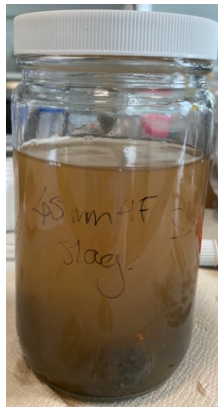
25/07/19



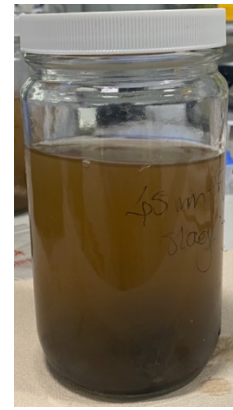
25/08/19



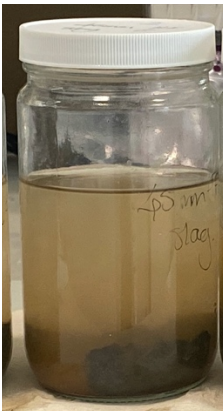
25/09/19



25/10/19



25/11/19



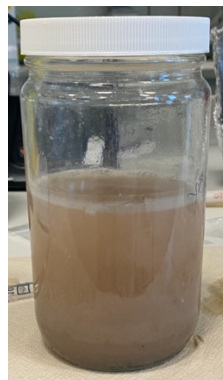
13/12/19



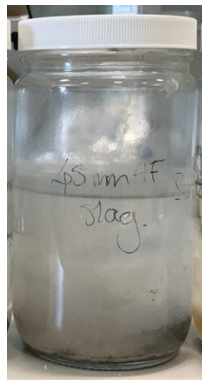
10/01/20



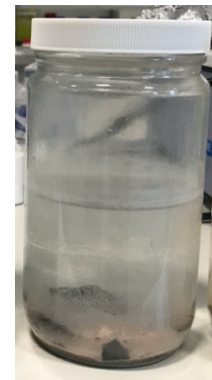
07/02/20



06/03/20



03/04/20



29/04/20

Figure 4. 6: Photographic images of Jar 2 from 25/06/19-29/04/2020.

Figure 4.6 shows the colour change over 12 months for Jar 2. There is a colour change between 25/6/19 and 25/7/19, suggesting more elements are being leached out. The model sea water seemed to get a progressively darker red throughout the experiment, like Jar 1, so it is most likely iron oxide leaching out and causing a red colour. The images of 7/02/20, 03/04.20 and 29/04/20 show a much lighter liquid appearance. This suggests that the iron oxide has been removed with each piece of slag. However, in these three images, red at the bottom of the jar

suggests the iron oxide has naturally separated and sunk to the bottom.

4.4.1: Weight Change of Slag

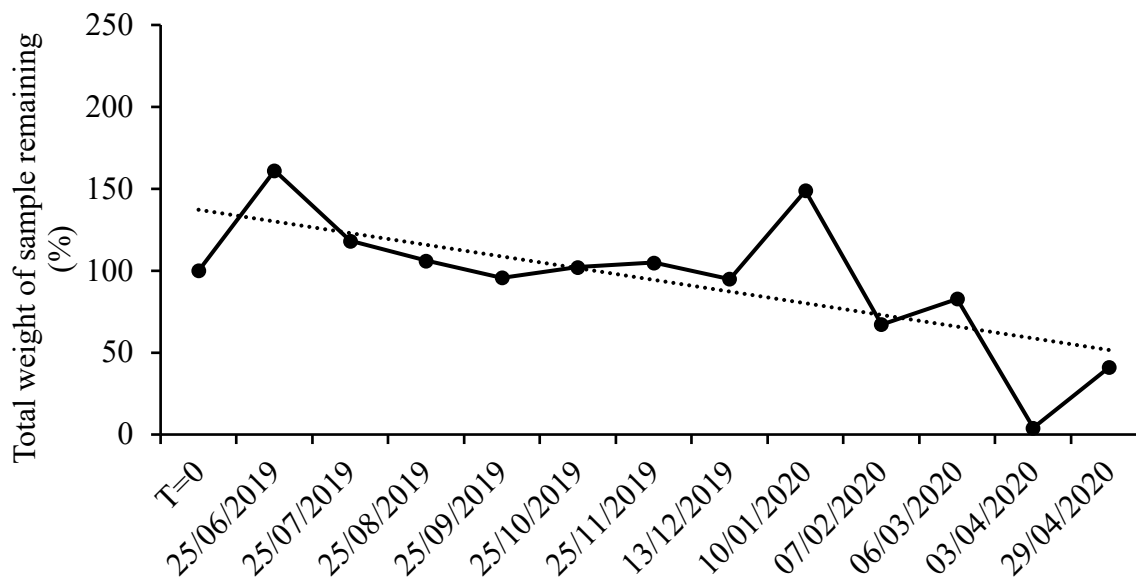


Figure 4. 7: Graph showing the weight of a solid slag sample from Jar 2 during the duration of the experiment with a trendline.

The graph in Figure 4.7 suggests that over the 12-month experiment, the slag samples decreased in weight, suggesting that elements of the slag were leaching out into the model seawater.

4.4.2: Microwave Plasma Atomic Emission Spectroscopy (MP-AES) of Model Sea Water

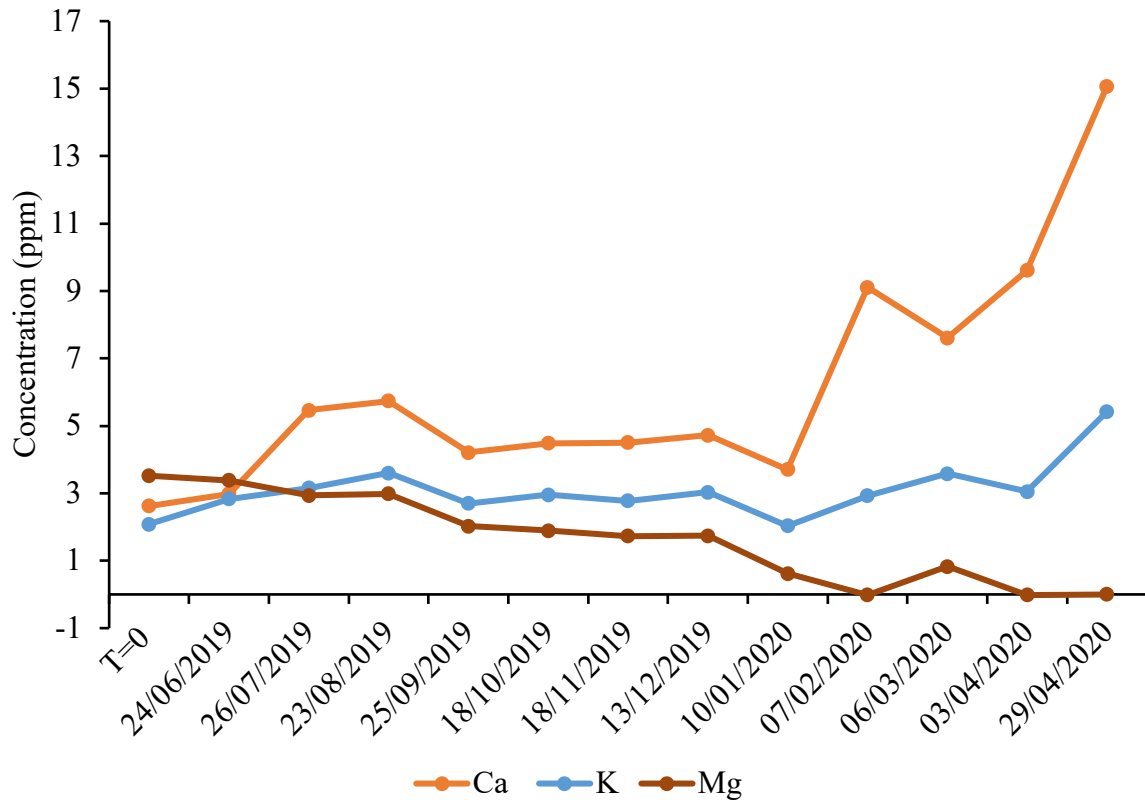


Figure 4. 8: Graph showing the change in Calcium (Ca), Potassium (K) and Magnesium (Mg) concentration in model sea water measured over 12 months in Jar 2.

Zinc (Zn), Iron (Fe), Copper (Cu), Manganese (Mn), Aluminium (Al) and Silicon (Si) concentrations were also measured over the 12 months; however they were only present in trace amounts so that data appears in Appendix A in Table A.2. Ca rises from 2.62 ppm to 15.07 ppm over the experiment, which is quite a dramatic rise. There is a significant increase in pH in months 10/01/2020 and 29/04/2020 suggesting the model sea water has broken the slag down enough to reach an area that perhaps has a large CaO or CaCO₃ concentration. K only rises from 2.08 ppm to 5.42 ppm, and Mg decreases from 3.52 ppm to 0 ppm.

4.4.3: pH Change of Model Sea Water in Jar 2

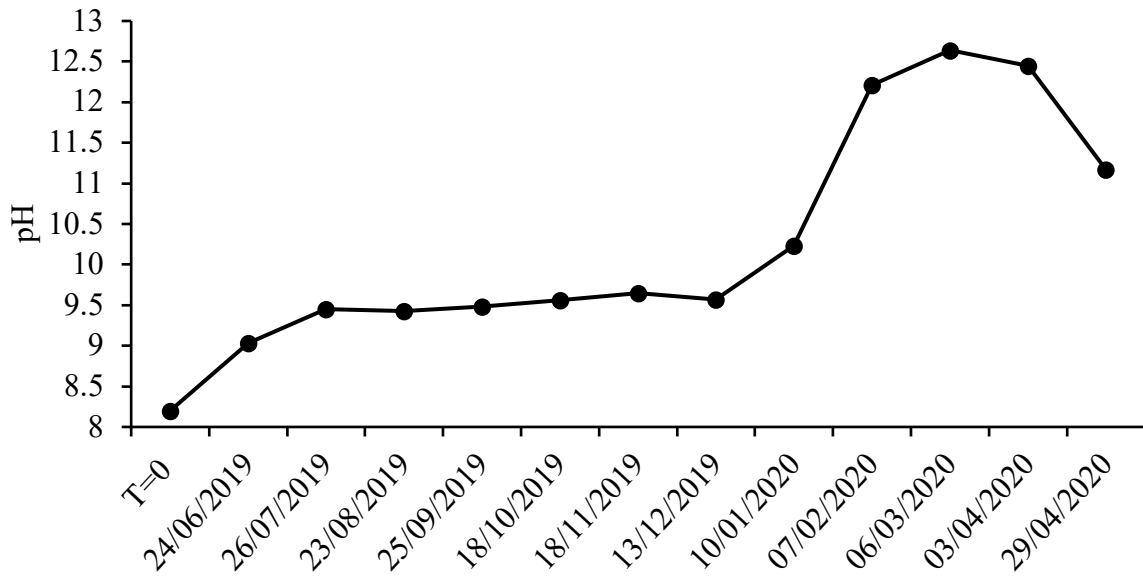


Figure 4. 9: Graph showing the pH change over 12 months for Jar 2: 45mm HF BOS slag.

There is a steady increase in the pH measurement over the 12 months from 8.2 to 11.17. There is a significant increase in the measurement taken on 10/01/20. This is similar to the Ca concentration increase that was seen in Figure 4.8, suggesting that the pH increase is due to a rise in Ca.

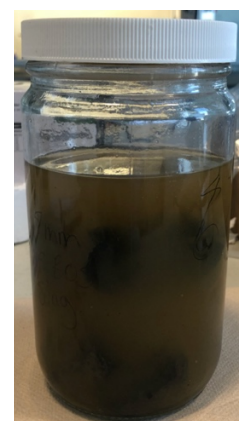
4.5: Results from Jar 3- 45mm LF BOS Slag (B)



25/06/19



25/07/19



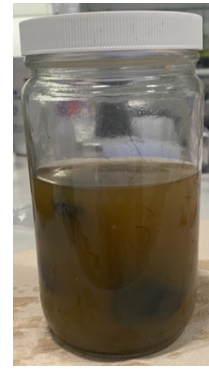
25/08/19



25/09/19



25/10/19



25/11/19



13/12/19



10/01/20



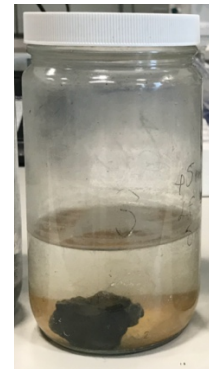
07/02/20



06/03/20



03/04/20



29/04/20

Figure 4. 10: Photographic images of Jar 3 from 25/06/19-29/04/2020.

From image 25/06/19 in Figure 4.9, it can be said that the slag has made the model seawater considerably darker over the first month. This is due to this grade of slag having much larger pieces than the last 2 jars. As more pieces of slag are removed over the 12 months, the colour gets progressively lighter, and more red iron oxide can be seen in the seawater. Again in the final 2 months, the iron oxide particles separated and sunk to the bottom of the jar.

4.5.1: Weight Change of Slag

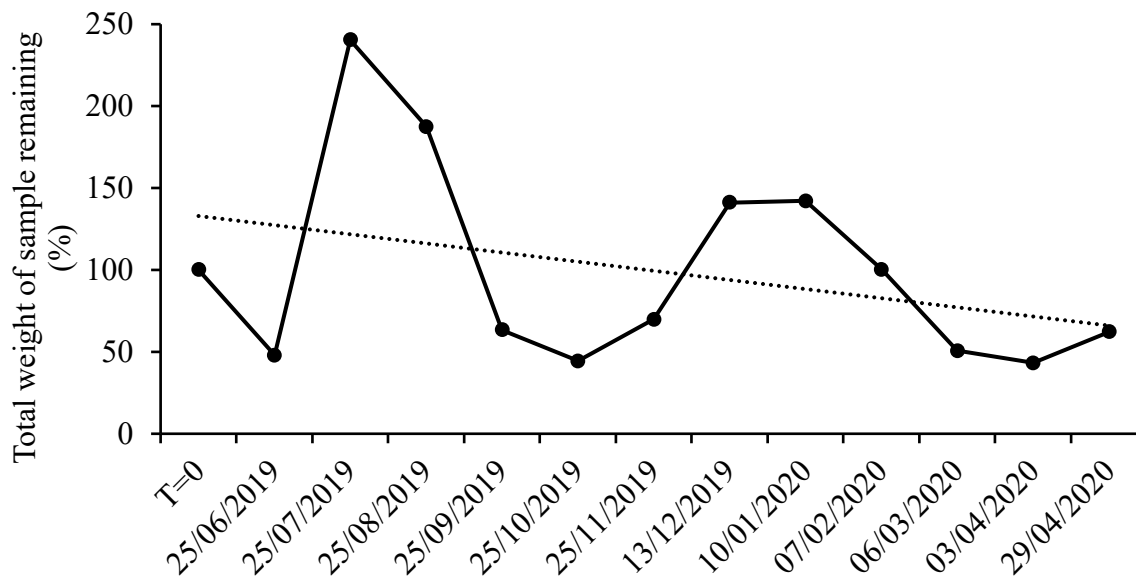


Figure 4. 11: Graph showing the weight of a solid slag sample from Jar 3 during the duration of the experiment with a trendline.

Figure 4.11 shows that the overall trend of the slag's weight generally trended downwards suggesting that elements were leaching out into the model sea water.

4.5.2: Microwave Plasma Atomic Emission Spectroscopy (MP-AES) of Model Sea Water

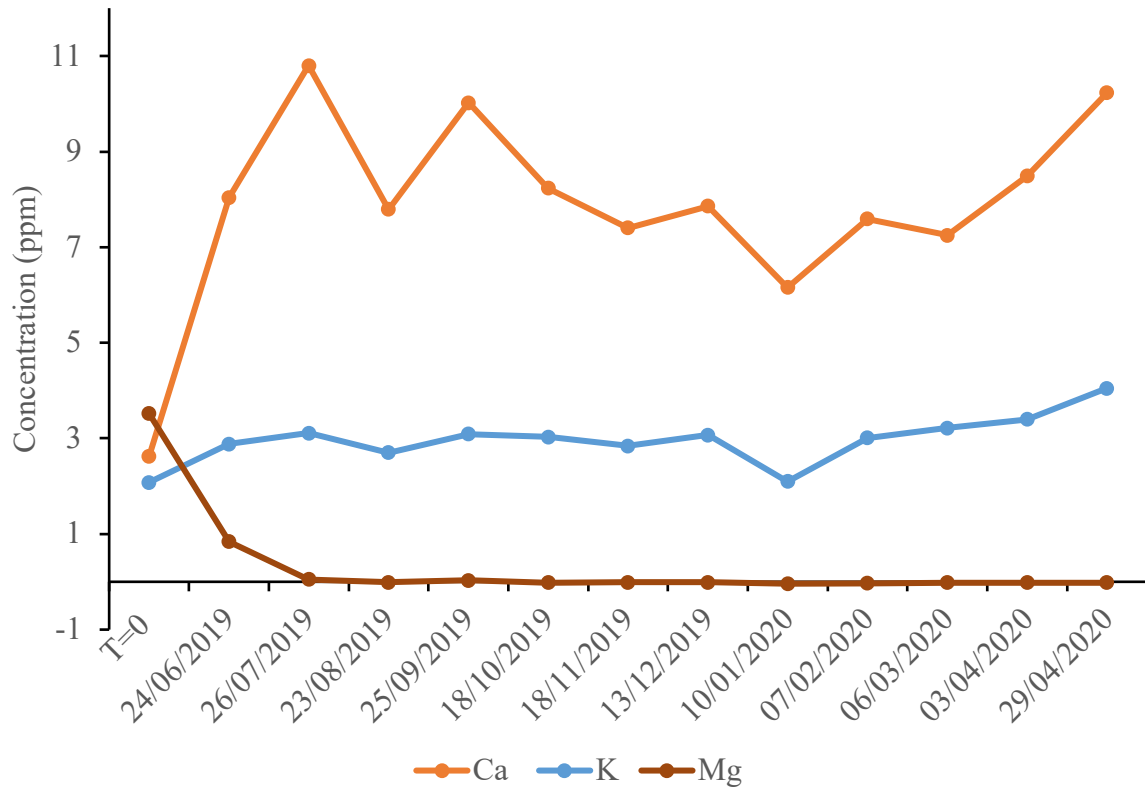


Figure 4. 12: Graph showing the change in Calcium (Ca), Potassium (K) and Magnesium (Mg) concentration in model sea water measured over 12 months in Jar 3.

Zinc (Zn), Iron (Fe), Copper (Cu), Manganese (Mn), Aluminium (Al) and Silicon (Si) concentrations were also measured over the 12 months; however, they were only present in trace amounts so that data appears in Appendix A in Table A.3. Figure 4.12 shows there were increases in both Ca and K concentrations, but the Mg concentration decreased. Ca increased from 2.62 ppm to 10.23 ppm with some fluctuations, but for the most part, it increased. K increased from 2.08 ppm to 4.05 ppm with slight fluctuation. Mg decreased from 3.52 ppm to -0.02 ppm.

4.5.3: pH Change of Model Sea Water in Jar 3

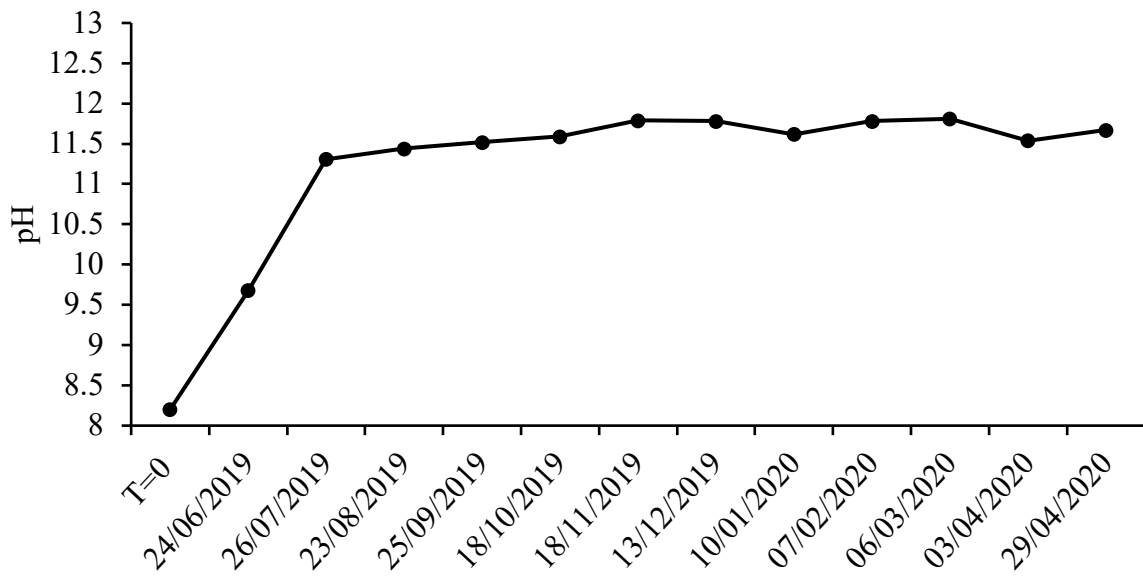
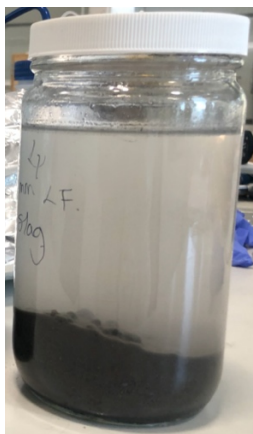


Figure 4. 13: Graph showing the pH change over 12 months for Jar 3: 45mm LF BOS slag.

Figure 4.12 shows that the pH increased over the first 2 months of the experiment and then plateaued at around 11.5. Overall the pH increased from 8.20 to 11.67 over the 12 months.

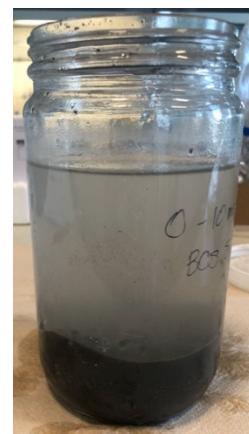
4.6: Results from Jar 4-0-10mm LF BOS Slag



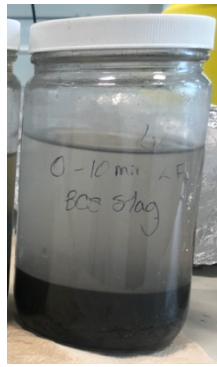
25/06/19



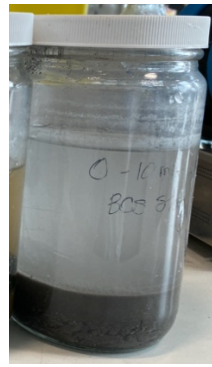
25/07/19



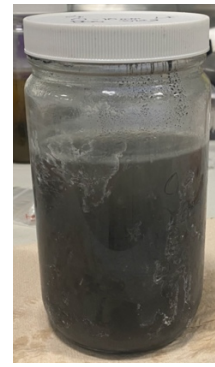
25/08/19



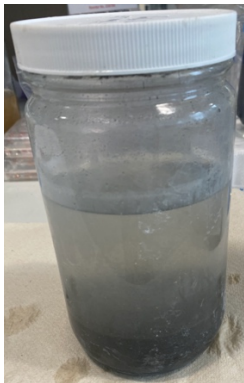
25/09/19



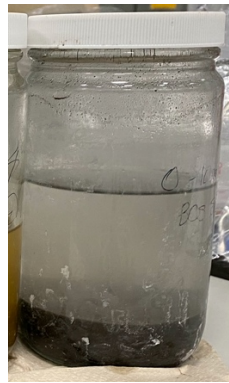
25/10/19



25/11/19



13/12/19



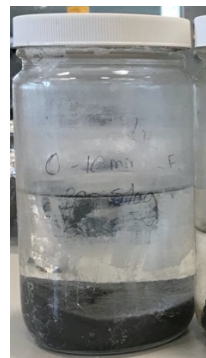
10/01/20



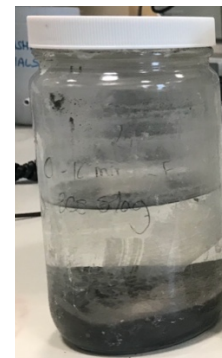
07/02/20



06/03/20



03/04/20



29/04/20

Figure 4. 14: Photographic images of Jar 4 from 25/06/19-29/04/2020.

Figure 4.14 shows that the model sea water in Jar 4 stayed a consistently clear colour throughout the experiment, with the slag consistently sitting on the bottom of the jar during the experiment.

4.6.1: Surface area change of slag

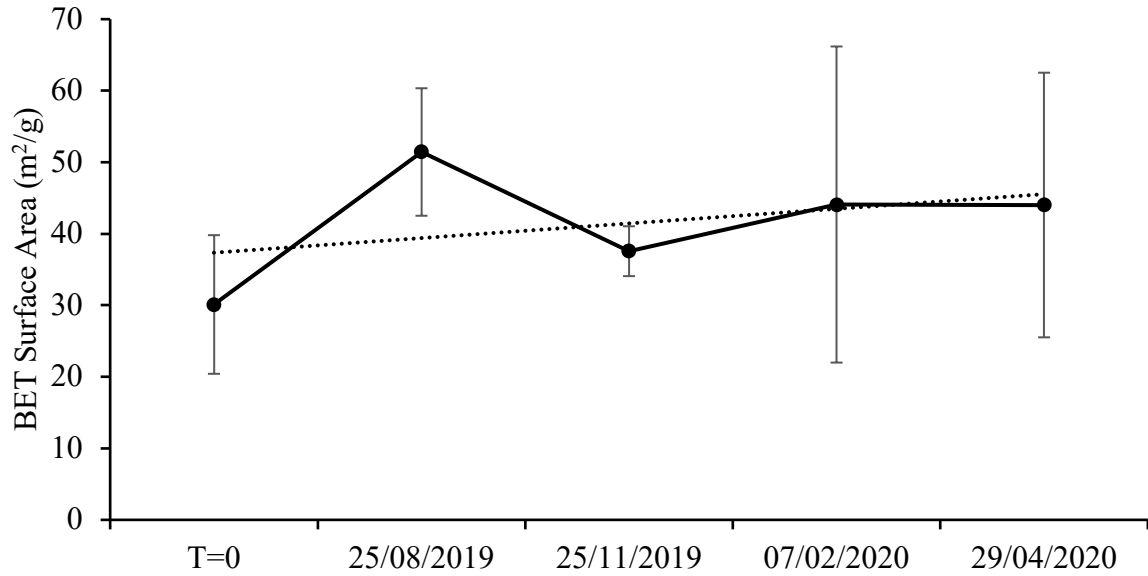


Figure 4. 15: Graph showing the change in the slag surface area from Jar 4 over the 12-month duration of the experiment. The standard deviation is shown by the error bars.

Due to sample 4 being a powder with particles of 0-10mm in diameter, BET surface area analysis was completed as an alternative to weighing the sample. The BET surface area shown is an average measurement taken from 3 different BET experiments of the same sample. The large error bars on the graph are due to the inhomogeneous nature of the samples tested. Figure 4.15 shows that the slag's surface area increased slightly across the 12-month experiment. The surface area increased from 30.11 m²/g to 44.02 m²/g.

4.6.2: Microwave Plasma Atomic Emission Spectroscopy (MP-AES) of Model Sea Water

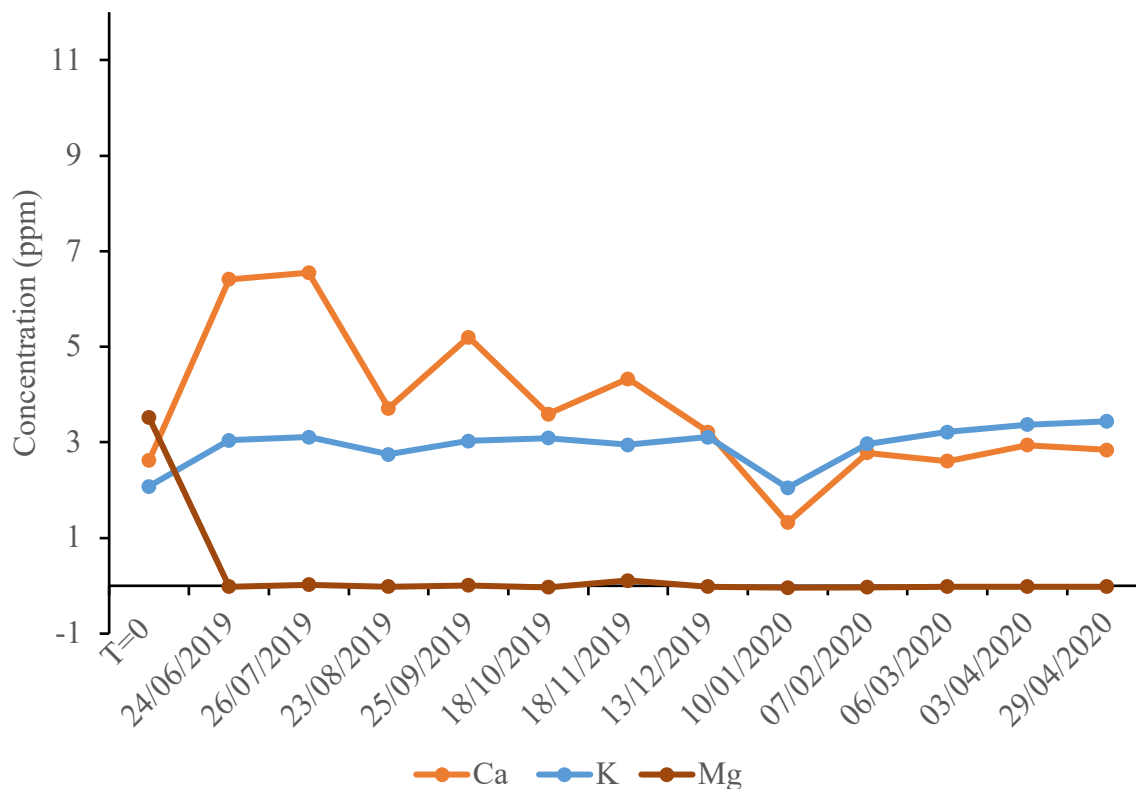


Figure 4. 16: Graph showing the change in Calcium (Ca), Potassium (K) and Magnesium (Mg) concentration in model sea water measured over 12 months in Jar 4.

Zinc (Zn), Iron (Fe), Copper (Cu), Manganese (Mn), Aluminium (Al) and Silicon (Si) concentrations were also measured over the 12 months; however, they were only present in trace amounts so that data appears in Appendix A in Table A.4. There was very little change in the amounts of Ca, Mg and K present in the model sea water throughout the experiment. Ca increased slightly from 2.62 ppm to 2.84 ppm. K increased from 2.08 to 3.44. Mg decreased from 3.52 to -0.02.

4.6.3: pH Change of Model Sea Water in Jar 4

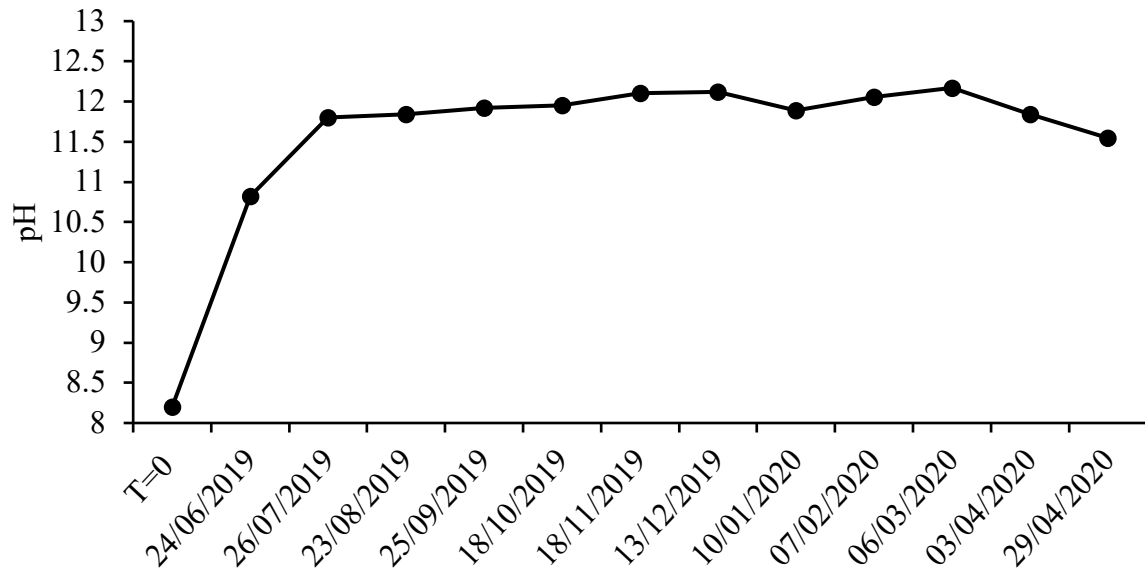


Figure 4. 17: Graph showing the pH change over 12 months for Jar 4: 0-10mm LF BOS slag.

Throughout the experiment, the pH increased from 8.5 to 11.55. It can be seen that the most significant increase happened over the first 2 months, with the pH then stabilising between 11.50 and 12 for the rest of the 12 months.

4.7: Results from Accelerated Leaching Experiment

4.7.1: Weight Change and Surface area change of Slag in Accelerated Leaching Experiments

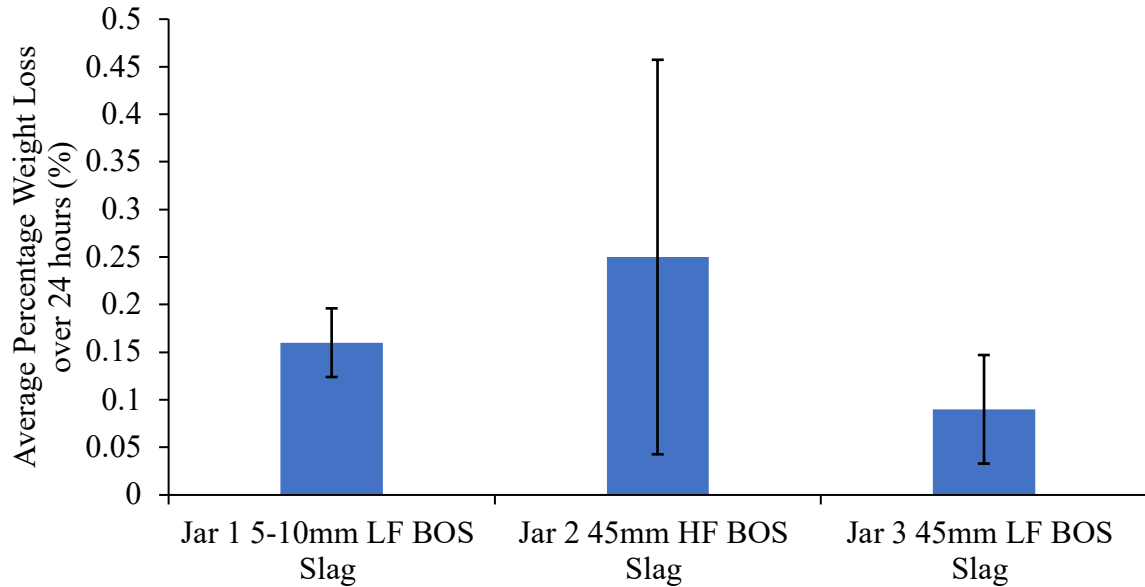


Figure 4. 18: Bar chart comparing the average percentage weight loss in the accelerated leaching experiment after 24 hours. The error bars show the standard deviation of the 3 measurements.

The accelerated leaching experiment was repeated 3 times for each variation of slag hence why the results are averaged. The results show that the 45mm HF slag lost the most weight on average during the accelerated leaching experiments. However, the error bars show a slight variation in the results of the 3 repetitions of the experiment, which is due to the variations in the composition of the slag.

Table 4. 4: Table showing the average BET surface area change after 24 hours in the accelerated leaching experiment.

	After 24 Hrs		
	T=0 (m ² /g)	(m ² /g)	Standard Deviation
Jar 4 0-10mm LF BOS Slag	30.11	72.42	6.37

The results in table 4.4 suggest that the BET surface area of the 0-10mm LF BOS slag sample increased significantly after 24 hours of the samples being agitated. The agitation of the water allowed the particles to be continuously moving encouraging soluble elements such as Ca, K and Mg to dissolve into the water, therefore leaving the slag particles a large surface area.

4.7.2: Microwave Plasma Atomic Emission Spectroscopy (MP-AES) of Model Sea Water in Accelerated Leaching Experiment

Table 4. 5: Table showing the Ca concentration after 24 hours of accelerated leaching in model seawater. The measurement is the average of the 3 experimental repeats completed, with the standard deviation also shown.

	T=0 (ppm)	After 24 Hrs (ppm)	STDEV
Jar 1 5-10mm LF BOS Slag	2.62	1.93	0.04
Jar 2 45mm HF BOS Slag	2.62	1.89	0.07
Jar 3 45mm LF BOS Slag	2.62	2.17	0.2
Jar 4 0-10mm LF BOS Slag	2.62	5.63	0.32

The Ca concentration in the model sea water in jars 1-3 decreases throughout the experiment. The Ca concentration in jar 4 increases from 2.62 ppm to 5.63 ppm.

Table 4. 6: Table showing the K concentration after 24 hours of accelerated leaching in model seawater. The measurement is the average of the 3 experimental repeats completed, with the standard deviation also shown.

	T=0 (ppm)	After 24 Hrs (ppm)	STDEV
Jar 1 5-10mm LF BOS Slag	2.08	2.78	0.09
Jar 2 45mm HF BOS Slag	2.08	2.65	0.02
Jar 3 45mm LF BOS Slag	2.08	2.92	0.16
Jar 4 0-10mm LF BOS Slag	2.08	3.47	0.54

The K concentration increased in all 4 Jars, with Jar 4 seeing the most significant increase.

Table 4. 7: Table showing the Mg concentration after 24 hours of accelerated leaching in model seawater. The measurement is the average of the 3 experimental repeats completed, with the standard deviation also shown.

	T=0 (ppm)	After 24 Hrs (ppm)	STDEV
Jar 1 5-10mm LF BOS Slag	3.52	3.33	0.08
Jar 2 45mm HF BOS Slag	3.52	3.27	0.03
Jar 3 45mm LF BOS Slag	3.52	3.54	0.12

Jar 4 0-10mm LF BOS Slag	3.52	1.37	0.28
--------------------------	------	------	------

The Mg concentration decreased in all 4 jars apart from jar 3 where it increased by a minimal amount.

4.7.3: pH Change of Model Sea Water in Accelerated Leaching Experiments

Table 4. 8: Table showing the pH change before and after 24 hours of the accelerated leaching experiment for all 4 jars. The measurement is the average of the 3 experimental repeats completed, with the standard deviation also shown.

	T=0	After 24 Hrs	STDEV
Jar 1 5-10mm LF BOS Slag	8.20	8.34	0.03
Jar 2 45mm HF BOS Slag	8.20	8.50	0.19
Jar 3 45mm LF BOS Slag	8.20	8.59	0.25
Jar 4 0-10mm LF BOS Slag	8.20	9.62	0.19

In all 4 of the experiments, the pH increased over the 24 hours, with slag in jar 4 causing the most significant increase in pH levels.

4.8: Discussion

One of the main observations from all four variations of slag used in the experiment was that Ca, Mg and K leached out in varying amounts. This is complemented by the fact that the average weight of all samples in 3 of the jars trended downward in the experiments. The samples in Jar 2 that were 45mm HF BOS slag lost the most considerable weight in both the 24-hour and 12-month experiments. The surface area of the slag in Jar 4 increased in both the static and agitated experiments, suggesting there was a dissolution of slag particles. This meant that the slag was left with a rougher surface with more crevices meaning the surface area increased.

The Ca concentration reached the highest when leaching out of the 45mm HF BOS slag sample in Jar 2; it reached 15.07 ppm. Increasing Ca concentration is a common effect slag causes in leaching experiments; Piatak, Li and Kashiwaya have previously seen it. Piatak states that the dissolution of calcium causes alkaline leachate to be formed, which raises the seawater's pH

(Kashiwaya et al., 2020; Li et al., 2019; Piatak, 2018). This can be visibly seen in Figures 4.7 and 4.8, which are both graphs related to Jar 2. They show an increase in Ca concentration and pH level in the same month, 10/01/20. The K concentration of Jar 2 also begins to increase simultaneously, suggesting that the Ca and K concentrations were in a similar area inside the slag. The K concentration increased the most in Jar 2, increasing from 2.08 ppm to 5.42 ppm.

The pH increases across the 4 experiments were not all of the same magnitudes, with Jar 1 increasing by the least from 8.2 to 9.53. This is possibly due to the low Ca concentration of 6.39 ppm observed at the end of the experiment. This suggests that perhaps the pieces of slag randomly picked for this analysis were not high in Ca concentration. As Chapter 3 highlights and other work within this thesis, the composition of steelmaking slag can be highly variable. The final pH value for Jars 2,3, and 4 were all in the same region of 11.17 -11.67. This is different for the same samples in the accelerated leaching experiment Jars 1,2, and 3's average final pH value was 8.34-8.59, whereas Jar 4's increased to 9.62. This has most likely been caused by the fact that the slag particles in this sample were much smaller and had a larger surface area meaning there was a far more extensive area to reach with the model seawater. This sample also showed the most significant Ca concentration increase across the 24-hour experiment. Li et Al. has previously seen similar results, and Kashiwaya et al., who both stated that the smaller the slag size fraction, the higher the pH rose and the more Ca leached out (Kashiwaya et al., 2020; Li et al., 2019).

The accelerated leaching experiment did highlight that when the slag and model sea water solution was agitated mass loss could be seen over 24 hours. This suggests that if the slag were to perhaps used in an undersea structural application, there may be a risk that the slag may erode away causing the structural application to fail. So if slag were to begin to be used then it would be worth taking this into consideration.

4.9: Conclusion

The work presented here assesses the effect that steelmaking slag has in model seawater. In both experimental setups, the weight of the individual pieces of BOS slag trended downwards, suggesting that particulates were leaching out. Whilst in the powdered slag experiments, the surface area increased. When the model sea water was tested, it was found that Ca, Mg and K

leach out throughout the experiment. This then causes the pH of the model seawater to increase, causing a more alkaline environment. However, as noted, the pH increases in the 4 jars were not all of the same magnitude, most likely due to the variable composition of the pieces of BOS slag.

The experiment aimed to assess the environmental impact the slag may have on its surrounding environment if it were to be used in a marine application. The MP-AES analysis in the chapter found that no heavy elements such as As, Cr or Pb leached out into the seawater, which was a positive result. However, the accelerated leaching experiment did highlight that if the slag were to be used in an undersea structural application, there may be a risk of structural failure due to erosion. With these results it does show that BOS slag would be suitable to be used in applications in the Swansea tidal lagoon project.

Chapter 5: Functionalization of Basic Oxygen Steelmaking Slag

The work presented in Chapter 5 was previously presented at the 8th Brunei International Conference on Engineering and Technology 2021. The conference proceeding were published online as of 10/1/2023 (Fisher & Barron, 2023) . There are further graphs and images from the work in Appendix B.

5.1: Introduction

To find new applications of BOS slag, it is essential to look at the significant individual components that make up the composition of BOS slag, e.g. calcium carbonate (CaCO_3), iron oxide (FeO), silicon dioxide (SiO_2) and aluminium oxide (Al_2O_3) and what applications they can be used in (Fisher & Barron, 2021). Several researchers have previously reported the hydrophobic properties of calcium carbonate when it has been functionalized using silanes and carboxylic acids such as stearic acid (Abeywardena et al., 2021; C. Wang et al., 2006, 2007). In research attempting to mimic natural bio-mineralization, CaCO_3 was first functionalized using stearic acid to become hydrophobic rather than hydrophilic through the formation of calcium stearate (C. Wang et al., 2006). Deionized water was mixed with CaO to form a $\text{Ca}(\text{OH})_2$ slurry; this allows Ca^{2+} ions to react with the steric acid ($\text{HO}_2\text{CC}_{17}\text{H}_{35}$) to form $\text{Ca}(\text{O}_2\text{CC}_{17}\text{H}_{35})_2$ precipitate. This precipitate then adheres to the surface and introduces hydrophobicity. Similar experiments have also been reported to create superhydrophobic behaviour of the CaCO_3 with contact angles in the range of 152 to 162° (Abeywardena et al., 2021; Arbatan et al., 2011). FeO has been reported to become superhydrophobic by functionalization, producing contact angles ranging from 150 to 159° (Hill et al., 2019; Z. T. Li et al., 2018). Interestingly, SiO_2 is made superhydrophobic when refluxed with silanes producing contact angles of 113 - 160° (Athauda et al., 2012; Karunakaran et al., 2011); however, when using lauric acid [$\text{HO}_2\text{C}(\text{CH}_2)_{10}\text{CH}_3$] the surface observed was not superhydrophobic, but instead hydrophobic with a contact angle of 132° (Y. Zhang et al., 2019); however, superhydrophobic contact angles can be produced using a mixture of two different SiO_2 sizes (Karunakaran et al., 2011).

It has previously been demonstrated that aluminium oxide particles and surfaces can be functionalized with carboxylic acids and that the resultant material can be varied from superhydrophobic (contact angle = 162°) to superhydrophilic (contact angle $<5^\circ$) depending on the choice of the carboxylic acid (Alexander et al., 2016; Al-Shatty et al., 2017; Hill et al., 2020; Maguire-Boyle et al., 2017; Maguire-Boyle & Barron, 2011). This work has also been extended to iron oxide particles (Maguire-Boyle et al., 2012). This led to the exploration of if you can functionalize the surface of BOS slag with various carboxylic acids. Lauric acid and isostearic acid [$\text{HO}_2\text{C}(\text{CH}_2)_{14}\text{CH}(\text{CH}_3)_2$] were chosen as routes to increased hydrophobicity surface functionalization, while cysteic acid ($\text{HO}_2\text{CCH}(\text{NH}_2)\text{CH}_2\text{SO}_3\text{H}$) was chosen for its

proven ability to increase the hydrophilicity of surfaces. Finally, the reaction of lanolin was investigated. Lanolin is a sterol ester (even though it was traditionally called “wool fat”) of various C₁₂-C₂₄ carboxylic acids. Thus, lanolin, a side product from wool production, could act as a “hidden” source of long-chain carboxylic acids for low cost sustainable hydrophobic functionalization.

5.2: *Experimental Methods*

Basic oxygen steelmaking slag was collected from Tata Steel, Port Talbot, UK. Toluene, lauric acid, cysteic acid and lanolin were purchased from Sigma-Aldrich and used as received. Isostearic acid was purchased from Tokyo Chemical Industry UK Ltd and used as received. Millipore distilled water (15 MΩ cm) was used throughout the experiments.

5.2.1: *Synthesis of Functionalized Slag*

The BOS slag particles were functionalized using a modification of previously reported methods (Alexander et al., 2016; Hill et al., 2019). Several different ratios of slag to carboxylic acid were tested, which are listed in Table 5.1. Several different ratios were used to find the optimum amount of chemical to starting material. In each experiment 15g of BOS slag was used as the starting material. The amount of functionalisation chemical was then worked out from this e.g. in a 1:1 ratio, 15 g of BOS slag: 15g of functionalisation chemical. The BOS slag used for all refluxes was 45mm HF BOS slag.

Table 5. 1: The ratio of slag:reagent used in functionalization experiments.

Reagent	Slag:reagent ratio
Isostearic acid	1:1, 1:1.25, 1:1.5
Lauric acid	1:1, 1:1.25, 1:1.5
Cysteic acid	1:1, 1:1.25, 1:1.5
Lanolin	1:2, 1:3, 1:5

For the hydrophobically functionalized slag, the appropriate carboxylic acid was refluxed overnight in 200 mL of toluene at 110 °C. Due to the magnetic nature of the slag, an overhead mechanical stirrer was used to stir the reaction. Once the reaction was finished, the

functionalized slag was centrifuged for 30 minutes at 5000 rpm. The supernatant was removed and disposed of, and the precipitate was then re-dispersed in fresh 2-propanol and centrifuged again. This process was repeated three times, and then the same process was repeated twice using ethanol. The remaining precipitate was dried overnight in an oven at 100 °C. Once dried, a small portion of the sample was reserved for thermogravimetric analysis (TGA), Fourier transform infrared spectroscopy (FTIR) and scanning electron microscopy (SEM) analysis. The rest of the sample was then pressed into a pellet using a 32 mm die and pellet press for water contact angle (WCA) measurements. This procedure was repeated exactly for the synthesis with cysteic acid, except it was refluxed overnight in 200 mL distilled water (15 MΩ cm). All of the syntheses were completed in triplicate.

5.2.2: Characterisation

FTIR measurements were taken using a Perkin Elmer spectrum two FTIR spectrometer. Scans were done over a range of 400-4000 cm⁻¹ with a total of 32 scans for each measurement. Using distilled water under ambient conditions, water contact angle (WCA) measurements were taken using Krüss DSA25 Expert Drop shape analyzer. Advanced and receding measurements were taken, as well as sessile drop measurements. For all measurements, the WCA quoted is the average of three measurements performed across the sample's surface. To measure the WCA, The Ellipse Tangent 1 fitting method was used. Figure 5.3 shows an example of a contact angle measurement. For samples functionalized with cysteic acid the contact angle could not be measured due to the surfaces hydrophilic nature, so instead the time for the water droplet to be absorbed into the sample was measured.

For all functionalisation experiments in Chapter 5, the sample was placed into an open alumina crucible under continuous argon gas flow. The sample was ramped to 1000 °C at a rate of 20 °C min⁻¹. The weight loss of the sample was used to calculate the grafting density of the carboxylic acids onto the BOS slag using equation 5.1. MW is the molecular weight of the carboxylic acid, and SSA is the specific surface area of the BOS slag. The specific surface area of the BOS slag was calculated using BET surface area analysis, and it was calculated to be 31.1 ± 8.4 m² g⁻¹. This value is for 45mm HF BOS Slag. A Quantachrome Nova 2000e surface area analyzer was used for this measurement

$$\left(\frac{Wt\%}{100-wt\%}\right) \times \left(\frac{Avogadros\ number}{MW \times SSA}\right) = \text{Grafting Density} \quad (5.1)$$

Table 5. 2: Table showing the molecular weight of each carboxylic acid used to calculate grafting density.

Carboxylic acid	Molecular weight (g/mol)
Isostearic Acid	284.5
Lauric Acid	200.3
Lanolin	508.9
Cysteic Acid	169.2

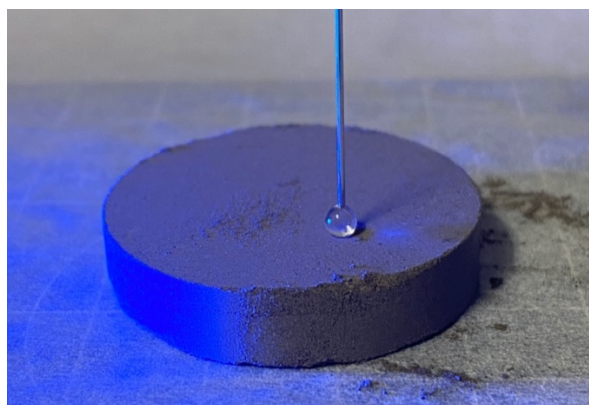


Figure 5. 1: A photograph showing the placement of a water droplet on a pressed pellet of BOS slag functionalised with lauric acid in a 1:1 ratio.

5.3: Results and Discussion

Unfunctionalized BOS slag is hydrophilic and a contact angle is not measurable; instead the time for the droplet to be absorbed is measured as 4s. In contrast, reaction of the BOS slag with isosteric acid, lauric acid, and lanolin result in a distinctly hydrophobic surface as is evidenced by the observation (e.g., Figure 5.2) of a measurable water contact angle (Table 5.3). The highest contact angle at $141^\circ \pm 4^\circ$ was produced by the sample functionalized with lauric acid in a 1:1 ratio. This is similar to the contact angle testing done by Zhang et al. (Y. Zhang et al., 2019). This sample also produced the largest grafting density at $8.7 \pm 1.7 \text{ nm}^{-2}$, which suggests that due to the straight-chain nature of lauric acid, more of the carboxylic acid was able to be reacted with the surface of the BOS slag, thus, increasing the hydrophobicity of the surface. Four points should be noted about the results. First, each measurement was repeated three times and across a specific sample, a significant variation in the measured contact angle (e.g., across the surface of one pellet the contact angle could be around 112° and in a spot on the same pellet

133°) was found out, resulting in a high error, most probably due to the heterogeneous nature of the BOS slag. Second, the error in the receding contact angle measurements is significantly larger than for advanced contact angle, and there is a large hysteresis (50 - 75°) between the advanced and receding measurements, which suggests that the surfaces are quite rough and not homogeneous. Third, the results do not follow the expected trend of increased contact angle with higher carboxylic acid content. This is also likely a function of the heterogeneous nature of the BOS slag between batches in the same sample, i.e., each reflux reaction was performed with a random sample of BOS slag that would have slightly different amounts of CaCO₃, SiO₂, FeO and Al₂O₃ leading to the results following an inconsistent trend as compared to what has been observed for the single-phase alumina analog (Maguire-Boyle & Barron, 2011). Finally, the results for lanolin are comparable to that of lauric and isosteric acid suggesting that the lanolin contains similar carboxylic acid components to produce the same hydrophobic effects.

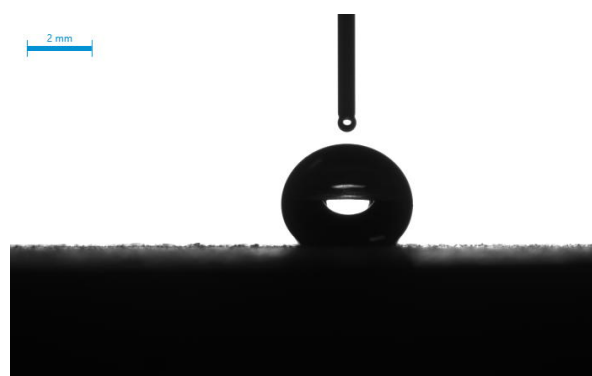


Figure 5. 2: Contact angle measurement of the lauric acid functionalized BOS slag (BOS slag:lauric acid = 1:1).

Table 5. 3: Contact angle and grafting density for BOS slag functionalized with isostearic acid, lauric acid and lanolin.

Reagent	BOS slag:reagent ratio	Static H ₂ O contact angle (°)	Dynamic contact angle (°)		Grafting density (nm ⁻²)
			Advancing	Receding	
Isosteric acid	1:1	135 ±8	147 ±6	97 ±29	2.6±0.7
Isosteric acid	1:1.25	135 ±7	143 ±10	72 ±21	2.7±1.3
Isosteric acid	1:1.5	124 ±8	139 ±5	69 ±20	4.5±2.9
Lauric acid	1:1	141 ±4	151 ±6	76 ±10	8.7±1.7

Lauric acid	1:1.25	138 ±6	150 ±4	86 ±18	4.8±4.5
Lauric acid	1:1.5	123 ±11	143 ±8	73 ±21	7.9±3.9
Lanolin	1:2	135 ±5	150 ±7	73 ±6	4.9±4.6
Lanolin	1:3	129 ±8	141 ±5	71 ±13	3.5±2.8
Lanolin	1:5	138±4	144 ±4	79 ±23	2.9±2.1

Table 5.4 compares the water adsorption time for unfunctionalized BOS slag to BOS slag functionalized with cysteic acid. It can be seen from the results that the addition of cysteic acid to the slag makes the surface slightly more hydrophilic, and thus water absorption is faster. This is similar to our prior results with alumina surfaces (Maguire-Boyle & Barron, 2011). It can be seen that the rate of water absorption does not increase with the addition of more cysteic acid, which as with the hydrophobic functionality is most likely due to the inhomogeneous nature of the slag. For example, during the measurement of the samples with a higher ratio of cysteic acid, one part of the slag pellet would adsorb in under 1 second. At the same time, the water would take approximately 10 seconds to be absorbed somewhere else on the same surface. This suggests that due to the heterogeneity of BOS slag, some parts of the sample have not been functionalized as well as others.

Table 5. 4: Time for water droplet adsorption and calculated grafting density for cysteic acid-functionalized BOS slag.

Sample	Time for absorption (s)	Grafting Density (nm ⁻²)
Unfunctionalized BOS slag	4.1 ±3.0	-
BOS slag: cysteic acid 1:1	1.8 ±1.3	6.7 ±3.8
BOS slag: cysteic acid 1:1.25	1.8 ±2.5	8.3 ±1.8
BOS slag: cysteic acid 1:1.5	3.1 ±2.8	10.4 ±4.4

The TGA of BOS slag (Figure 5.4) shows a mass loss due to dehydration at about 150 °C and a second loss at 650 °C associated with decarbonization of CaCO₃ (Fisher & Barron, 2021). Each functionalized sample shows a significant additional weight loss associated with the decomposition of the organic substituents (Al-Shatty et al., 2017). Figure 5.5 shows the mass loss TGA of pure Isostearic acid. The derivative of the plot shows that the largest change in mass loss happens between 150-325 °C. When this is compared to Figure 5.4 which shows the mass loss of BOS slag functionalised with isostearic acid in a 1:1 ratio. It can be seen from the

derivative of this graph that there is an increase in the rate of mass loss between approximately 150-375 °C. This shows that the BOS slag was successfully functionalised with isostearic acid. In each case the TGA of the reacted product is distinct from the base acid confirming the covalent attachment of the carboxylic acid to the surface of the BOS slag (Bethley et al., 1997). The TGA measurements of the products from the reaction of lanolin with BOS slag confirm its ability to act as a “hidden” source of long-chain carboxylic acids for low cost sustainable hydrophobic functionalization (Ghobadi et al., 2021; Jiang et al., 2018; Sagiri et al., 2013). As shown in Figure 5.4a, the TGA plot for lanolin-BOS slag is close to that of lauric acid-BOS slag, and this is to be expected since both should result in the functionalization with a long chain aliphatic carboxylic acid. For the hydrophobic substituents, the mass loss due to decarbonization of CaCO_3 is retained (Figure 5.4a). However, in the case of the product from the reaction with cysteic acid (Figure 5.4b) it is missing, presumably since the reaction is run in water. Soluble $\text{Ca}[\text{O}_2\text{CCH}(\text{NH}_2)\text{CH}_2\text{SO}_3\text{H}]_2$ derivative has been formed resulting in its removal from the BOS slag (C. Wang et al., 2006). The hydrophilic nature of the cysteic acid derivative is also seen in the continuous mass loss associated with adsorbed water. Further TGA graphs can be found in Appendix B.

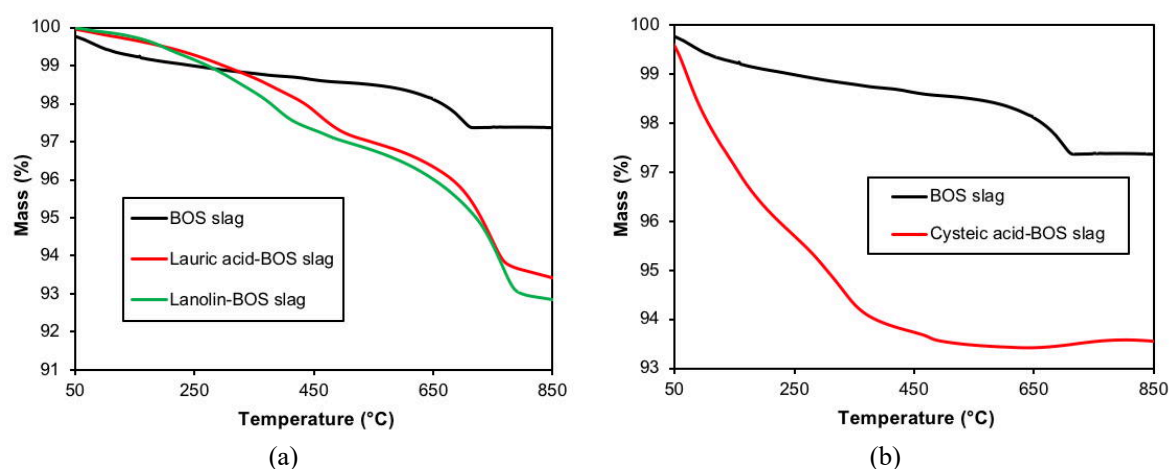


Figure 5. 3: TGA plots under air of (a) BOS slag, lauric acid-BOS slag, and lanolin-BOS slag, and (b) BOS slag and cysteic acid-BOS slag.

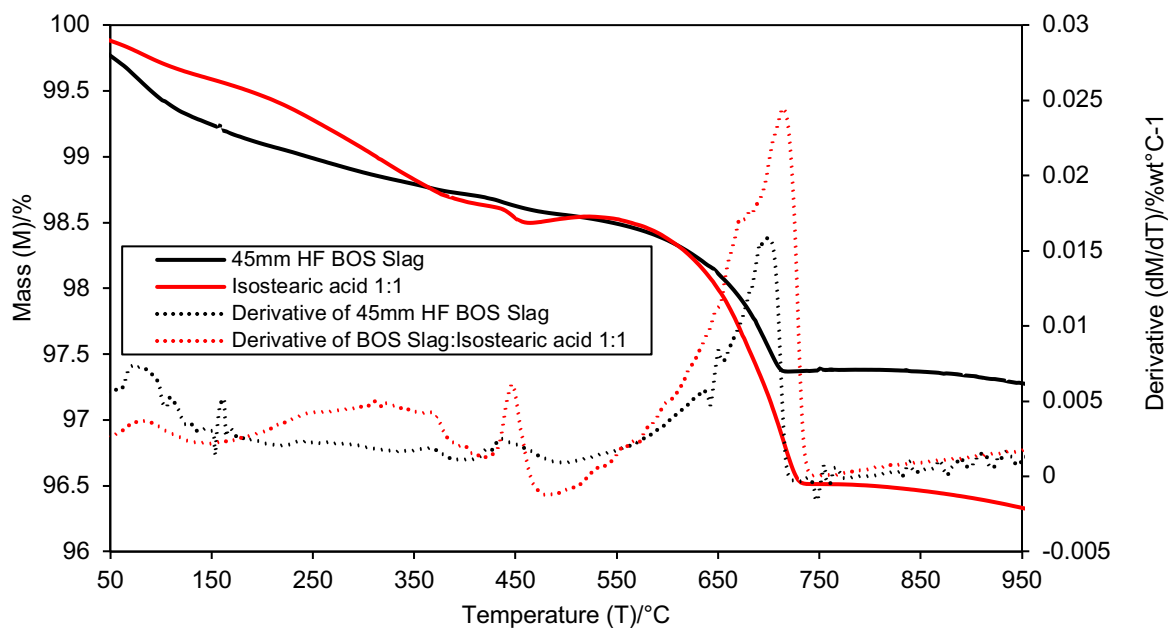


Figure 5. 4: TGA plot under air for 45mm HF BOS slag functionalised with Isostearic acid in a 1:1 ratio with derivative plots.

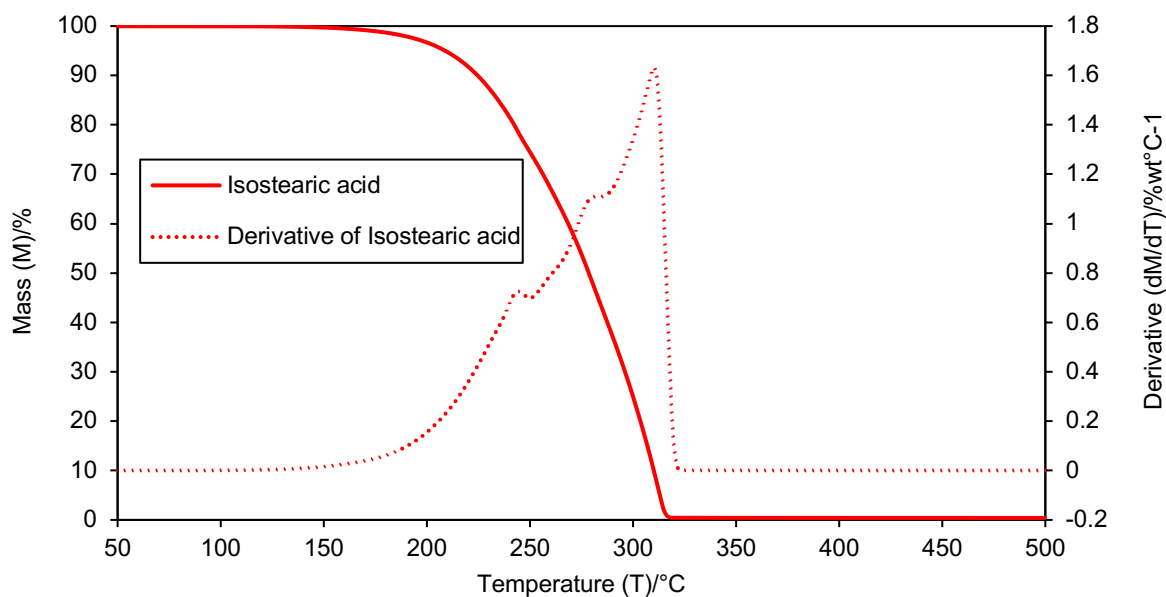


Figure 5. 5: TGA Plot under air of Isostearic acid with derivative plot of isostearic acid.

Further confirmation of the chemical reaction of the acids with the BOS slag is obtained from the FT-IR spectra (Figure 5.7-5.10), shows the formation of peaks associated with both the carboxylate functionality and the hydrocarbon substituents. Across all FTIR spectra the C-H stretch can be seen in the spectra of Isostearic acid, Lauric acid, Lanolin and Cysteic acid. This peak is then evidenced in the spectra of all the functionalised samples. The IR spectra of the products from the reaction with the slag contain peaks at $1460\text{--}1470\text{ cm}^{-1}$ [$\nu_{\text{asymm}}(\text{CO}_2)$] and

1380–1390 cm^{-1} [$\nu_{\text{symm}}(\text{CO}_2)$] consistent with bridging structures (Alcock et al., 1976; Bethley et al., 1997). Importantly, they preclude unidentate coordination of a carboxylic acid group to the surface whose IR spectrum would contain stretches at 1680–1640 and 1610–1570 cm^{-1} . As expected, the IR spectrum of the product from the reaction with cysteic acid shows a peak around 2976 cm^{-1} associated with the N-H stretch, while peaks 1066–1148 cm^{-1} can be attributed to the stretching vibration of the S=O bond (Si et al., 2015; Suzuta et al., 2016). Further FTIR spectra can be found in Appendix B.

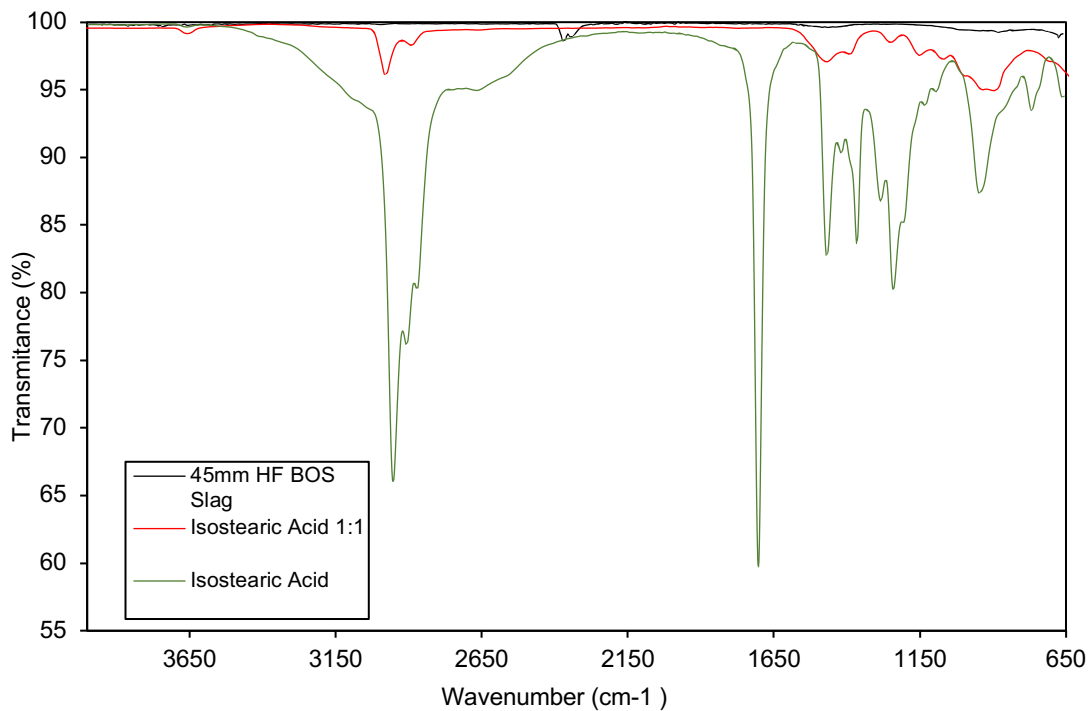


Figure 5. 6: FTIR spectra of the Isostearic acid functionalized BOS slag (BOS slag: Isostearic acid = 1:1)

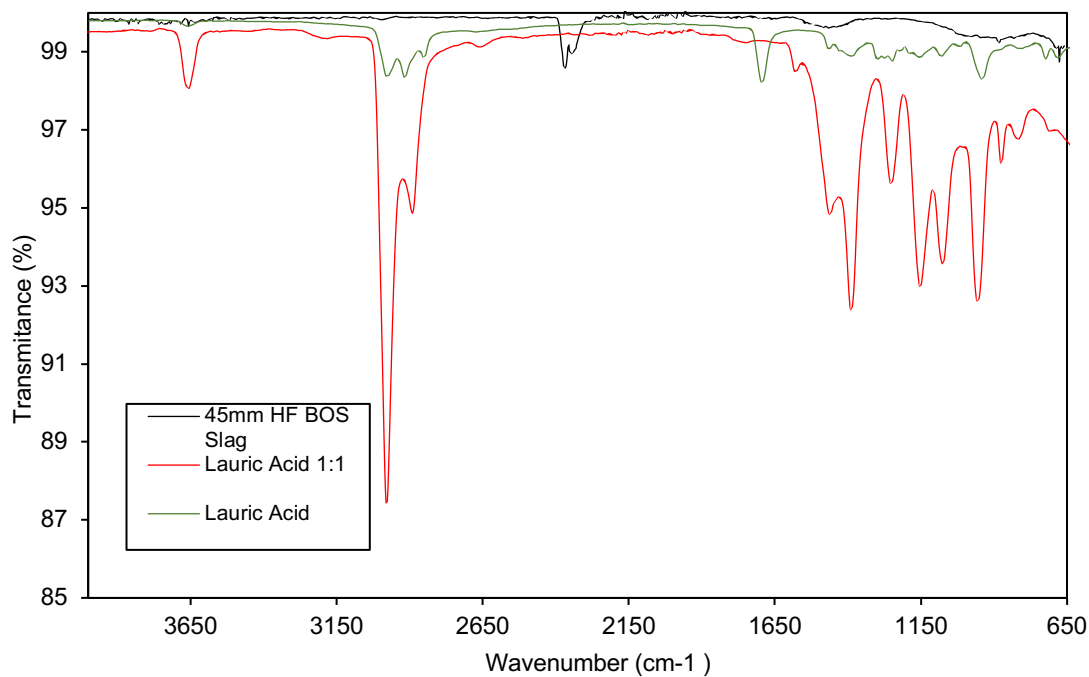


Figure 5. 7: FTIR spectra of the Lauric acid functionalized BOS slag (BOS slag: Lauric acid = 1:1).

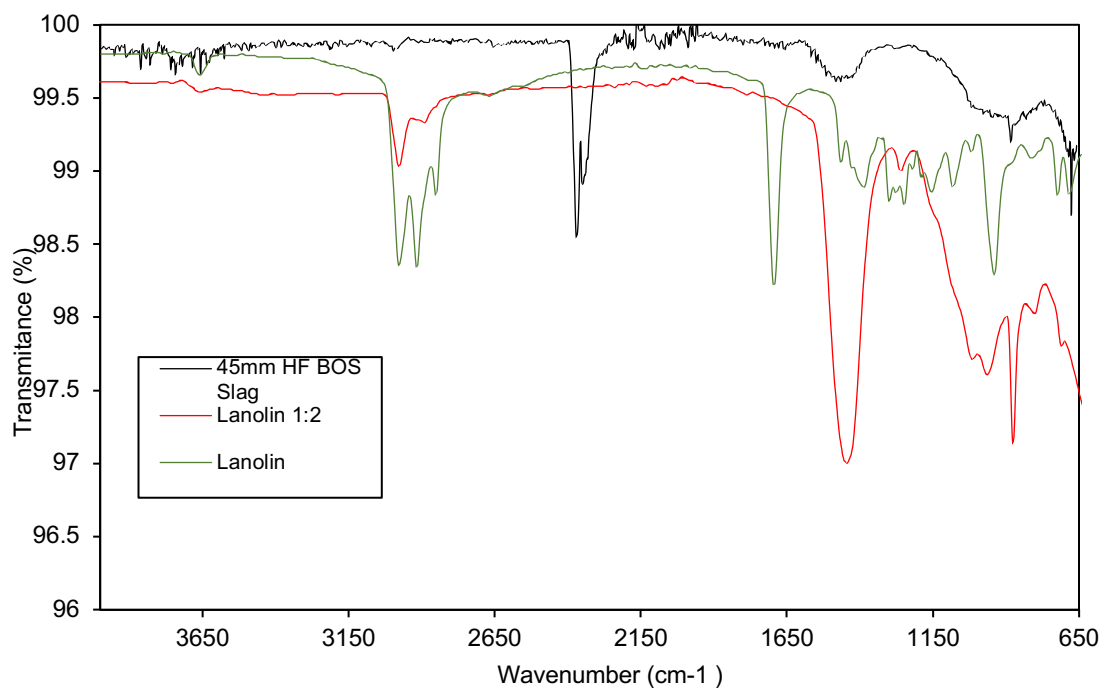


Figure 5. 8: FTIR spectra of the Lanolin functionalized BOS slag (BOS slag: Lanolin = 1:2).

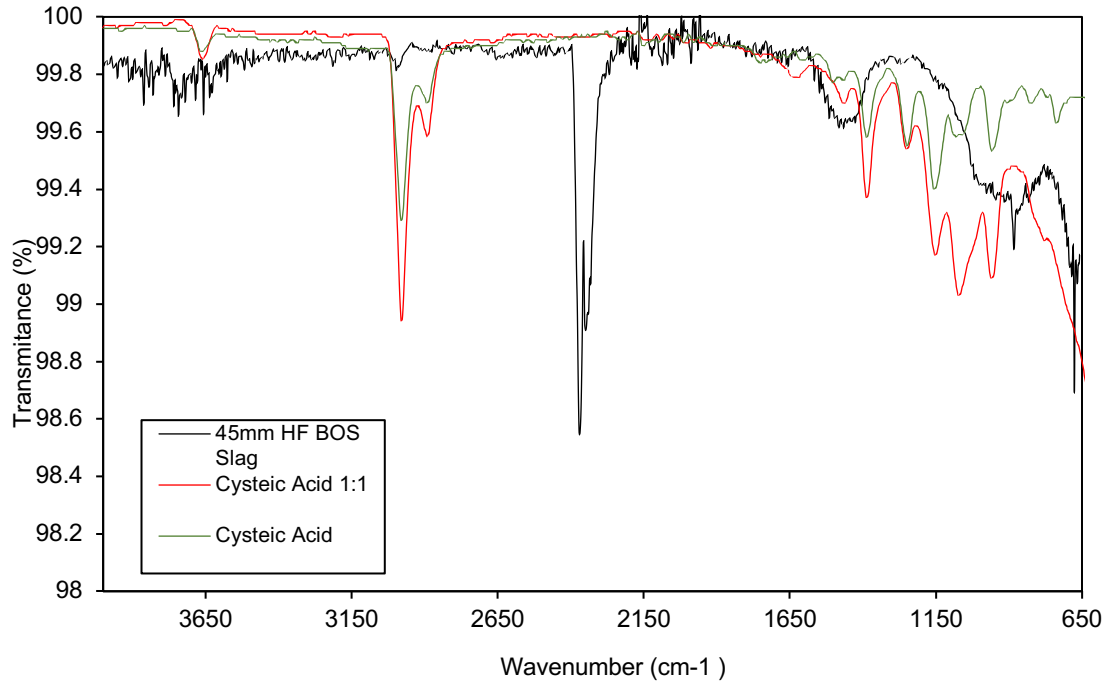


Figure 5. 9: FTIR spectra of the Cysteic acid functionalized BOS slag (BOS slag: Cysteic Acid = 1:1).

5.4: Conclusion

It has been demonstrated that BOS slag may be functionalized to create either a hydrophobic or improved hydrophilic surface. This is favorable as it is a new way for BOS slag to be recycled and provides a new starter material for surface functionalization research. Although, each of the carboxylic acid tested, successfully functionalized the surface of the steelmaking slag and created a hydrophobic surface, lauric acid was seen to produce the highest static contact angle measurement. However, the simplicity and availability of lanolin as a natural resource suggest that its role as a “hidden” source of long-chain carboxylic acids that creates surfaces analogous to those made from petroleum sourced products is a potential green alternative. Although BOS slag has been used as a fertilizer, its potential to be made hydrophobic offers the potential use as a base for plant growth where water resources are limited (S. M. Lee et al., 2018).

Chapter 6: Effect of Functionalized and
Unfunctionalized Basic Oxygen
Steelmaking Slag on the Growth of
Cereal Wheat (*Triticum aestivum*)

Chapter 6 of this thesis was previously published in the Elsevier publishing Journal ‘Resources, Conservation and Recycling Advances’. The paper was published on 27th May 2022. It has been inserted into this thesis with permission from the original publisher (Fisher & Barron, 2022).

6.1: Introduction

Due to BOS slag containing a high amount of CaCO_3 , the material has become an ideal candidate for a fertilizer. Due to BOS slag's alkaline nature and other nutrients. It has previously caused crops to grow in great abundance (Annunziata Branca et al., 2014). It has been previously reported that steelmaking slags can promote microalgae growth (T. Liu et al., 2021). Under the right conditions, the slag can promote algae reproduction and the accumulation of metabolites and encourage lipids to accumulate. The slag makes an ideal nutrient to culture the microalgae as it provides a significant source of Fe and reduces the cost of culturing microalgae. Another study assessed the leaching effect of BOS slag in agriculture (T. Branca et al., 2019). It was found that the presence of the slag increased the availability of P and Ca in the soil, and none of the heavy metals, e.g. Cr and V, that may be present in the slag leached out. In 2018 work was conducted on the ability of BOS slag to decrease CH_4 emissions and arsenic levels in rice plants (Gwon et al., 2018). In a greenhouse experiment, it was found that the grain yield of the rice plants was significantly increased by 10.3%-15.2%, and CH_4 emissions were suppressed by 17.8-24.0%. The rise in yield was attributed to the higher levels of nutrients in the soil made available by the steelmaking slag. The CH_4 reduction was attributed to the higher Fe availability, which acted as an alternate electron acceptor and decreased CH_4 emissions. Due to the formation of Fe-plaque around the roots of the plants, arsenic was sequestered (Gwon et al., 2018; Hansel et al., 2001). Research has also been conducted on the effect of power plant ash and bottom plant slag deposits on different crops such as autumn rye (*Secale cereale L.*) and barley (*Hordeum Sativum Jessen*) (Dželetović & Filipović, 1995). The characteristics of power plant ash are similar to that of BOS slag in that there are aluminosilicates and Fe, Ca and Mg. It was found that there were no adverse effects on the growth profile of the samples when grown on the deposits, and in some cases, enhanced fertilization occurred in the case of autumn rye (*Secale cereale L.*), alfalfa (*Medicago sativa L.*) and Barley (*Hordeum sativum Jessen*). The effects were not seen to be as prominent in winter rapeseed (*Brassica napus L.*) samples.

Lee et al., reported the effect of iron oxide particles and carbon nanotubes on wheatgrass growth, in which growth is enhanced with iron oxide particles, and the hydrophobic nature of the carbon nanotubes enhanced the growth of the seeds by providing a water reservoir for the seeds (Lee et al., 2018). In Chapter 5 it was shown that BOS slag has been functionalized to be

both hydrophobic and hydrophilic. These findings led to the exploration of if the BOS slag, a known source of several plant nutrients, e.g. Ca, Fe, and Si, could be used to fertilize cereal wheat seeds and improve their growth.

6.2: Methods

6.2.1: Chemicals and Materials

Basic oxygen steelmaking (BOS) slag was collected from Tata Steel, Port Talbot, South Wales, UK. We have previously reported the composition of the BOS slag used in this study (Fisher & Barron, 2021). Rainwater was collected from Neath, South Wales, UK. Toluene, lauric acid, cysteic acid and lanolin were purchased from Sigma-Aldrich and used as received. Nitric acid and hydrochloric acid were purchased from Fisher Scientific. Isostearic acid was purchased from Tokyo Chemical Industry UK Ltd and used as received. Millipore distilled water (15 M Ω cm) was used throughout the experiments. Cereal wheat seeds were purchased from Aconbury Sprouts. Analytical reference standards for MP-AES were purchased from Sigma-Aldrich Ltd. 45mm HF BOS slag was used in all experiments.

6.2.2: Functionalized BOS slag synthesis and characterization

The method used for the BOS slag synthesis was previously reported in Chapter 5 as well as in several scientific publications (Fisher & Barron, 2023; Hill et al., 2019; S. M. Lee et al., 2018). In order to make the slag hydrophobic isostearic acid, lanolin and lauric acid were used. Each carboxylic acid was tested in several different ratios to find the optimum amount to functionalize the BOS slag. The appropriate carboxylic acid was refluxed overnight with 20 g of BOS slag in 200 mL of toluene. The reflux was heated and wrapped in foil at 110 °C and stirred using an overhead mechanical stirrer due to the magnetic nature of the slag. Once the reflux was completed, the solution was centrifuged at 5000 rpm for 30 minutes. The supernatant was then removed and disposed of, and the slag was re-dispersed in isopropanol and centrifuged. This process was repeated 3 times, and then the same process was repeated 2 times using ethanol. Once the purification was complete, the slag was dried in an oven overnight. Part of the functionalized slag was reserved for Fourier transform infrared (FTIR), and thermogravimetric analysis (TGA), and the rest was pressed into a pellet using a 32 mm

dye and a pellet press. The pellet was then used for contact angle measurements. The exact process was repeated for the hydrophilic functionalized samples, which were functionalized using cysteic acid. Each reflux was also completed in triplicate.

Contact angle (CA) was used to assess the degree to which the slag was functionalized, and a Krüss DSA25 Expert Drop shape machine was used for all measurements. All measurements were performed using distilled water under ambient conditions. Sessile drop water contact angle measurements were performed on the pellet in three different spots across the surface. Advanced and receding contact angle measurements were performed on three different spots on the pellet. For all measurements, the Eclipse Tangent 1 fitting method was used. TGA was performed using a TA instruments SDT Q600. The experiment was done in an open alumina crucible using continuous argon gas flow. The sample was ramped from 0-1000 °C at a ramp rate of 20 °C/min. From the TGA measurements grafting density was also calculated using the value of the organic weight loss. The surface area to calculate grafting density was calculated using the Brunauer-Emmett-Teller (BET) method. The surface area calculated was 31.1 ± 8.4 m²/g. A Quantachrome Nova 2000e surface area analyzer was used for this measurement. FTIR was performed using a Thermo-fisher scientific i10 Nicolet FTIR. The scans were performed from 4000 - 400 cm⁻¹. 32 scans were performed for each sample.

6.2.3: Plant growth

In methods adapted from previous work, several petri dishes were filled with cotton wool (S. M. Lee et al., 2018). All of the variations of slag listed in Table 6.1 were tested as fertilizer. 20 seeds were grown for each variation of BOS slag in order to replicate the testing and be able to reduce error. A control sample of seeds was also grown, planted without BOS slag. The deposits of BOS slag were spaced 1 cm away from the next. Each deposit of BOS slag was weighed out using an analytical balance. The seeds were soaked in distilled water overnight before planting, as the producer of the seeds recommended. The planted seeds were placed in a dark drawer with no light. Distilled water (1 mL) was then placed on each seed for 8 days. Each day the height of each plant was measured and the qualitative visual growth rating system was used to monitor the plants progress each day. The qualitative visual growth rating system is shown in Table 6.2 and was previously used by Lee et al., (S. M. Lee et al., 2018). In one instance, cereal wheat was also watered using rainwater (1 mL) to examine the effect of

rainwater on cereal wheat seed growth. The pH of the water was measured using a Mettler Toledo Fivego pH meter. After the analysis was completed, the plant samples were digested using aqua regia in line with a previously reported method (Rodushkin et al., 1999). The digested plant samples were then analyzed using microwave plasma atomic emission spectroscopy (MP-AES). An Agilent 4200 MP-AES was used for the analysis. Analytical reference standards were used, and the analysis was calibrated for a range of 0-20 ppm. All elements were calibrated using this range. Optical microscopy was also used to look at the plants and roots, and a Keyence VHX1000 was used for this work. The plant height data was statistically analyzed using a one-way Analysis of Variance (ANOVA) test with a Tukey post hoc test if required. The analysis was performed using Origin Pro 8.5 Software (Kaufmann & Schering, 2014).

Table 6. 1: Summary of samples and BOS slag dosage used.

Sample number	Sample functionalization	BOS:carboxylic acid ratio	BOS Slag dosage (mg)
1	No BOS slag	N/A	0
2	Unfunctionalized BOS slag	N/A	1.0
3	Isosteric acid	1:1	1.0
4	Isosteric acid	1:1.25	1.0
5	Isosteric acid	1:1.5	1.0
6	Lauric acid	1:1	1.0
7	Lauric acid	1:1.25	1.0
8	Lauric acid	1:1.5	1.0
9	Lanolin	1:2	1.0
10	Lanolin	1:3	1.0
11	Lanolin	1:5	1.0
12	Cysteic acid	1:1	1.0
13	Cysteic acid	1:1.25	1.0
14	Cysteic acid	1:1.5	1.0

Table 6. 2: Qualitative Visual Growth Rating System (S. M. Lee et al., 2018).

Rating Number	Qualitative Visual Growth Rating System
1	No change
2	Very little to almost no root
3	Short root, no shoot
4	Medium length root, no shoot
5	Shoot (<1 cm)
6	Shoot (<3 cm)
7	Shoot (<5 cm)
8	Shoot (<7 cm)
9	Shoot (<9 cm)
10	Shoot (<11 cm)
11	Shoot (<13 cm)
12	Shoot (<15 cm)
13	Shoot (<17 cm)

6.3: Results and Discussion

6.3.1: Optical Microscopy

As shown from Fig. 1, the optical micrograph of the BOS slag shows a particularly rough heterogeneous texture. The image also demonstrates the material's porous nature, as a large pore can be seen in the top right-hand corner. It can be seen that dispersed within the material; several inclusions were consistent with iron oxide formed upon long-term exposure to air. Several small white particles throughout the material are consistent with CaCO_3 or CaSiO_3 since it is known that they represent a significant component of BOS slag (Fisher & Barron, 2021; Mallick, 2018).

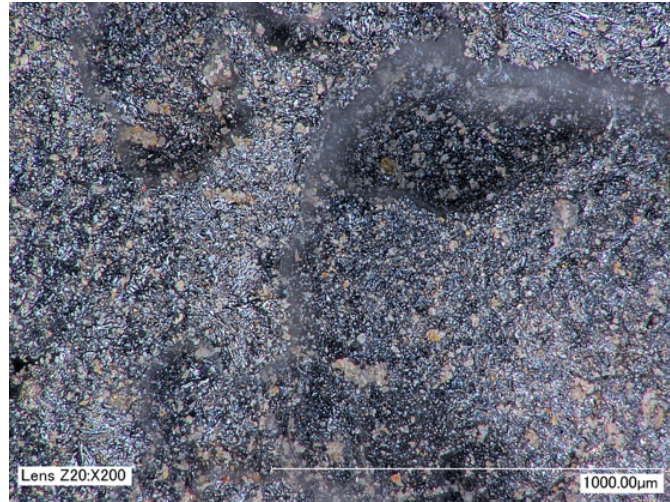
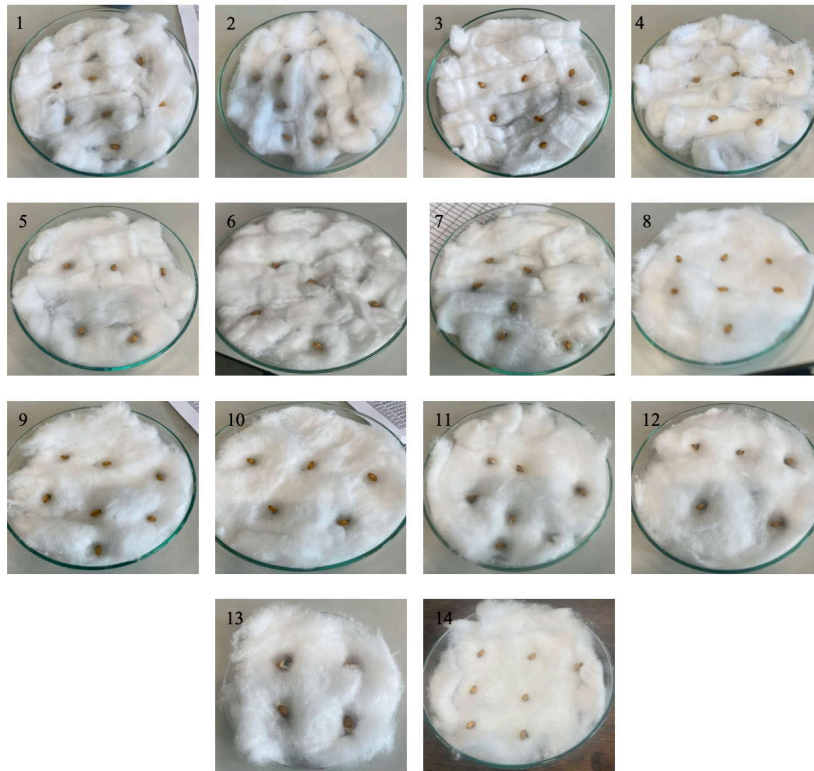


Figure 6. 1: Optical microscopy image of BOS slag used in the study ($\times 200$).

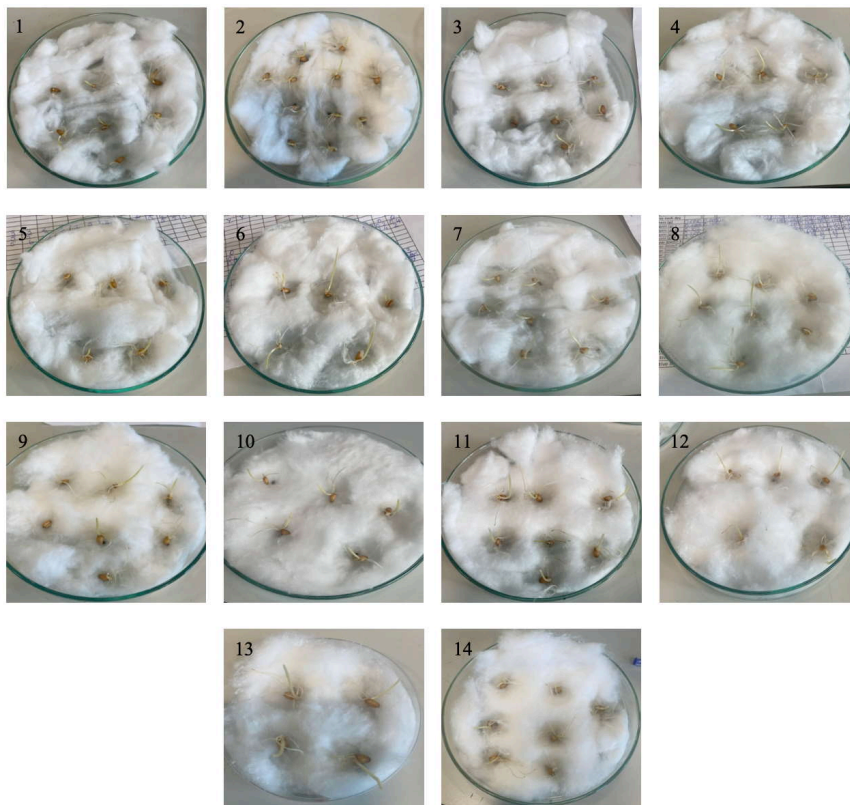
6.3.2: Plant growth

Images of the plant growth can be seen in Fig. 2, where a noticeable difference occurs between days 1, 4 and 8. On day 1, there was no change to the seeds as they had not had time to absorb the water yet and initiate the germination process, but the BOS slag deposits can be visibly seen underneath the seeds. By day 4, the seeds have germinated and sprouted roots and begun to grow a shoot, but the shoot is still very short in all cases. There is an apparent variance in the rate that the seeds germinate, as only some of the seeds can be visibly seen to have roots; this is due to the stochastic nature of the seeds. By day 8, it can be seen that all samples have grown a healthy green shoot. The shoot lengths do vary; however, the trends of variance in shoot length continued to be exhibited as there seemed to be a trend of seeds that germinated later, not being able to grow an as large shoot by day 8. For example, some of the plants in sample sets 10 and 11. The appearance of the plants is similar to that of plants seen in previous work (S. M. Lee et al., 2018).

Day 1



Day 4



Day 8

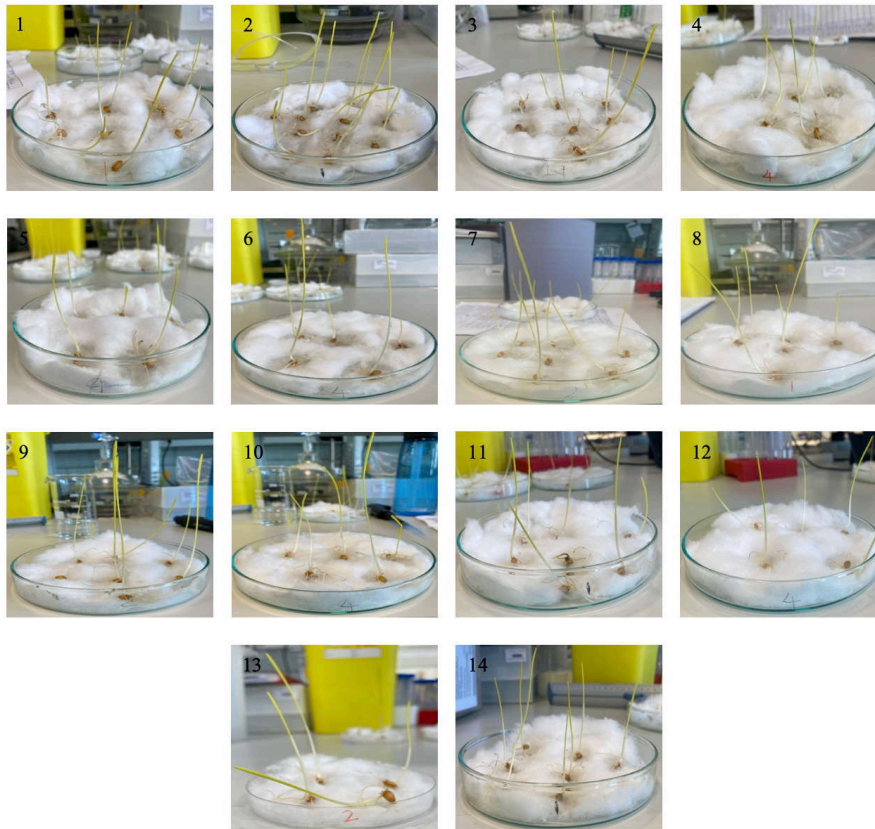


Figure 6. 2: Photographic images of the plant growth are shown on days 1, 4 and 8. The sample numbers correspond to those in Table 1.

6.3.3: Mass gain from plants

A plot of plant mass as a function of growth day is shown in Figure 6.3. For the reference sample (*i.e.*, no slag), the most significant rate of change of mass was on day 2, whereas for the unfunctionalized BOS slag sample, the greatest change occurred on day 3. For all other samples, it can be seen that the day on which the most mass gain occurs varies between days 2 and 3 for the samples. The large standard deviation bars show much statistical variability between the seed's mass gain rates.

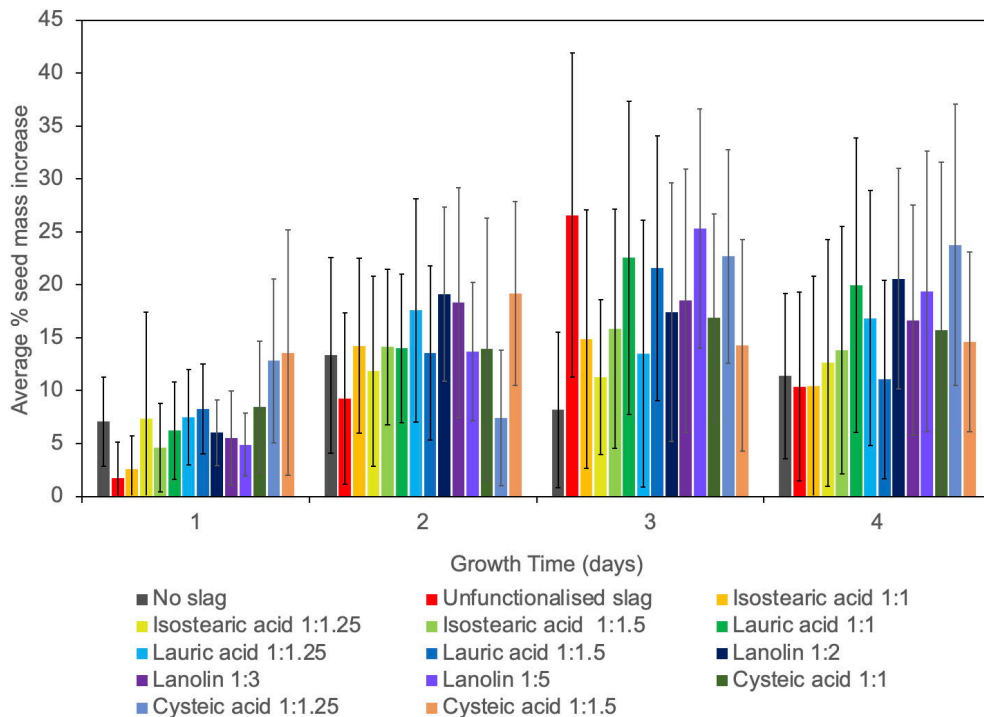


Figure 6. 3: Plots of seed mass gain as a function of time (days) for samples dispersed in DI water. Error bars represent one standard deviation.

6.3.4: Average height of plants

Figure 6.4 shows the average height of the seeds in each sample set on the final day (day 8). The standard deviation error bars for all the samples seem to be of similar height; the variation in plant heights has been caused by the natural variations in the plant seeds. When the sample set of plants grown with no slag and the samples grown with slag are compared, it can be seen there is a significantly better amount of growth, suggesting that the slag has worked well as fertilizer (Annunziata Branca et al., 2014). The samples containing lanolin have performed the best, with a small number of the samples managing to grow over 12 cm in length (see Figure 6.2 and 6.4). Samples containing lauric acid have managed to grow a significant amount. The similarity between lanolin and steric acid is reasonable given that lanolin is a sterol ester (even though it was traditionally called "wool fat") of various C_{12} - C_{24} carboxylic acids. Thus, lanolin, a side product from wool production, has been shown to act as a "hidden" source of long-chain carboxylic acids, *c.f.*, lauric acid (Fisher & Barron, 2023).

An ANOVA test was conducted across all samples to see if the slag variants significantly affected the plant growth height. The p-value used for the analysis was 0.05. The calculated p-

value was 0.02, meaning the difference between the groups is statistically significant. The calculated values can be viewed below in Tables 6.3 and 6.4. A Tukey *post hoc* analysis test was performed in order to find out between which groups the samples were significantly different. The only samples that were significantly different from each other were Lanolin 1:3 and Isostearic acid 1:1. This comparison had a p-value of 0.05. However, none of the other samples compared were seen as being significantly different.

Table 6. 3: ANOVA variance table for all samples.

Sample number	Sample functionalization	BOS:carboxylic		Sum	Average	Variance
		acid ratio	Count			
1	No BOS slag	N/A	20	132.20	6.61	4.52
2	Unfunctionalized BOS slag	N/A	20	151.40	7.57	2.79
3	Isostearic acid	1:1	20	124.40	6.22	8.07
4	Isostearic acid	1:1.25	20	147.50	7.38	6.41
5	Isosteric acid	1:1.5	20	146.30	7.32	4.27
6	Lauric acid	1:1	20	169.30	8.47	10.92
7	Lauric acid	1:1.25	20	144.60	7.23	5.59
8	Lauric acid	1:1.5	20	155.00	7.75	10.27
9	Lanolin	1:2	20	180.30	9.02	13.40
10	Lanolin	1:3	20	183.30	9.17	6.51
11	Lanolin	1:5	20	165.50	8.28	9.85
12	Cysteic acid	1:1	20	132.70	6.64	10.00
13	Cysteic acid	1:1.25	20	152.80	7.64	6.24
14	Cysteic acid	1:1.5	20	146.60	7.33	6.24

Table 6. 4: ANOVA summary table of calculated values for all samples

Source of Variation	SS	df	MS	F	P-value	F crit
Between Groups	196.70	13.00	15.13	2.02	0.02	1.76
Within Groups	1996.32	266.00	7.50			
Total	2193.02	279.00				

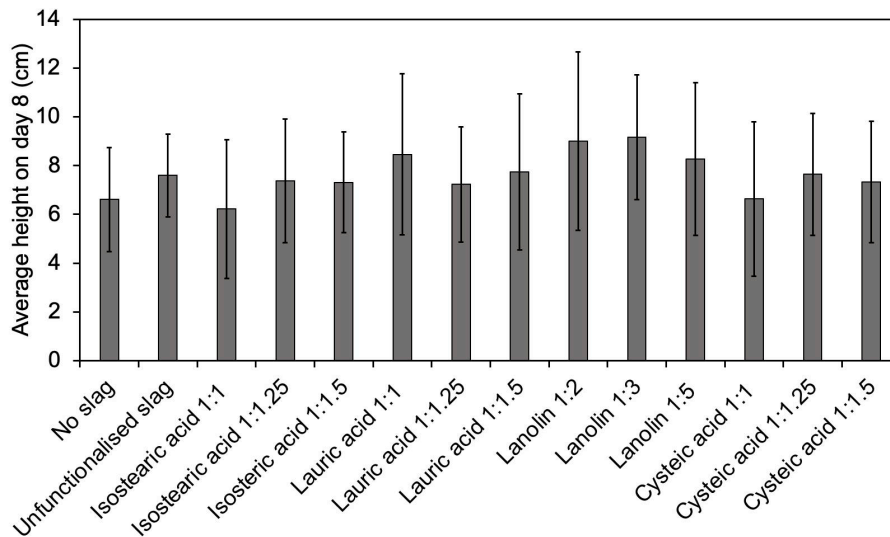


Figure 6. 4: Plot of average plant height after 8 days for all samples studied. Error bars represent one standard deviation.

6.3.5: Germination rate

The germination rate (GR) was observed to be similar for all the slag samples (Figure 6.5), although the GR for the sample grown with no slag (0.92 day^{-1}) is faster than that for the unfunctionalized BOS slag (0.66 day^{-1}). This suggests that the presence of BOS slag inhibits germination. Nevertheless, the functionalized slag samples perform better than unfunctionalized. While the standard deviation bars are large, the hydrophobic functionalized slag samples (isosteric, lauric and lanolin) show a decreasing germination rate with increasing functionality (and hence hydrophobicity). The MGT in Figure 6.6 is in line with the GR as it shows that samples with a slower rate of germination took longer to germinate.

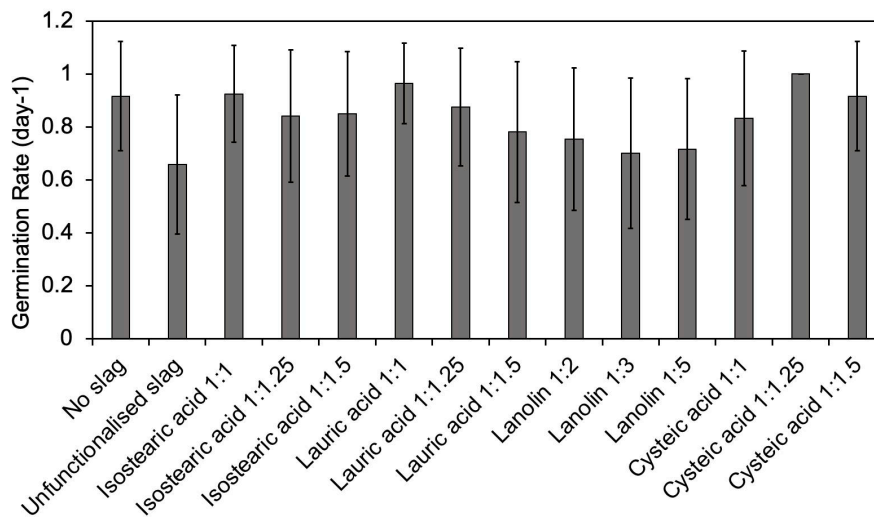


Figure 6. 5: Plot of mean germination rate (GR) for samples studied. Error bar represents one standard deviation.

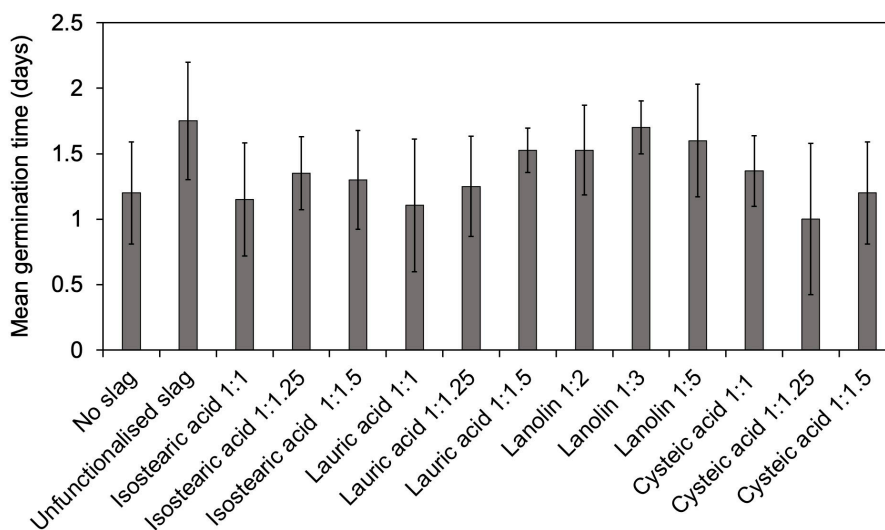
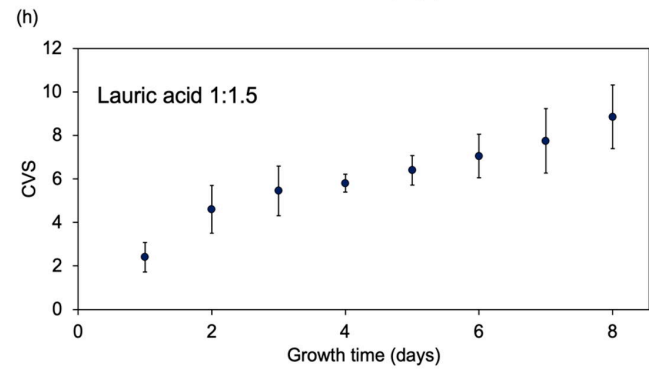
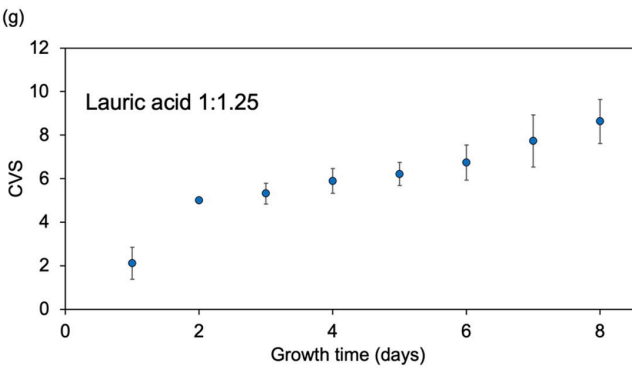
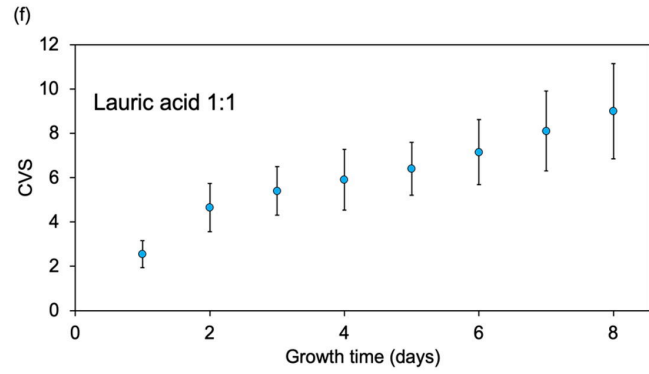
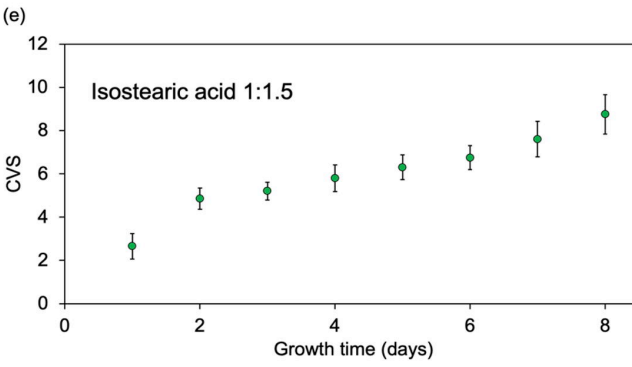
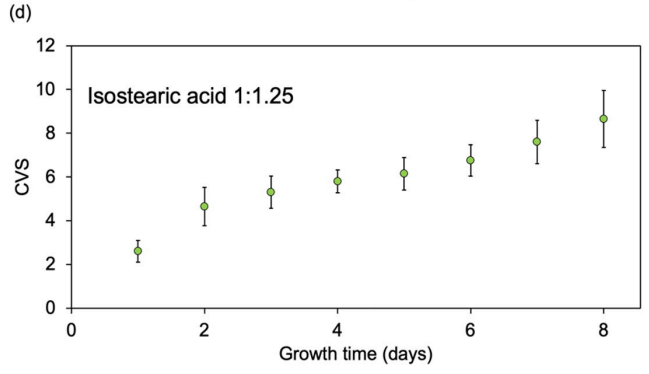
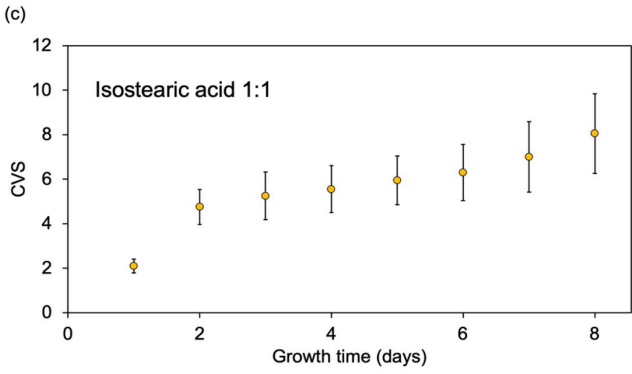
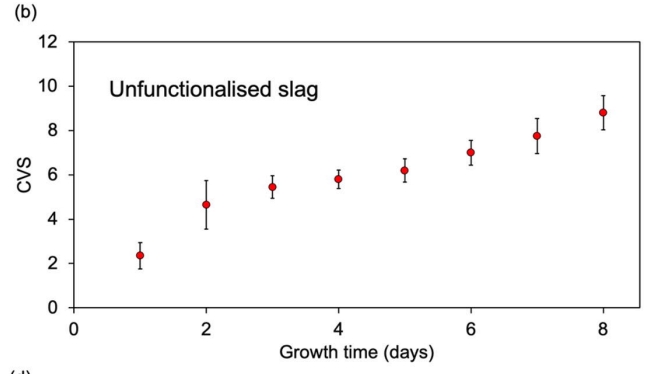
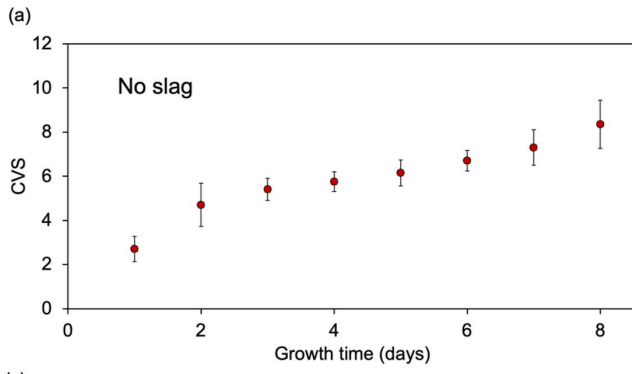


Figure 6. 6: Plot of mean germination time (MGT) for samples studied. Error bar represents one standard deviation.

6.3.6: Composite visual score graphs (CVS)

The CVS graphs in Figure 6.7 show that all the samples seem to grow at a similar rate, as all the graphs seem to follow a similar S-like curve pattern. On days 3-6 for most samples, the error bars from standard deviation on most of the samples are small, showing that there is little to no variance in the growth of the plants in the middle of the growing stage. However, past day 6, it can be seen that large error bars are saying that there is variance in how well the plants perform beyond this point. This is again due to the variance between the different cereal wheat seeds. If the no slag sample and unfunctionalized sample are compared, it can be seen that they follow a similar rate of growth.



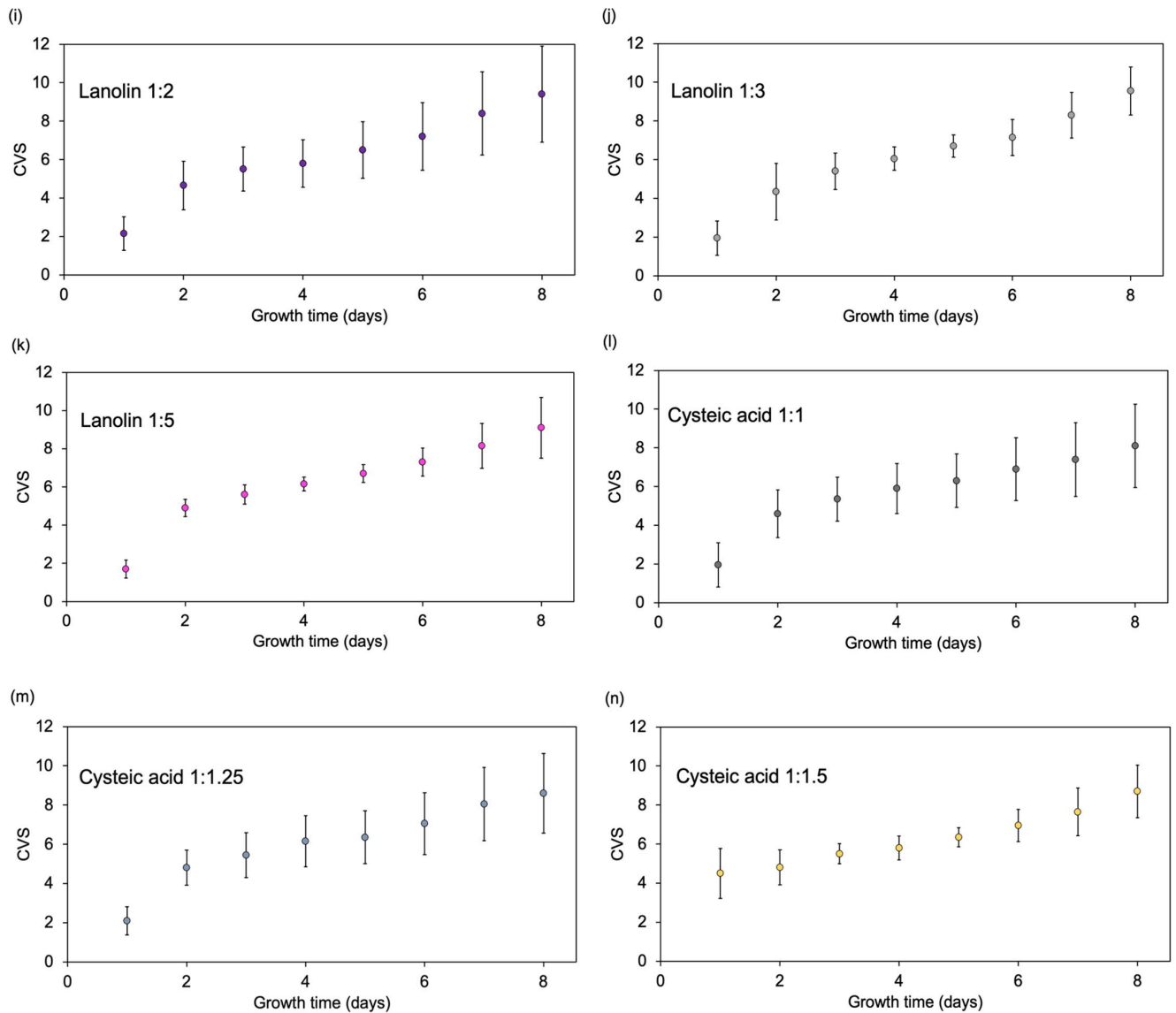


Figure 6. 7: Plots (a-n) of composite visual growth scores (CVS) for samples studied. Error bars represent one standard deviation.

6.3.7: Microwave plasma atomic emission spectroscopy (MP-AES)

Although BOS slag is predominantly calcium silicates, iron oxides, and aluminum silicates, it contains a wide range of trace elements (Fisher & Barron, 2021), some of which may be undesirable to be up-taken into plants. In order to determine the effects of the slag on the plants, MP-AES was employed, and the results are shown in Table 6.5.

Notably, there appears to be no statistical change in the presence of Al, Mg, Mn, and Zn between samples with slag and the reference without slag. In contrast, P shows a slight decrease

in uptake for all the slag samples compared to the reference, while Si is slightly increased; however, the ubiquitous nature of silicon makes analysis difficult (Doostdar et al., 2011). There is a marked increase in Cu for the sample grown on raw slag but no effect on the functionalized slag samples. We propose that the carboxylic acid covalent functionality on the surface (Bethley et al., 1997; Koide & Barron, 1995) inhibits its leaching out of the slag. Interestingly, Fe is seen to leach out of the unfunctionalized slag but not the hydrophobic versions. Finally, an increase in Ca is found in all the plants grown on the unfunctionalized and hydrophobic slags compared to the reference sample and plants grown with hydrophilic functionalized slag (*i.e.*, cysteic acid functionalized).

Table 6. 5: MP-AES data for all samples. The error represents one standard deviation.

Sample number	Sample	Al (ppm)	Ca (ppm)	Cu (ppm)	Fe (ppm)	K (ppm)	Mg (ppm)	Mn (ppm)	P (ppm)	Si (ppm)	Zn (ppm)
1	No BOS slag	0.03 ±0.01	0.18 ±0.04	0.02±0.01	0.12 ±0.12	1.48 ±0.06	0.52 ±0.11	0.04 ±0.01	1.47 ±0.19	0.05 ±0.02	0.02 ±0.01
2	Unfunctionalized BOS slag	0.04 ±0.02	0.35 ±0.05	0.52 ±0.22	0.21 ±0.10	1.34 ±0.06	0.45 ±0.06	0.03 ±0.01	1.29 ±0.09	0.10 ±0.03	0.05 ±0.02
3	Isostearic acid 1:1	0.06 ±0.01	0.27 ±0.04	0.08 ±0.06	0.01 ±0.01	1.28 ±0.16	0.45 ±0.07	0.02 ±0.01	1.29 ±0.24	0.08 ±0.01	0.02 ±0.01
4	Isostearic acid 1:1.25	0.18±0.16	0.53 ±0.32	0.07 ±0.03	0.36 ±0.01	2.80 ±2.22	0.45 ±0.04	0.04 ±0.02	1.12 ±0.05	0.28 ±0.24	0.03 ±0.03
5	Isostearic acid 1:1.5	0.11 ±0.1	0.39 ±0.11	0.08 ±0.04	0.14 ±0.01	1.35 ±0.08	0.47 ±0.01	0.02 ±0	1.30 ±0.05	0.14 ±0.08	0.02 ±0.01
6	Lauric acid 1:1	0.03 ±0.01	0.28 ±0.06	0.08 ±0.09	0.14 ±0.07	1.25 ±0.09	0.40 ±0.02	0.02 ±0.01	1.15 ±0.07	0.07 ±0.01	0.05 ±0.05
7	Lauric acid 1:1.25	0.08 ±0.08	0.37 ±0.22	0.02 ±0.01	0.31 ±0.33	1.38 ±0.14	0.41 ±0.09	0.06 ±0.05	1.14 ±0.05	0.09 ±0.07	0.03 ±0.02
8	Lauric acid 1:1.5	0.09 ±0.01	0.52 ±0.29	0.05 ±0.03	0.34 ±0.32	1.58 ±0.49	0.53 ±0.12	0.05 ±0.03	1.38 ±0.05	0.13 ±0.07	0.04 ±0.02
9	Lanolin 1:2	0.03 ±0.01	0.30 ±0.02	0.02 ±0.01	0.11 ±0.03	1.13 ±0.04	0.36 ±0.05	0.02 ±0.01	0.99 ±0.08	0.08 ±0.03	0.02 ±0
10	Lanolin 1:3	0.08 ±0.07	0.68 ±0.56	0.01 ±0.01	0.37 ±0.37	1.22 ±0.18	0.60 ±0.19	0.06 ±0.05	1.30 ±0.09	0.14 ±0.10	0.03 ±0.01
11	Lanolin 1:5	0.05 ±0.02	0.38 ±0.04	0.01 ±0.01	0.15 ±0.04	1.48 ±0.01	0.55 ±0.01	0.04 ±0.02	1.37 ±0.06	0.10 ±0.01	0.02 ±0.01
12	Cysteic acid 1:1	0.01 ±0	0.18 ±0.02	0.01 ±0.01	0.02 ±0.01	1.02 ±0.13	0.32 ±0.03	0.01 ±0	0.84 ±0.10	0.03 ±0.01	0.00 ±0.01
13	Cysteic acid 1:1.25	0.02 ±0.01	0.17 ±0.05	0.01 ±0.01	0.05 ±0.02	1.50 ±0.27	0.45 ±0.02	0.01 ±0.01	1.30 ±0.19	0.03 ±0.01	0.02 ±0.01
14	Cysteic acid 1:1.5	0.01 ±0.01	0.14±0.02	0.01 ±0.01	0.02 ±0.01	1.61 ±0.05	0.51 ±0.01	0.01 ±0	1.45 ±0.07	0.03 ±0.01	0.01 ±0.01

Figure 6.8 shows an optical microscopy image of a plant root from the unfunctionalized sample set that has been watered with DI water. It can be seen that in the root, there is a black particle, which could be particles of the slag entrained.



Figure 6. 8: Optical microscopy image of sample 2 plant root ($\times 200$).

6.3.8: Functionality versus growth

From the data, it can be said that the BOS slag had a positive effect on the growth of the cereal wheat seeds. This is because of the high amount of Ca present in the BOS slag samples, an essential mineral for plant growth, which assists with cell structure, elongation, and division (Hepler, 2005). Between the unfunctionalized and functionalized slags, it was found that the best fertilizer for the plants was BOS slag functionalized with lanolin in a 1:3 ratio. This sample set was seen to have the highest average height overall, with 9.17 cm. The highest mass gain for this seed was seen on day 2, with the GR rate being slower also. This sample also has a higher amount of Fe (Table 6.5), a slight increase in Al, retention of Mg, but no increase of undesirable elements. Al has been previously reported to increase root growth in low concentrations (Silva & Uchida R, 2000). In previous studies, Fe has been shown to encourage plant enzyme production and speed up the metabolism of the plants (Rout & Sahoo, 2015). Mg also contributes to enzyme activity in plants (Shaul, 2002).

The increased mass gain of the sample on day 2 may be due to the high Ca content recorded by the MP-AES measurements at 0.68 ppm. This suggests that the high Ca content encourages faster cell structure formation and cell elongation leading to the mass gain on day 2. It can be said that the lanolin component of the sample also played a role in the increased plant growth. Lanolin is a natural lubricant and has been used in plant research as a carrier for plant growth regulators (Lv et al., 2021; Redemann et al., 1950; T. Wu et al., 2020). The lanolin does not have a physiological effect on the plant tissue but instead allows the easier transport of nutrients towards the seed.

6.3.9: *Distilled water versus rainwater*

Figure 6.9 shows images comparing the plants grown with no BOS slag, with unfunctionalized BOS slag watered with distilled water (DI water) and unfunctionalized BOS slag watered with rainwater. It can be seen that there is no noticeable difference between the seeds on day 1 as the seeds have not yet had enough time to absorb water and germinate. On day 4, all sample sets have evidence of considerable root growth, with some shoots being present. On day 8, it can be seen that all the samples set have grown a considerable shoot with there being some variation in the height of the plants.

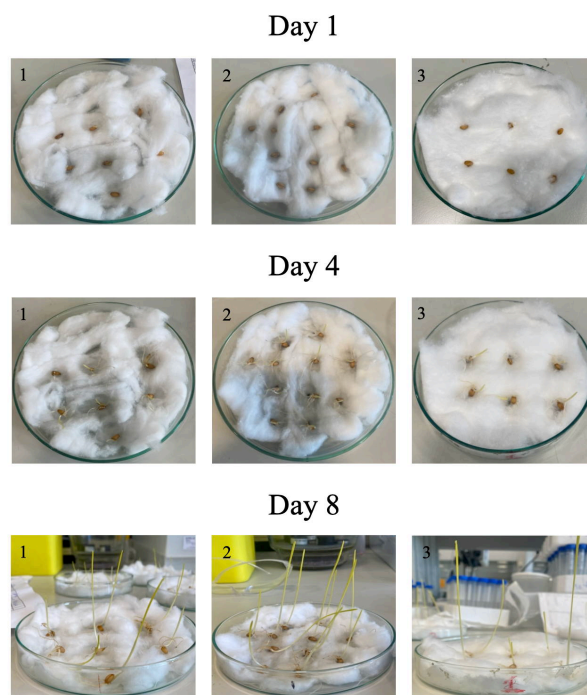


Figure 6. 9: Photographic images of the plant growth shown on days 1, 4 and 8 for Sample 1

(no slag), sample 2 (unfunctionalized slag with DI water), and sample 3 (unfunctionalized slag with rainwater).

Figure 6.10 shows the mass gain of the 3 sample sets over a 4-day period, where it can be seen that there is the most significant mass gain by the rainwater sample set on day 3. This follows a similar pattern to the other samples fertilized with BOS slag. The sample grown without any BOS slag being present had the best growth rate on day 2. However, the average height data in Figure 6.11 shows that the sample set watered with DI water performed better during the height measurements than the sample watered with rainwater. It can also be seen that the sample set grown with no BOS slag performed better in the height measurements.

Nevertheless, it can be seen from the variance in the standard deviation error bars on the graph that, in some cases, the samples did grow to be taller than the sample set with no BOS slag. The samples were again subjected to ANOVA analysis with a p-value of 0.05. The calculated p-value for the variance between samples was 0.083, suggesting no significant statistical difference between the samples and, therefore, no difference between the samples grown with rainwater vs DI water. The ANOVA summary data can be seen in Tables 6.6 and 6.7.

Table 6. 6: ANOVA variance table for no slag, unfunctionalized slag and unfunctionalized slag with rainwater.

Groups	Count	Sum	Average	Variance
No slag	20.00	132.20	6.61	4.52
Unfunctionalized slag	20.00	151.40	7.57	2.79
Rainwater	20.00	115.40	5.77	11.44

Table 6. 7: ANOVA summary table of calculated values for no slag, unfunctionalized slag and unfunctionalized slag with rainwater.

Source of Variation	SS	df	MS	F	P-value	F crit
Between						
Groups	32.45	2.00	16.22	2.60	0.08	3.16
Within Groups	356.32	57.00	6.25			

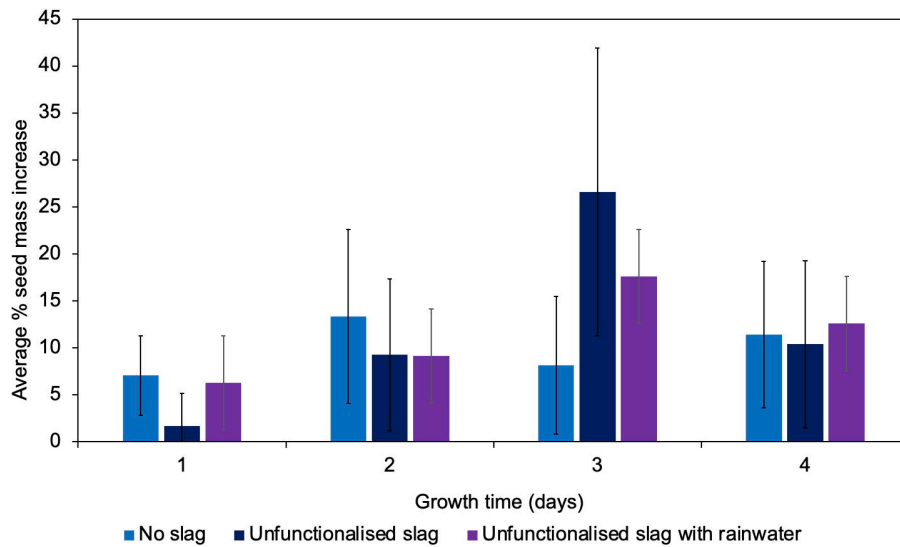


Figure 6. 10: Plots of seed mass gain as a function of time (days). Error bars represent one standard deviation.

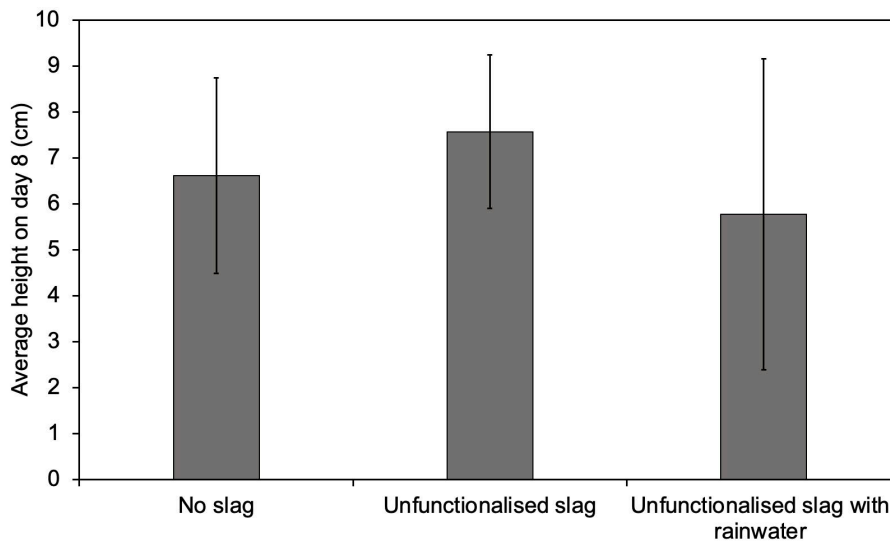


Figure 6. 11: Plot of average plant height after 8 days for all samples studied. Error bars represent one standard deviation.

Samples watered with rainwater have germinated faster than those watered with DI water but not as fast as the sample set grown with no BOS slag, as shown in Figure 6.12. The GR of the DI water unfunctionalized sample was 0.66 day^{-1} , and the rainwater sample was 0.79 day^{-1} . So,

with the addition of rainwater watering, it can be said that the addition of rainwater increases the GR rate. The MGT graph in Figure 6.13 shows that rainwater samples germinated faster than the sample watered with DI water.

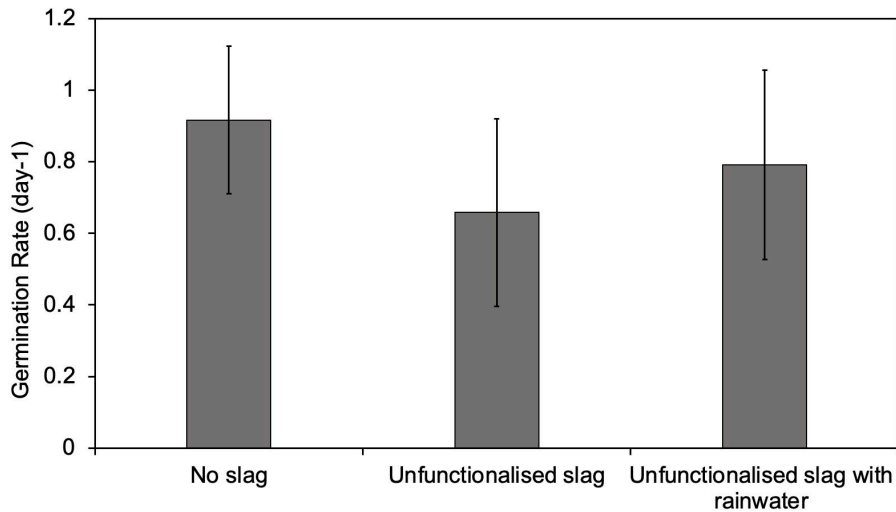


Figure 6. 12: Plot of mean germination rate (GR) for samples studied. Error bar represents one standard deviation.

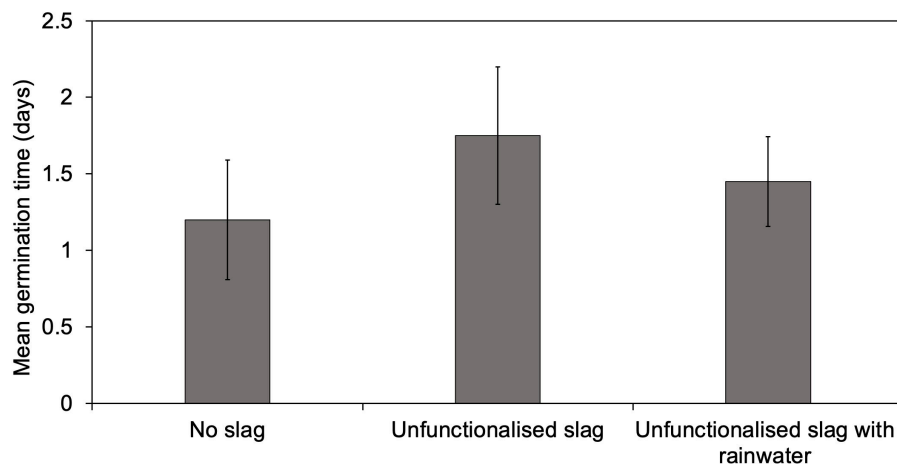


Figure 6. 13: Plot of mean germination time (MGT) for samples studied. Error bar represents one standard deviation.

The CVS graph depicting the growth of the sample watered with rainwater is shown in Figure 6.14 and can be seen to follow an “S” like pattern where the rate of change is rapid towards the start, slower towards the middle. Then the change begins to happen faster again towards day 8. Nevertheless, there is a significant variance between the different samples in the sample set, as seen in the standard deviation error bars on the graph.

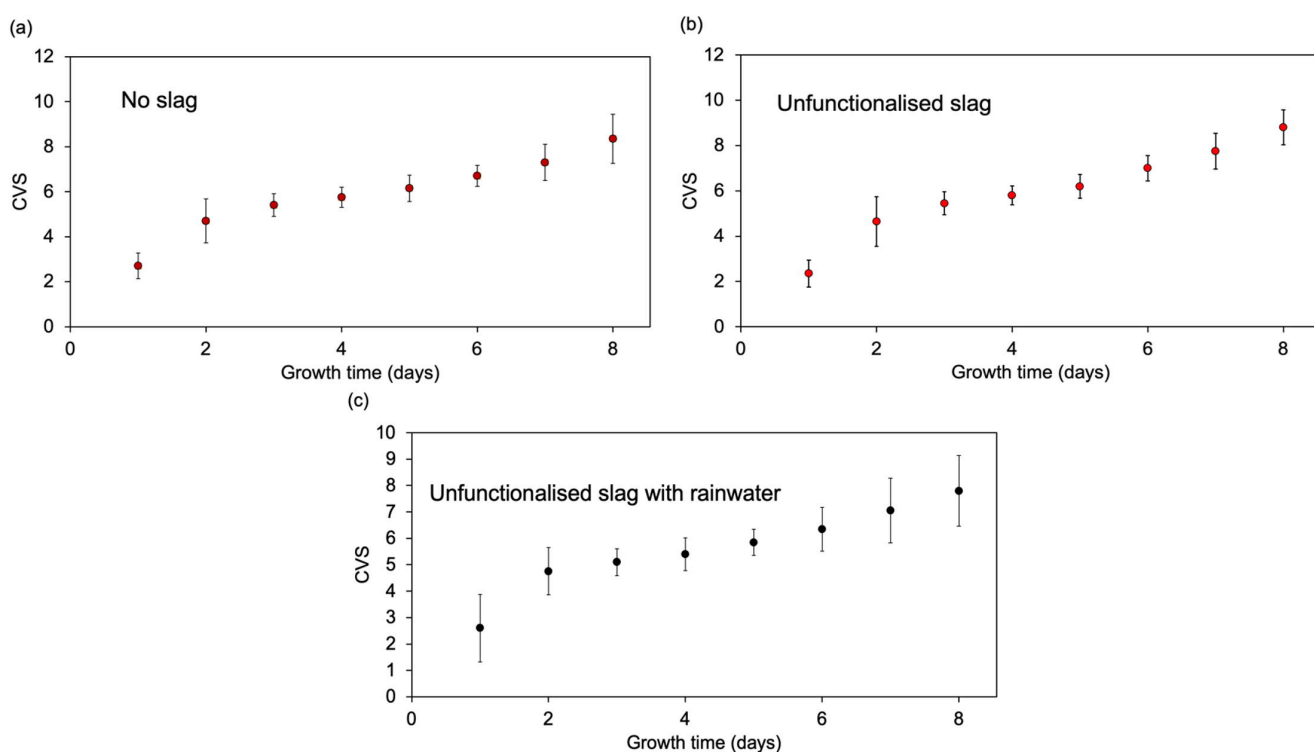


Figure 6. 14: Plots of composite visual growth scores (CVS) for samples studied for (a) no slag, (b) unfunctionalized slag with DI water, and (c) unfunctionalized slag with rainwater. Error bars represent one standard deviation.

In the MP-AES data shown in Table 6.8, it may be seen that the elemental uptake is generally directly proportional to the composition of the water source. The exception is that the high Ca content in rainwater is not replicated by the uptake for the sample with unfunctionalized slag, suggesting that the Ca is absorbed onto the slag rather than the plant. In contrast, there is also a direct correlation with DI water, except that Cu is leached from the slag into the plants.

We note that the calcium content of the rainwater was measured as having a value of 12.35 ppm, not in line with previous data recorded for rainwater from the South Wales area. Previous recordings of Rainwater in South Wales have had readings ranging between 0.085-0.448 ppm) (DEFRA, 2021). This suggests that when the rainwater fell, the precipitation had been transported from an area with high calcium levels in the rainwater.

Table 6. 8: MP-AES data for all samples. The error represents one standard deviation.

Sample	Al (ppm)	Ca (ppm)	Cu (ppm)	Fe (ppm)	K (ppm)	Mg (ppm)	Mn (ppm)	P (ppm)	Si (ppm)	Zn (ppm)
No BOS slag with DI water	0.03 ±0.01	0.18 ±0.04	0.02±0.01	0.12 ±0.12	1.48 ±0.06	0.52 ±0.11	0.04 ±0.01	1.47 ±0.19	0.05 ±0.02	0.02 ±0.01
Unfunctionalized BOS slag with DI water	0.04 ±0.02	0.35 ±0.05	0.52 ±0.22	0.21 ±0.10	1.34 ±0.06	0.45 ±0.06	0.03 ±0.01	1.29 ±0.09	0.10 ±0.03	0.05 ±0.02
Unfunctionalized BOS slag with rainwater	0.02 ±0	0.22 ±0.14	0.01 ±0.01	0.11 ±0.02	1.80 ±0.27	0.52 ±0.08	0.02 ±0.01	1.31 ±0.21	0.07 ±0.03	0.02 ±0.01
DI water	0.01	0.16	0.01	0.1	1.22	0.68	0.02	1.45	0.51	0.01
Rainwater	0.02	12.35	0.01	0.11	1.81	0.60	0.02	1.31	0.5	0.01

It was found that the rainwater had a pH reading of 6.89, and the DI water had a pH reading of 7.03. When the data is compared of samples watered with rainwater and samples watered with DI water, it is clear that the DI water was better for plant growth as these plants grew taller and germinated faster than the other plants. This suggests that high levels of Ca can inhibit plant growth. This has previously been reported that growth is inhibited when cereal wheat is grown with Ca in a 500 µg/mL concentration (He et al., 2018). This is due to calcium toxicity, which has previously been reported when excess calcium is detected within the rhizosphere, the area around the roots, then plant growth rates and germination rates are inhibited (White & Broadley, 2003).

6.4: Conclusions

Overall it can be concluded that the BOS slag worked well as a fertilizer for the samples. This can be seen from the fact that after day 8, a large proportion of the sample sets grew taller than the control set grown with no BOS slag. This can be due to the Ca and Fe nutrients that the BOS slag has provided to the cereal wheat seed. It could be seen that samples functionalized with carboxylic acids to become hydrophobic worked the best because of the water reservoir created around the rhizosphere by the hydrophobic slag; this is in line with previous reports (S. M. Lee et al., 2018). The data also shows that the sample functionalized with cysteic acid did not work as well as fertilizer due to the hydrophilic water-loving nature of the sample, where the water may have been absorbed too quickly by the slag before the seed sample had enough time to absorb the water. We propose that the use of lanolin makes a viable reagent as a low cost sustainable hydrophobic functionalization for BOS slag. It must be noted that the ANOVA tests showed that none of the results were statistically significant. This may suggest that there is no relationship between the BOS slag as fertilizer or that the sample size for the experiment was not large enough to gather enough data on the effects of the BOS slag on the cereal wheat seed.

If BOS slag is to be used as fertilizer, it should be noted that the concentration of heavy metals, *e.g.* V and Cr, in the BOS slag should be screened to check that the concentration is not over the limit and will not do harm to the environment around it. In this case, DI water produced the best results instead of rainwater due to the high Ca content of the rainwater, which may have caused calcium toxicity to occur in the seed, meaning that the growth of the sample was

potentially stunted. This research can be useful in arid regions where water is scarce and is absorbed too quickly by the soil for the seed to get the full benefit, as a hydrophobic layer of slag can be used to create a water reservoir that would provide both water and nutrients to the seed.

Chapter 7: Conclusions and Further Work

7.1: Conclusions

This thesis aimed to assess all available technologies for valorising steelmaking slag in land and marine applications. The literature review found that there was a wide range of different applications that steelmaking slag could be used for due to its composition consisting of precious components to industry, such as calcium oxides and iron oxides. A range of slags from different parts of the steelmaking process was considered as there may have been an application that could be applied to a different slag. The review found that the slags were highly recyclable. There was much research on using slag in the construction industry as aggregate in concrete, cement clinker, or supplementing the cement matrix with calcium silicates. Applications where the slags could be used as received, seemed to be popular as this would mean there was a minimal processing cost for the steelmaking or company using it. Examples of this come from slags used as railway ballast, fertiliser, adsorbent material and CO₂ sequestration; in all examples, the slag can be used as is.

Chapter 3 was a study completed in order to validate if BOS slag from UK steel plants e.g. Tata Steel could be used to sequester carbon emissions. As there was no research testing if slag produced in the UK could be used. There was only research surrounding legacy slag deposits. All the samples proved capable of capturing and sequestering CO₂, with the CO₂ sequestration ability being enhanced when the studies were done in a moist environment. All samples showed high adsorption capacity. It was found that Sample C which had a higher concentration of Ca and Si performed the best out of all samples.

The next area of research completed was static and accelerated leaching experiments looking at the reaction between model sea water and BOS slag. The static experiments were completed over 12 months in static water. The accelerated leaching was completed with model seawater being mechanically stirred over 24 hours. The main findings of the experiments were that Ca, Mg and K were the main elements that leached out. All other elements assessed were only present in trace amounts. There was a direct positive correlation between the Ca concentration and the pH level. The pH level was also heavily influenced by the size fraction of the slag, with the 0-10mm size fraction slag assessed raising the pH by the most in the accelerated leaching experiments. The accelerated leaching experiment highlighted the fact that when the slag is agitated erosion of the slag occurs. This would suggest that if the slag were to be used in a

marine application it should not be used in a structural application as there may be a risk of failure.

BOS slag undergoes functionalisation testing to become hydrophobic or hydrophilic using carboxylic acids in chapter 5. These experiments found that Isosteric acid, Lauric acid, Lanolin and cysteic acid can all be used to functionalise the slag and changes its surface properties. The best hydrophobicity result was achieved with Lauric acid in a 1:1 ratio. This sample achieved a contact angle of $141^{\circ} \pm 4^{\circ}$. Lauric acid proved the best due to its straight-chained nature, creating a more hydrophobic surface. However, each sample's advanced and receding contact angles revealed a large hysteresis between the 2 angles, which suggested the surface had high roughness and was inhomogeneous. The samples also did not follow the expected trend of a higher, more hydrophobic surface with more carboxylic acid being added. Instead, there was no trend, but this was most likely caused by the varying amounts of CaCO_3 , SiO_2 , FeO and Al_2O_3 in each sample. This was successful when cysteic acid was used to make the surface more hydrophilic, and the surface was shown to absorb water faster. Nevertheless, the functionalisation level was found to be inconsistent across the surface. For example, in one area of the pellet, water would absorb in under a second, and in a different section, it would take around 10 seconds for the same amount of water to be absorbed.

The samples from Chapter 5 then underwent a further study in which the slags were used to fertilise wheatgrass plants and assess if the carboxylic acids added had any effect on the plant growth. The study found no significant growth until day 4 of the study, by which point the seeds had germinated and begun to grow roots and a shoot. Seeds germinating any later than day 4 did not grow as a significant a shoot by day 8. The mass gain results showed that the most significant mass gains happened on days 2 and 3 of the study. An ANOVA statistical test was conducted on the plant height data to determine if any results were statistically significantly different. The results found that the only significant comparison data was the Lanolin 1:3 to Isostearic acid 1:1 data. An interesting result was that the germination rate of the sample grown with no slag was faster than the sample grown with unfunctionalized slag, suggesting that the slag inhibited growth in some way. Composite visual score graphs showed that the samples followed a similar growth progression, as all the graphs are similar to S-shape. The MP-AES data of the plants revealed that the carboxylic acids surrounding the slags prevented Fe and Cu from leaching out during the experiment. However, the data showed increased Ca levels leached out of the slag and into the plant in the unfunctionalized and

hydrophobic samples. This Ca, in increased amounts, most likely contributed to plant growth as Ca is known to enhance plant growth. The Lanolin 1:3 sample performed best, and this sample had a high Ca concentration. Lanolin is also a natural lubricant and has previously been used as a medium to transfer nutrients to plants. The hydrophobic nature of the slag also enhanced plant growth as it created a water reservoir around the seed. The samples grown with cysteic acid functionalised slag did not reach the same heights as the others; this was due to the slag's hydrophilic nature, which absorbed the water too fast before the seed had time to benefit. In the rainwater to DI water comparison, rainwater was found to inhibit the growth of the plants. This was thought to be because of the high Ca concentration in the rainwater found in the MP-AES analysis. Extremely high levels of Ca can be toxic to plants.

7.2: Further work

The experimental studies detailed throughout the thesis provided a good idea of how the slag could be utilised. However, there is some further work I would have liked to look at and experiment with. However, this work was not possible due to constraints caused by the COVID-19 pandemic and the time out of the lab environment, but I would like to detail it below.

A helpful topic to explore further from chapter 5 would be a different method of making the contact angle sample. In these tests, a pellet press was used to make a 32mm pellet. However, this pellet would often crumble, for example. It was tough to achieve a consistently uniform flat surface on the pellet. An alternative may be to spray a uniform slag film onto a glass slide and use this to measure the contact angle. It would have also been interesting to see if enhanced hydrophobic effects could be achieved using a combination of carboxylic acids. Lanolin is a by-product of the wool trade that is available in large amounts and is a green product. Whereas lauric acid is not as readily available, It would be interesting to see if the two can be combined for use in an industry where lauric acid may not be as readily available.

Additional time for testing a more extensive sample set of plants would also have been helpful as it may have yielded more statistically significant results. As the slag could be made both hydrophobic and hydrophilic and was not harmful to plants, the research could be applied in arid regions where water is scarce. The hydrophobic slag could channel water towards the seed

and prevent it from evaporating or being absorbed by the soil before reaching it. A follow on from the studies in this thesis would have been to look at the water channelling concept and test it on a lab scale to assess its viability.

Finally, it is imperative to be mindful of the circular economy with the imminent threat of climate change, so an exciting area of work may be to combine several of the applications in this thesis. For example, as received, the slag could be used to sequester CO₂ from the steelmaking process. For optimum results it is suggested that this should be completed in a moist environment. Slag could then undergo a functionalisation process to become either hydrophobic or hydrophilic and could then go on to enhance plant growth. As the slag is working as a fertiliser with only a limited amount of nutrients, the slag may need to be removed and replenished. The removed slag could then go on to be used as one of starting materials for cement. This would permanently store the slag and the CO₂.

Appendix A: Additional Tables for
Chapter 4: Nutrient Leaching
Experiment with Model Sea Water

Table A. 1: Table showing the amounts of Zn, Fe, Cu, Mn, Al and Si found in trace amounts in Jar 1: 5-10mm LF BOS slag over the 12 month duration of the nutrient leaching experiment.

	Zn (ppm)	Fe (ppm)	Cu (ppm)	Mn (ppm)	Al (ppm)	Si (ppm)
T=0	2.72	0.2	0.02	0.03	0	-0.15
24/06/2019	0.7	0.06	0.01	0.003	0.01	0.79
26/07/2019	-0.07	-0.1	0	0.04	-0.01	-0.22
23/08/2019	-0.1	-0.04	0	0.01	0	-0.22
25/09/2019	-0.03	0.03	0	0	0.01	-0.22
18/10/2019	-0.02	0.05	0	0	0	-0.23
18/11/2019	-0.03	0.04	0	0.01	0	-0.22
13/12/2019	-0.02	0.04	0	0	0	-0.22
10/01/2020	0.52	-0.06	0.02	-0.01	0.05	-0.22
07/02/2020	-0.03	0.04	0	0	0	-0.22
06/03/2020	-0.03	0.04	0	0.01	0	-0.2
03/04/2020	-0.02	0.05	0	0.01	0	-0.22
29/04/2020	-0.03	0.04	0	0.01	0	-0.2

Table A. 2: Table showing the amounts of Zn, Fe, Cu, Mn, Al and Si found in trace amounts in Jar 2: 45 mm HF BOS slag over the 12 month duration of the nutrient leaching experiment.

	Zn (ppm)	Fe (ppm)	Cu (ppm)	Mn (ppm)	Al (ppm)	Si (ppm)
T=0	2.72	0.2	0.02	0.03	0	-0.15
24/06/2019	-0.01	0.05	0.01	0.01	0.01	-0.09
26/07/2019	-0.14	-0.12	0	0.04	-0.01	-0.22
23/08/2019	-0.04	0	0	0.02	0	-0.22
25/09/2019	-0.03	0.02	0	0.01	0	-0.23
18/10/2019	-0.02	0.05	0	0	0	-0.23
18/11/2019	-0.03	0.04	0	0.01	0	-0.22
13/12/2019	-0.03	0.04	0	0	0	-0.23
10/01/2020	0.03	-0.07	0.02	0	0.05	-0.22
07/02/2020	-0.03	0.03	0	0.01	0	-0.22
06/03/2020	-0.02	0.05	0	0	0	-0.23
03/04/2020	-0.03	0.05	0	0.01	0	-0.22

29/04/2020	-0.02	0.06	0	0.01	0	-0.22
------------	-------	------	---	------	---	-------

Table A. 3: Table showing the amounts of Zn, Fe, Cu, Mn, Al and Si found in trace amounts in Jar 3: 45 mm LF BOS slag over the 12 month duration of the nutrient leaching experiment.

	Zn (ppm)	Fe (ppm)	Cu (ppm)	Mn (ppm)	Al (ppm)	Si (ppm)
T=0	2.72	0.2	0.02	0.03	0	-0.15
24/06/2019	-0.01	0.05	0.01	0	0	-0.12
26/07/2019	-0.12	-0.12	0	0.04	-0.01	-0.24
23/08/2019	-0.04	0.02	0	0	0	-0.22
25/09/2019	-0.09	-0.11	0	0.04	-0.01	-0.22
18/10/2019	-0.02	0.05	0	0	0	-0.21
18/11/2019	-0.03	0.05	0	0	0	-0.21
13/12/2019	-0.03	0.03	0	0.01	0	-0.21
10/01/2020	0.02	0.07	0.2	0	0.05	-0.22
07/02/2020	-0.03	0.04	0	0.01	0	-0.2
06/03/2020	-0.03	0.05	0	0.01	0	-0.22
03/04/2020	-0.03	0.05	0	0	0	-0.17
29/04/2020	-0.05	0.05	0	0.01	0	-0.17

Table A. 4: Table showing the amounts of Zn, Fe, Cu, Mn, Al and Si found in trace amounts in Jar 4: 0-10 mm LF BOS slag over the 12 month duration of the nutrient leaching experiment.

	Zn (ppm)	Fe (ppm)	Cu (ppm)	Mn (ppm)	Al (ppm)	Si (ppm)
T=0	2.72	0.2	0.02	0.03	0	-0.15
24/06/2019	-0.01	0.05	0.01	0	0	-0.16
26/07/2019	-0.14	-0.12	0	0.04	-0.01	-0.21
23/08/2019	-0.03	0.03	0	0.01	0	-0.22
25/09/2019	-0.16	-0.13	0	0.04	-0.01	-0.23
18/10/2019	-0.02	0.05	0	0	0	-0.22
18/11/2019	-0.02	0.04	0	0	0	-0.23
13/12/2019	-0.04	0.04	0	0	0	-0.22
10/01/2020	0.01	-0.07	0.01	-0.01	0.06	-0.22
07/02/2020	-0.04	0.04	0	0.01	0	-0.22

06/03/2020	-0.03	0.04	0	0.01	0	-0.23
03/04/2020	-0.04	0.04	0	0.01	0	-0.17
29/04/2020	-0.03	0.04	0	0.01	0	-0.21

Appendix B: Additional Figures for
Chapter 5: Functionalization of Basic
Oxygen Steelmaking Slag

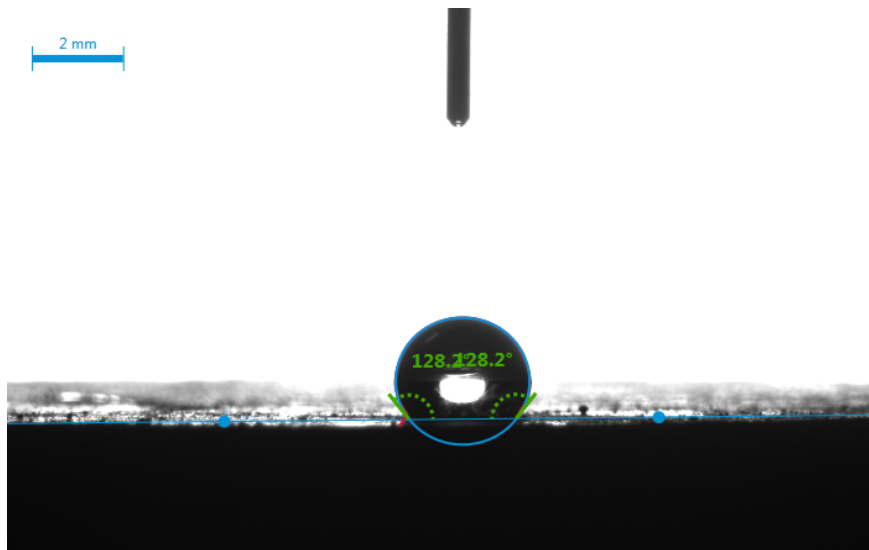


Figure B. 1: Contact angle measurement of isosteric acid functionalised BOS slag (1:1)

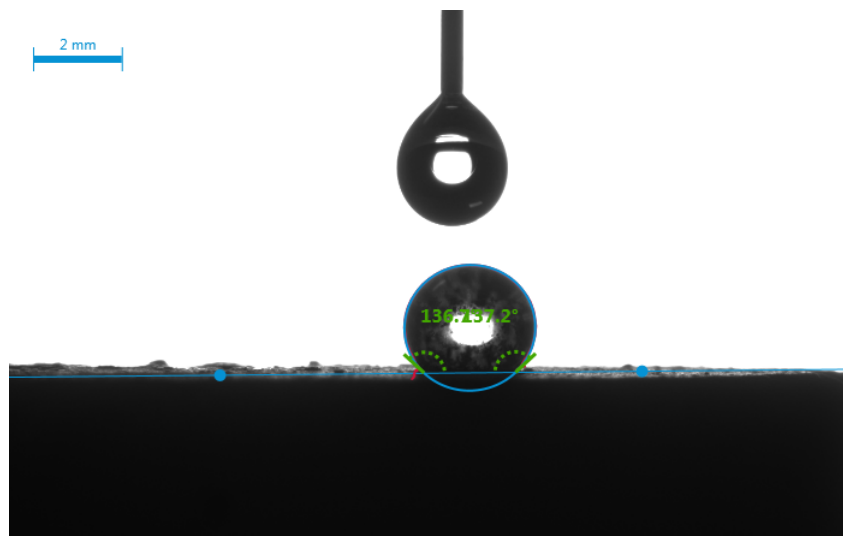


Figure B. 2: Contact angle measurement of isosteric acid functionalised BOS slag (1:1.25)

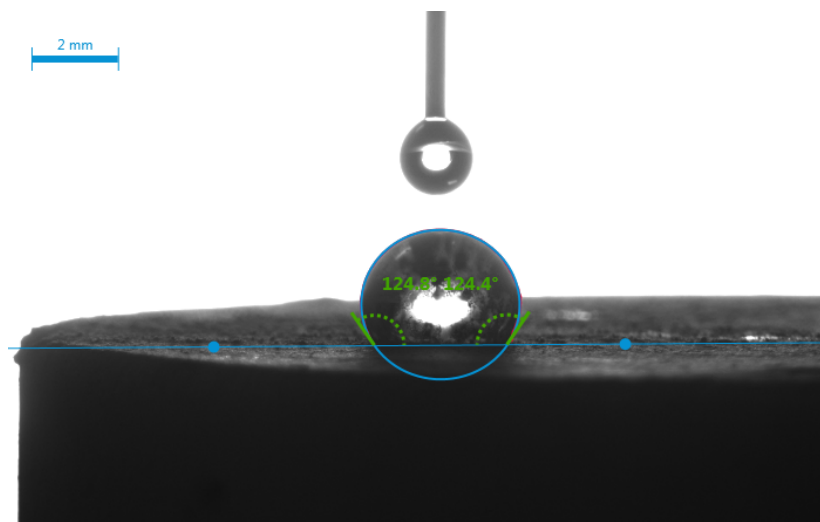


Figure B. 3: Contact angle measurement of isosteric acid functionalised BOS slag (1:1.5)

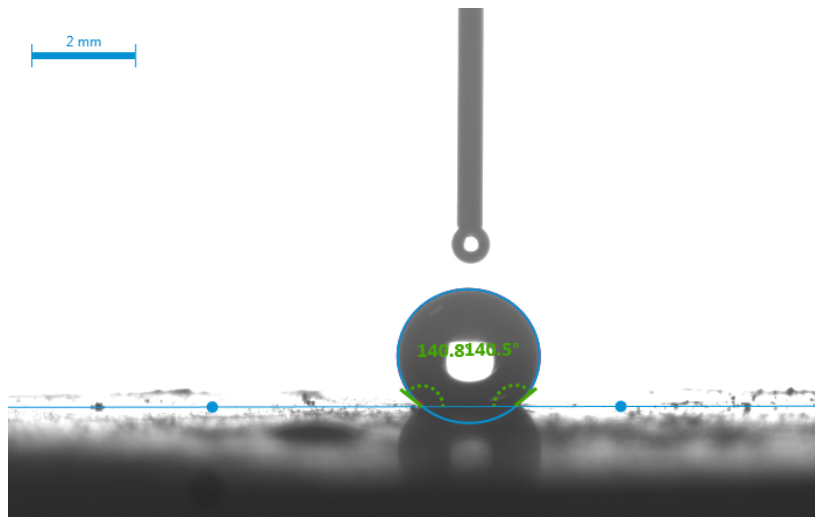


Figure B. 4: Contact angle measurement of Lauric acid functionalised BOS slag (1:1)

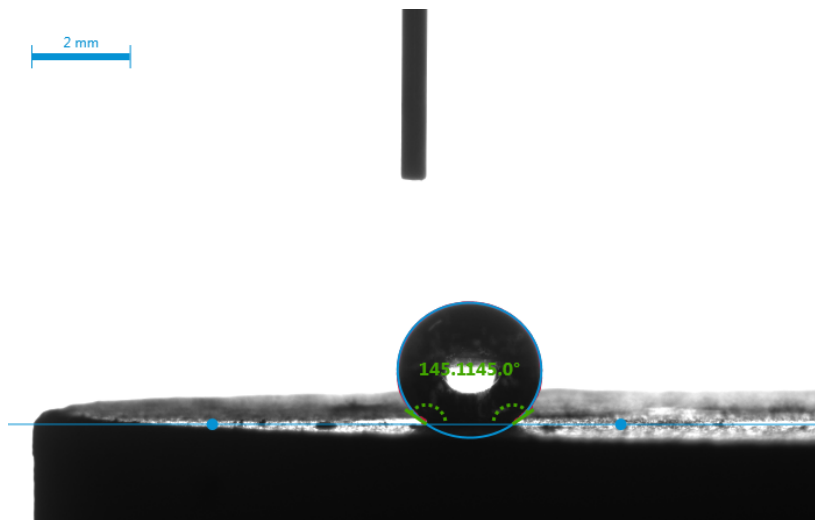


Figure B. 5: Contact angle measurement of Lauric acid functionalised BOS slag (1:1.25)

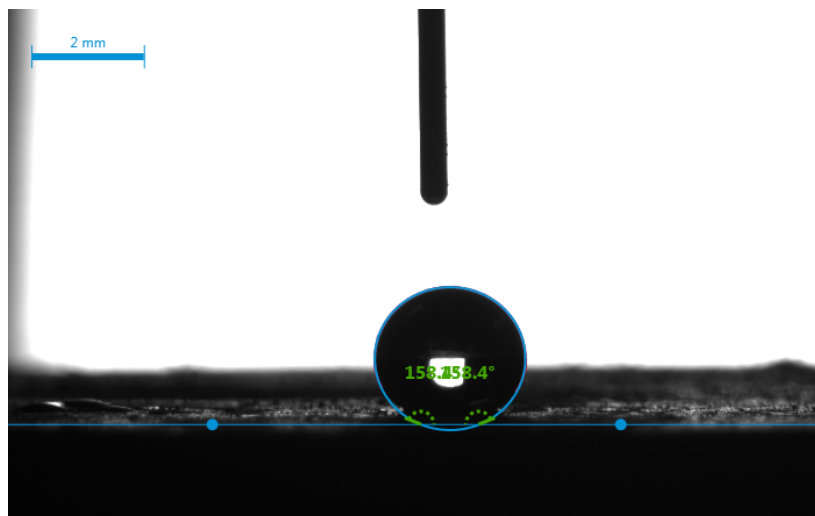


Figure B. 6: Contact angle measurement of Lauric acid functionalised BOS slag (1:1.5)

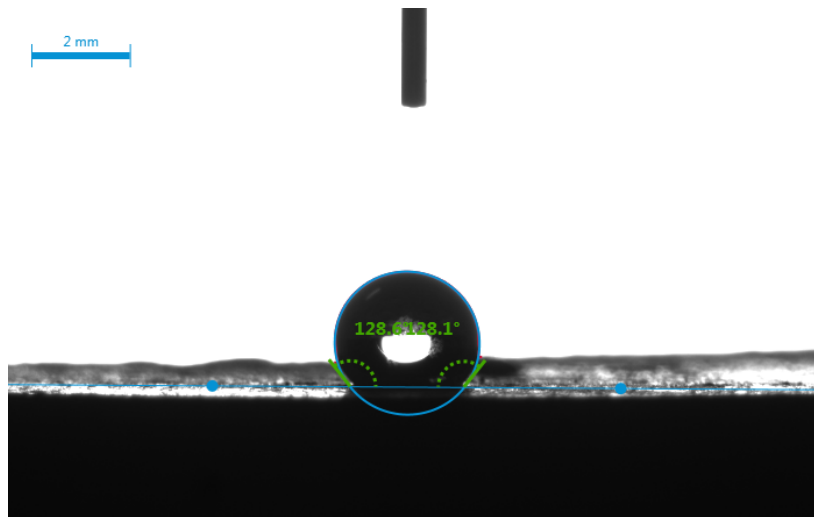


Figure B. 7: Contact angle measurement of Lanolin functionalised BOS slag (1:2)

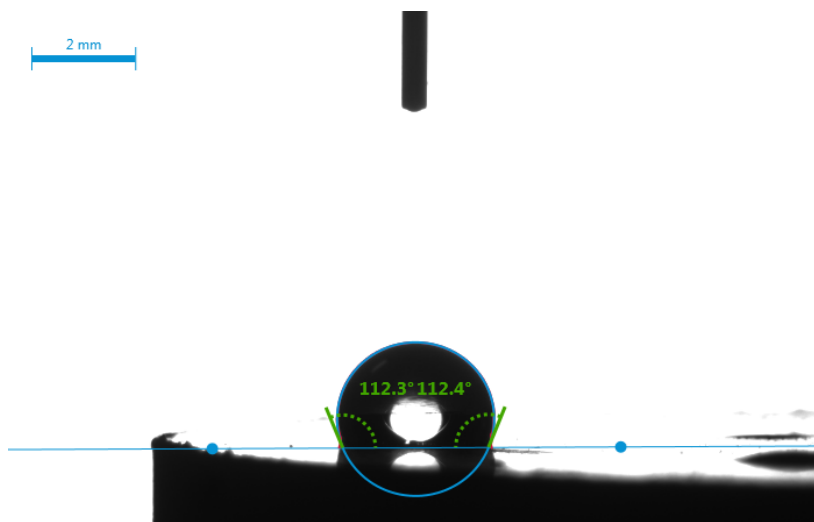


Figure B. 8: Contact angle measurement of Lanolin functionalised BOS slag (1:3)

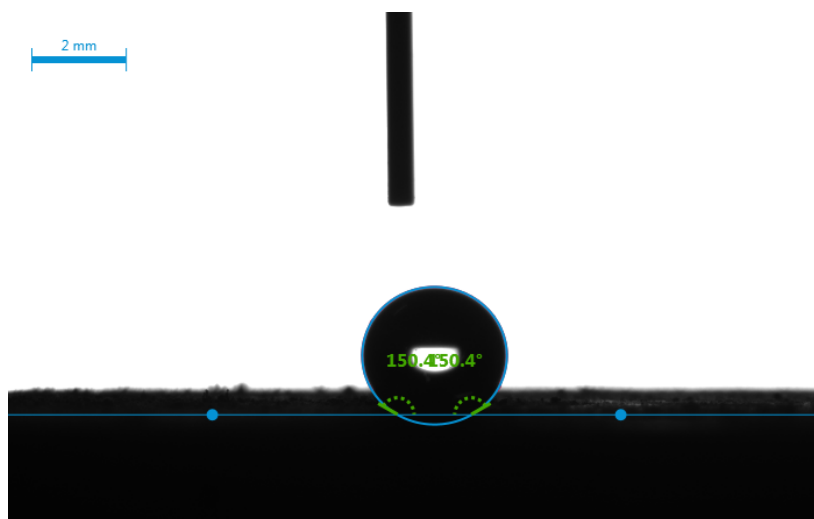


Figure B. 9: Contact angle measurement of isosteric acid functionalised BOS slag (1:5)

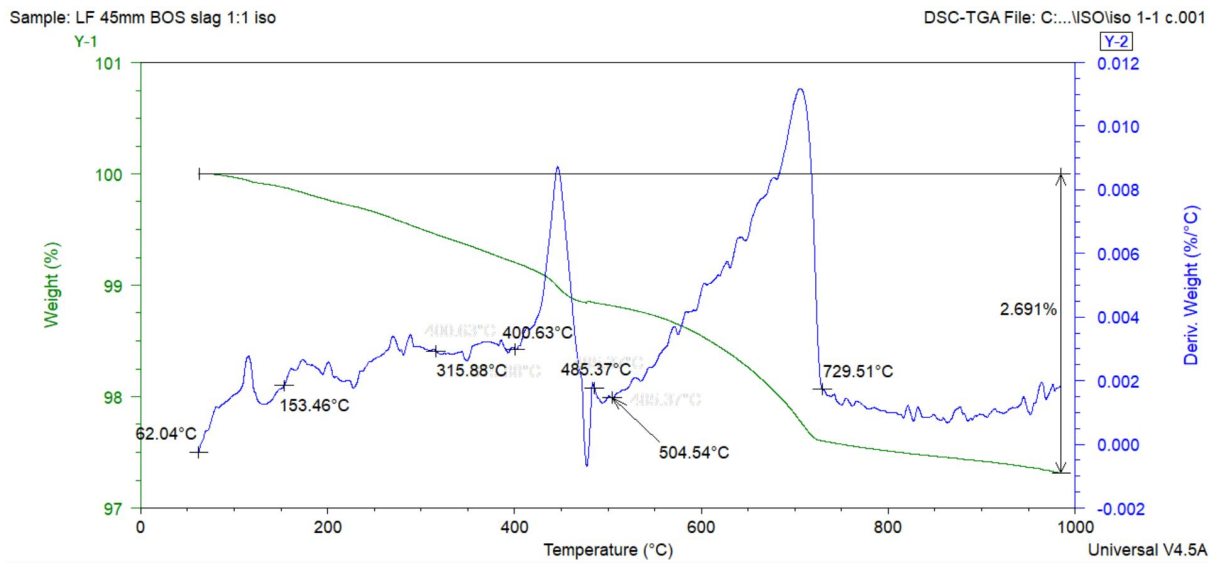


Figure B. 10: TGA plot used to calculate grafting density of BOS slag: Isosteric acid in a 1:1 ratio.

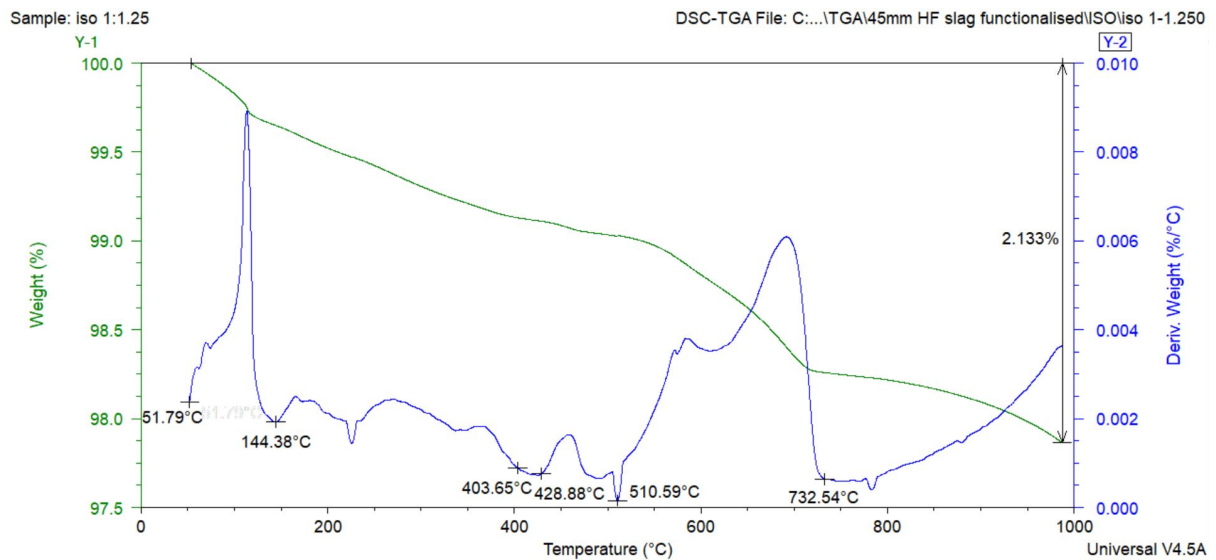


Figure B. 11: TGA plot used to calculate grafting density of BOS slag: Isosteric acid in a 1:1.25 ratio.

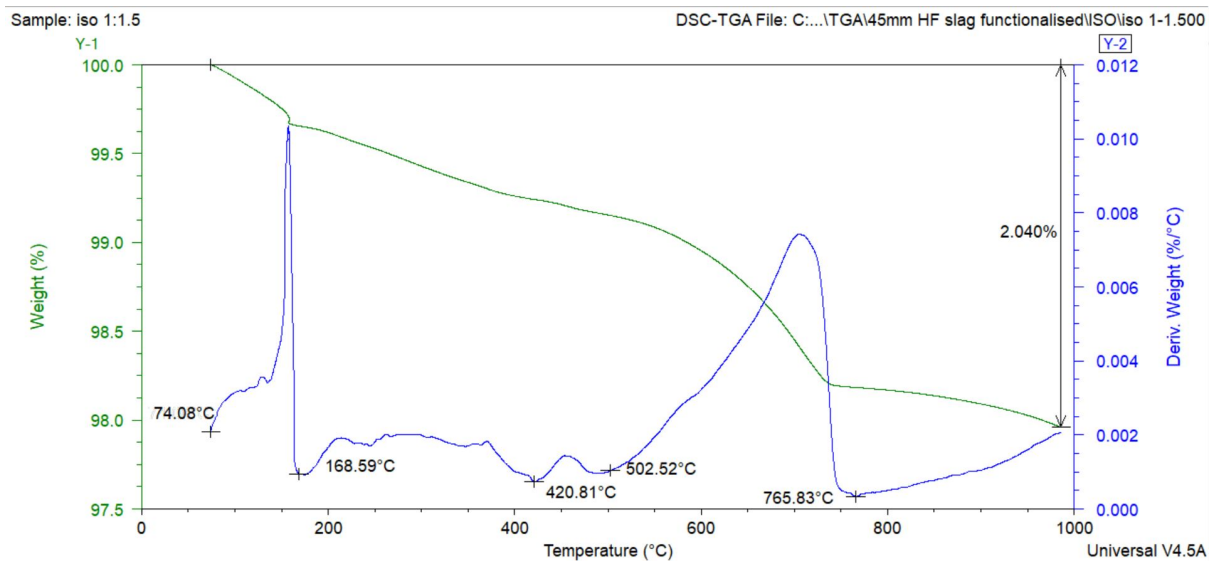


Figure B. 12: TGA plot used to calculate grafting density of BOS slag: Isosteric acid in a 1:1.5 ratio.

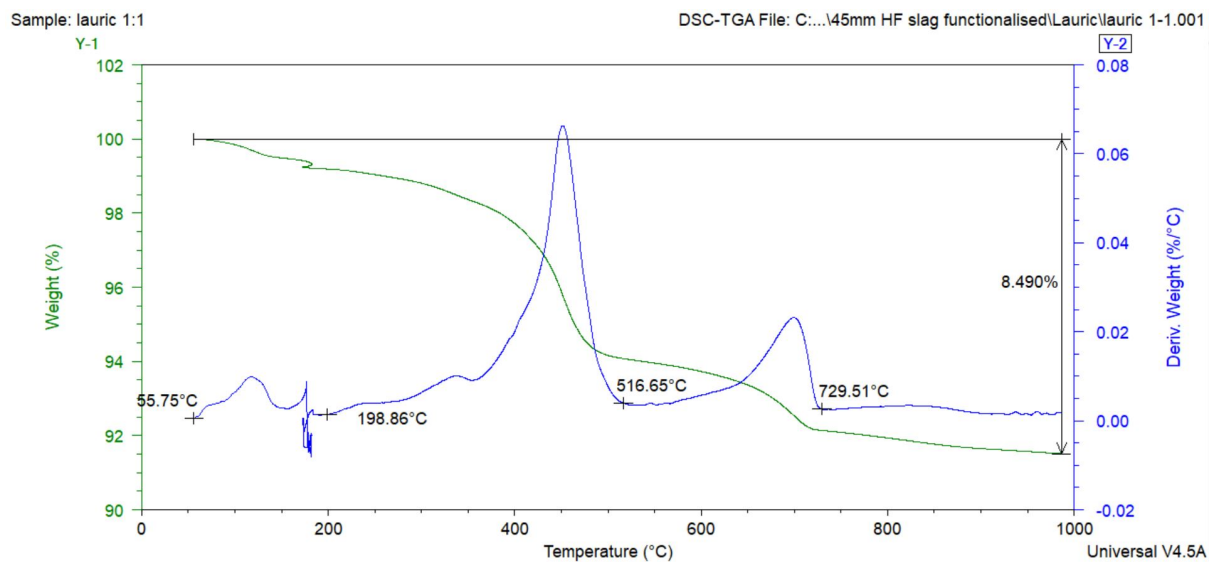


Figure B. 13: TGA plot used to calculate grafting density of BOS slag: Lauric acid in a 1:1 ratio.

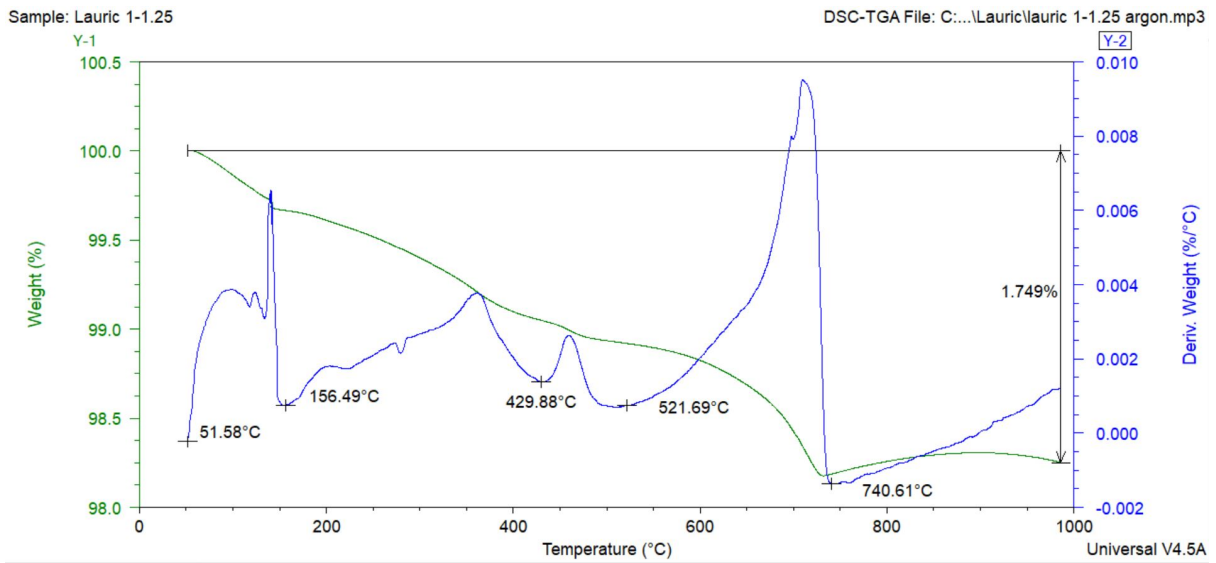


Figure B. 14: TGA plot used to calculate grafting density of BOS slag: Lauric acid in a 1:1.25 ratio.

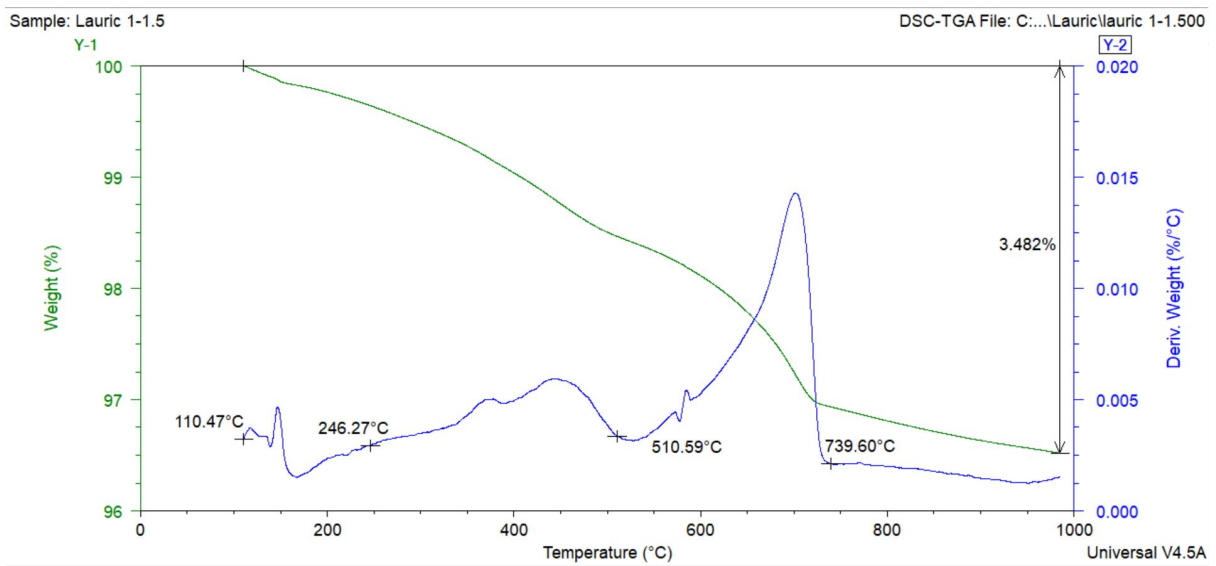


Figure B. 15: TGA plot used to calculate grafting density of BOS slag: Lauric acid in a 1:1.5 ratio.

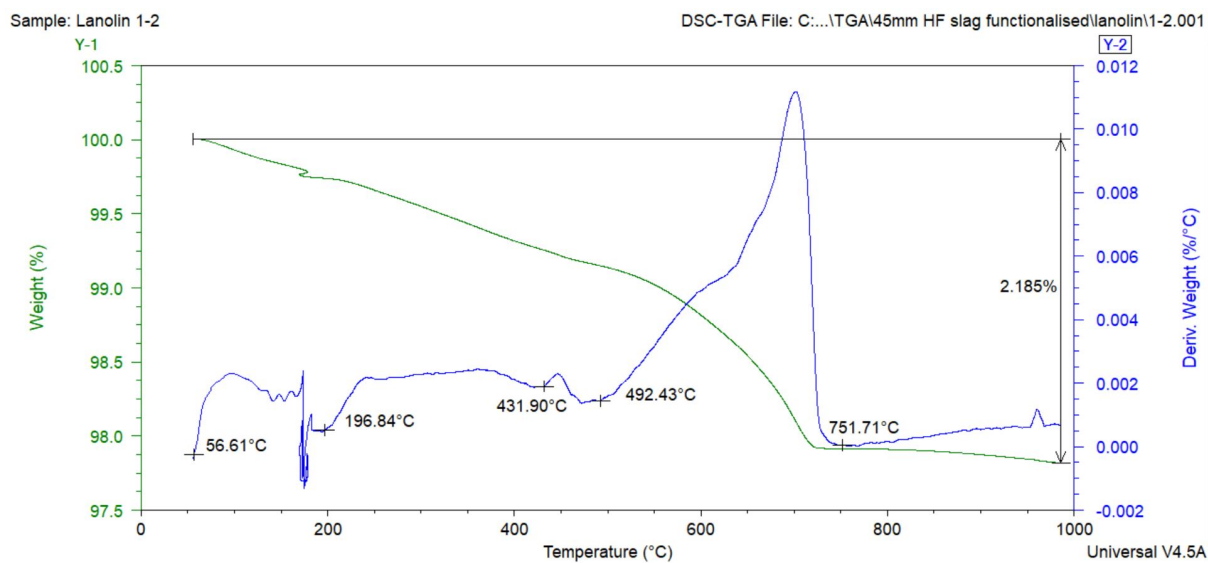


Figure B. 16: TGA plot used to calculate grafting density of BOS slag: Lanolin in a 1:2 ratio.

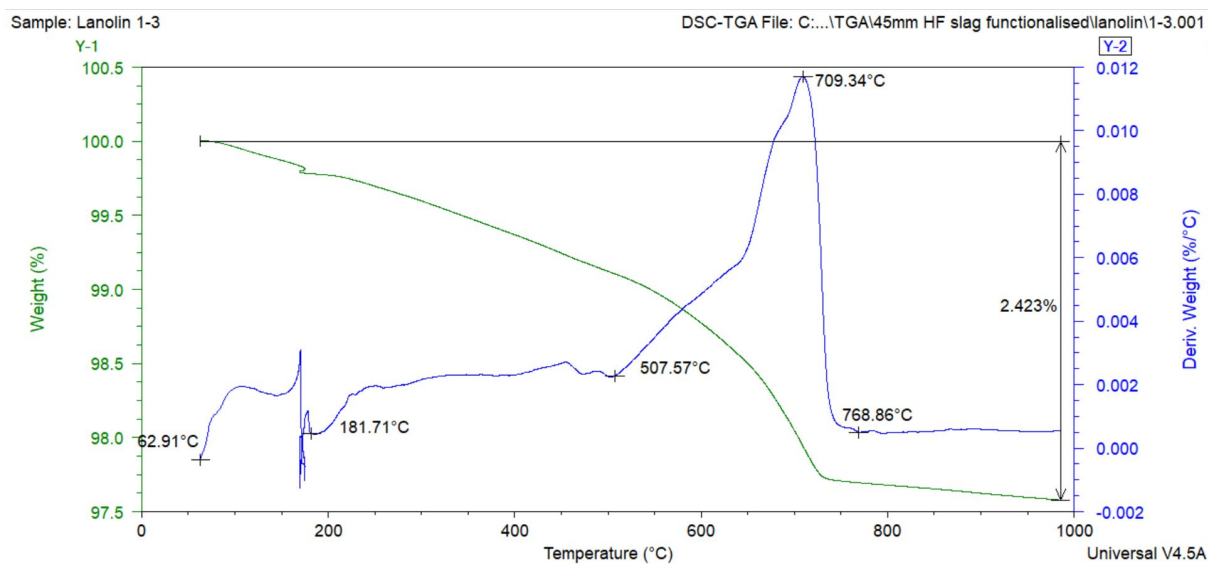


Figure B. 17: TGA plot used to calculate grafting density of BOS slag: Lanolin in a 1:3 ratio.

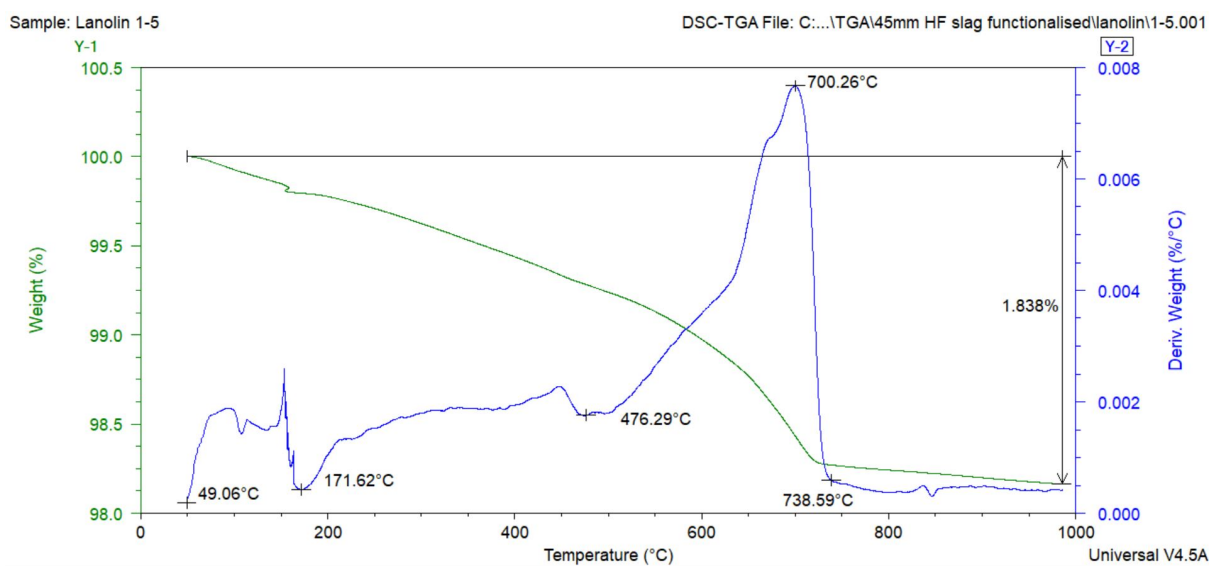


Figure B. 18: TGA plot used to calculate grafting density of BOS slag: Lanolin in a 1:5 ratio.

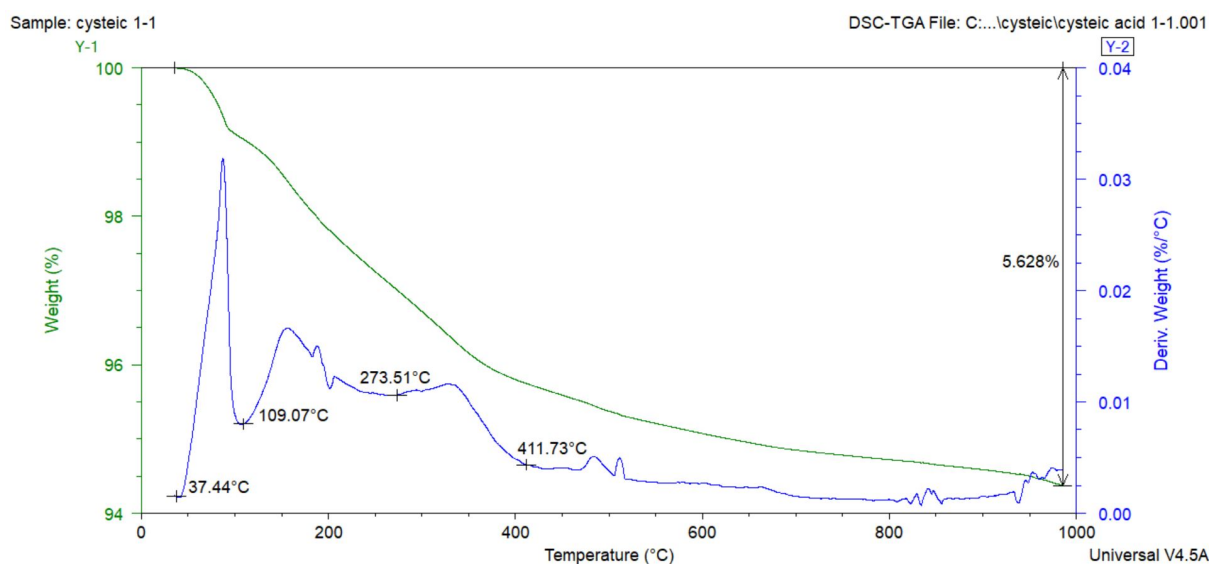


Figure B. 19: TGA plot used to calculate grafting density of BOS slag: Cysteic Acid in a 1:1 ratio.

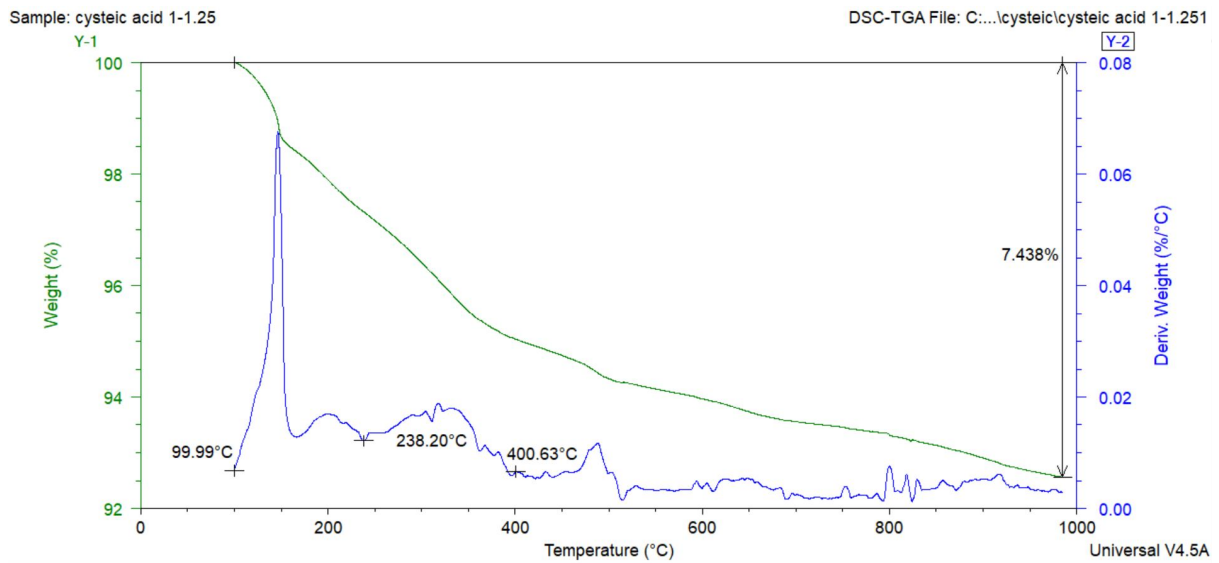


Figure B. 20: TGA plot used to calculate grafting density of BOS slag: Cysteic Acid in a 1:1.25 ratio.

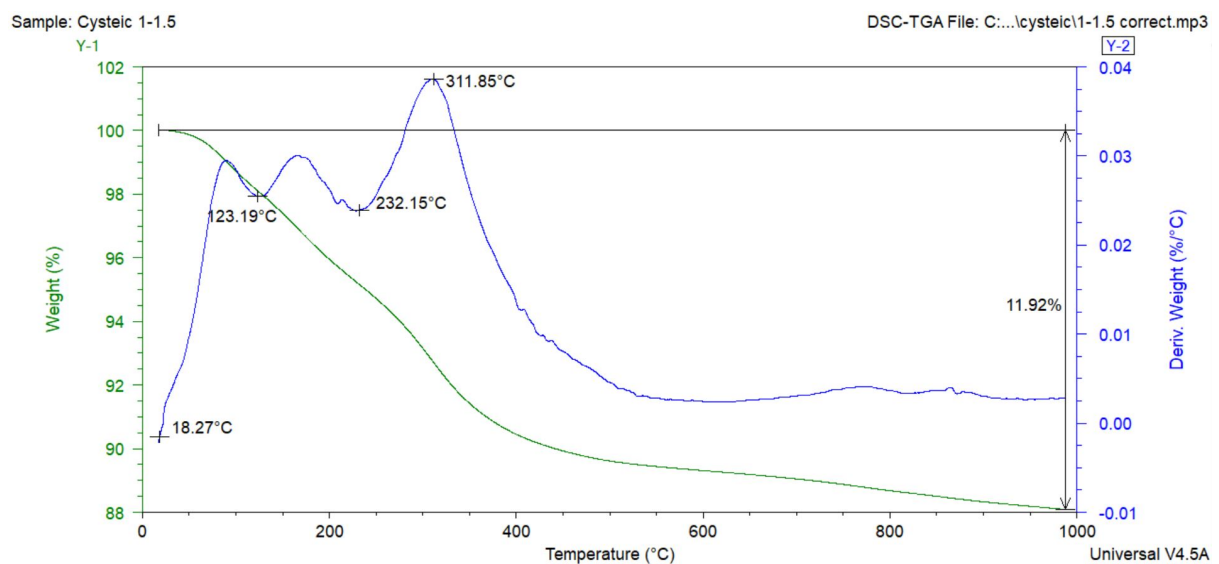


Figure B. 21: TGA plot used to calculate grafting density of BOS slag: Cysteic Acid in a 1:1.5 ratio.

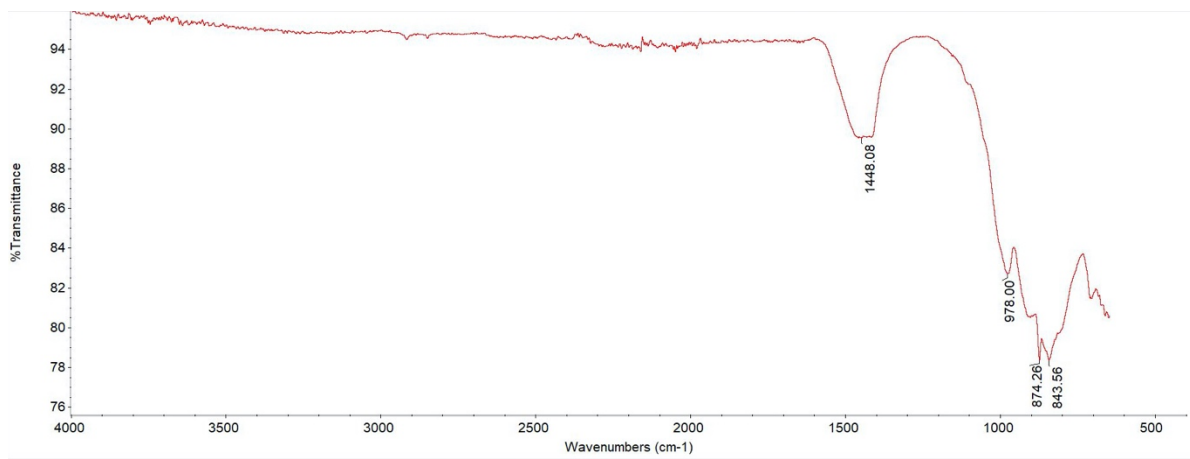


Figure B. 22: FTIR spectra of isosteric acid functionalised BOS slag (1:1)

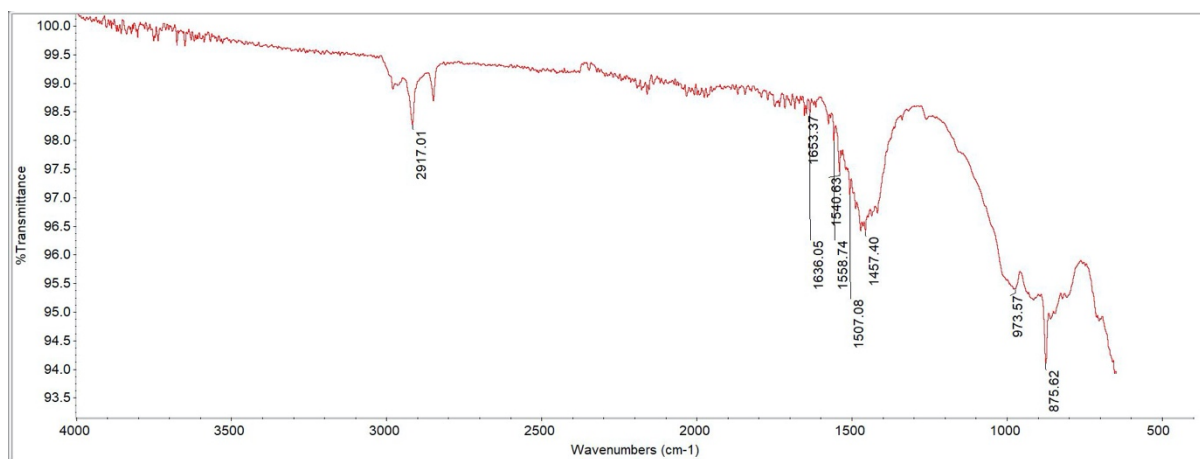


Figure B. 23: FTIR spectra of isosteric acid functionalised BOS slag (1:1.25)

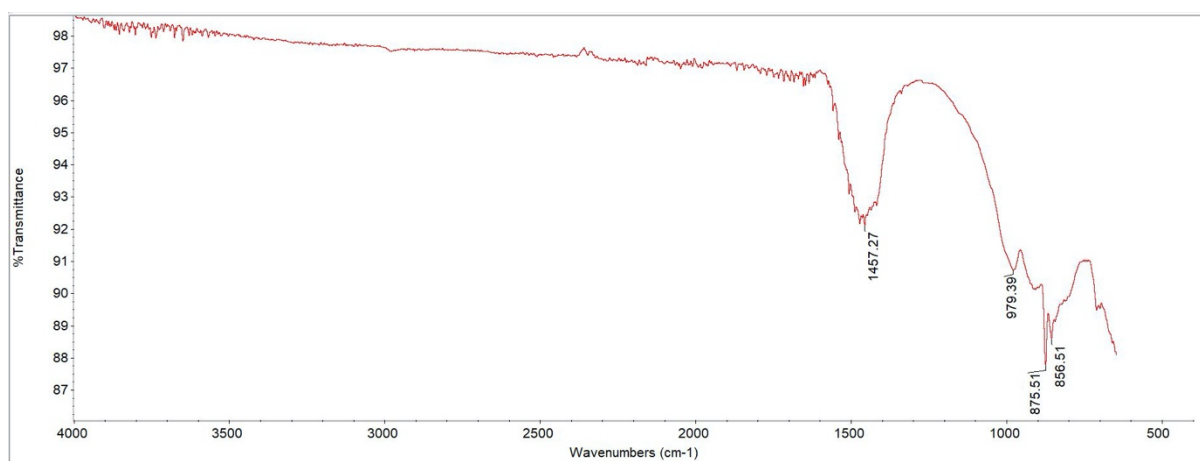


Figure B. 24: FTIR spectra of isosteric acid functionalised BOS slag (1:1.5)

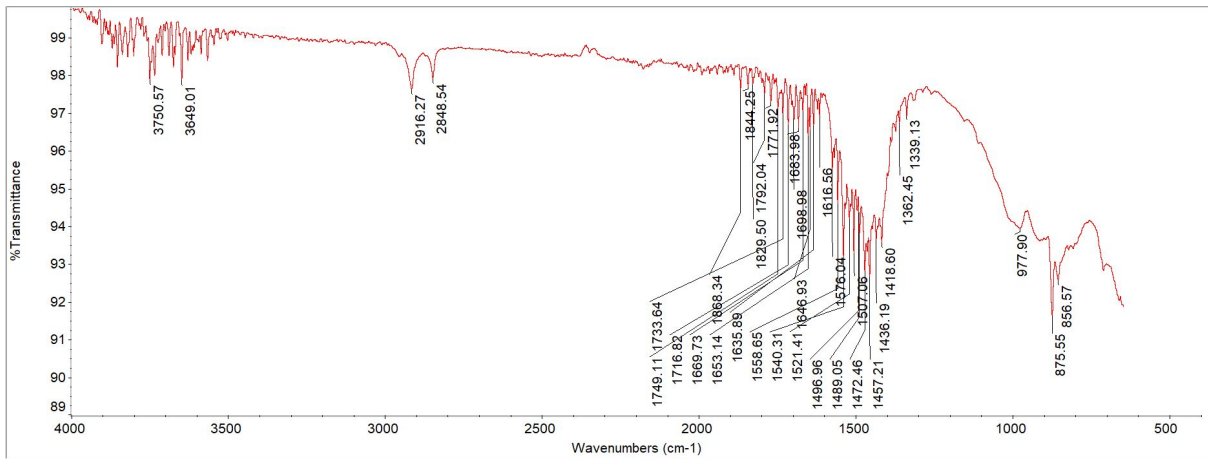


Figure B. 25: FTIR spectra of Lauric acid functionalised BOS slag (1:1)

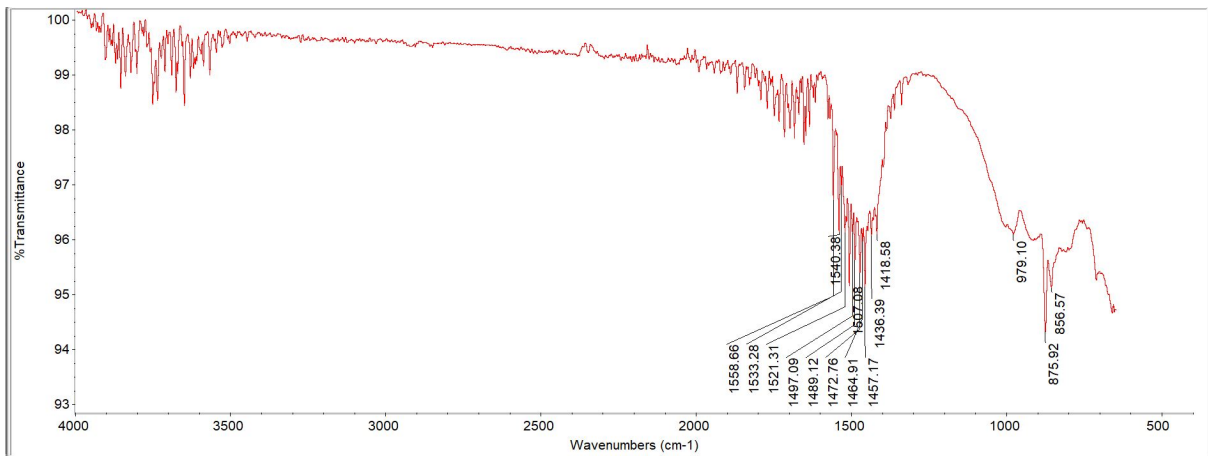


Figure B. 26: FTIR spectra of Lauric acid functionalised BOS slag (1:1.25)

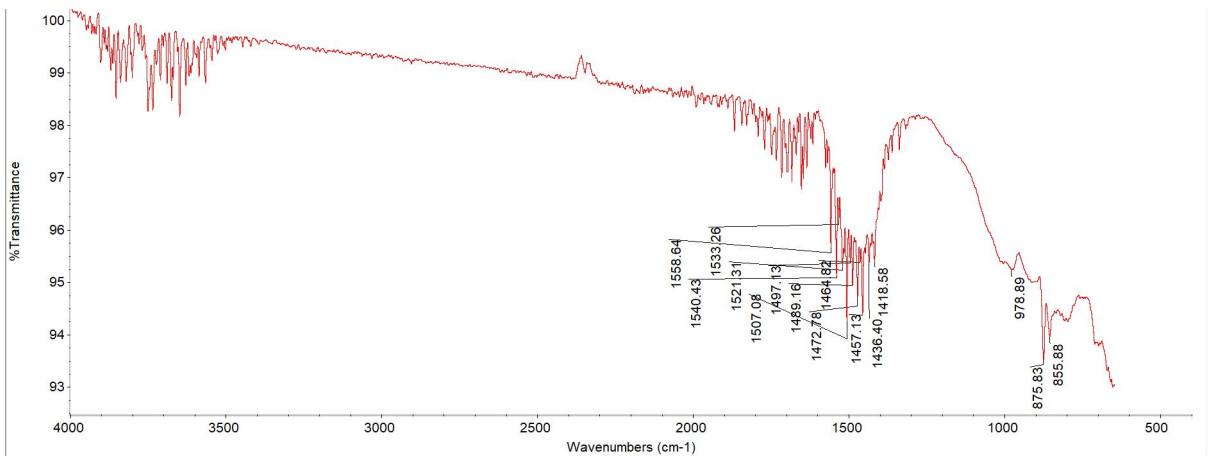


Figure B. 27: FTIR spectra of Lauric acid functionalised BOS slag (1:1.5)

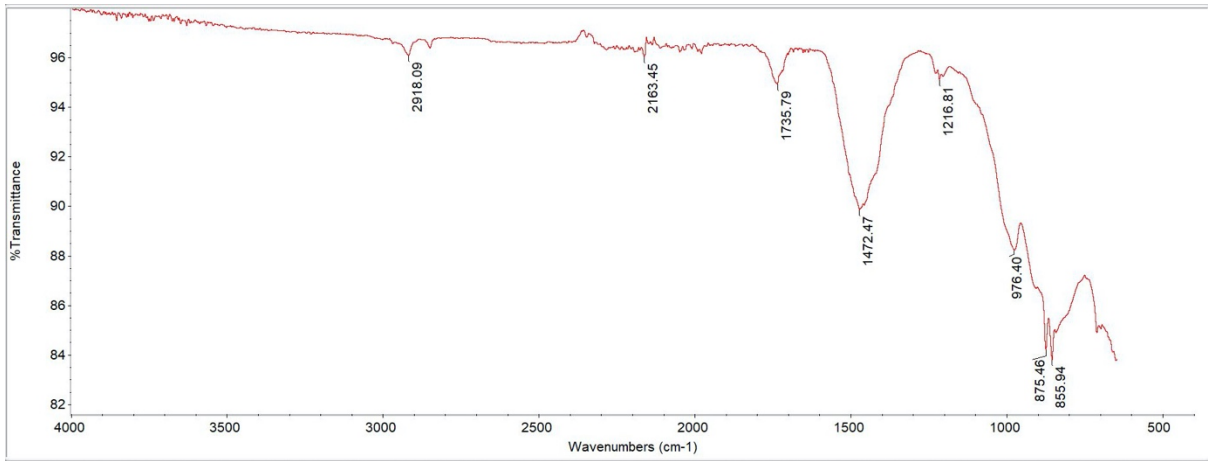


Figure B. 28: FTIR spectra of Lanolin functionalised BOS slag (1:2)

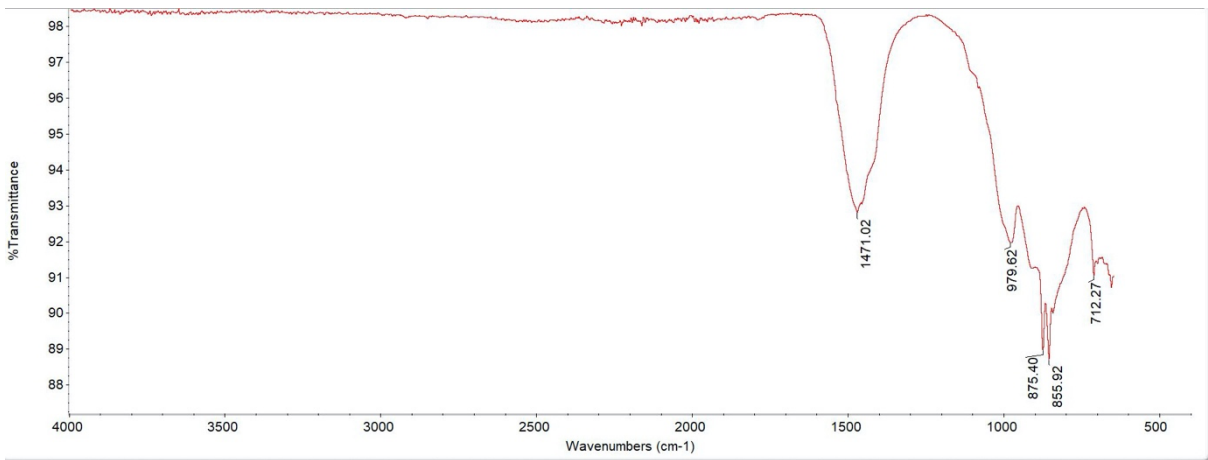


Figure B. 29: FTIR spectra of Lanolin functionalised BOS slag (1:3)

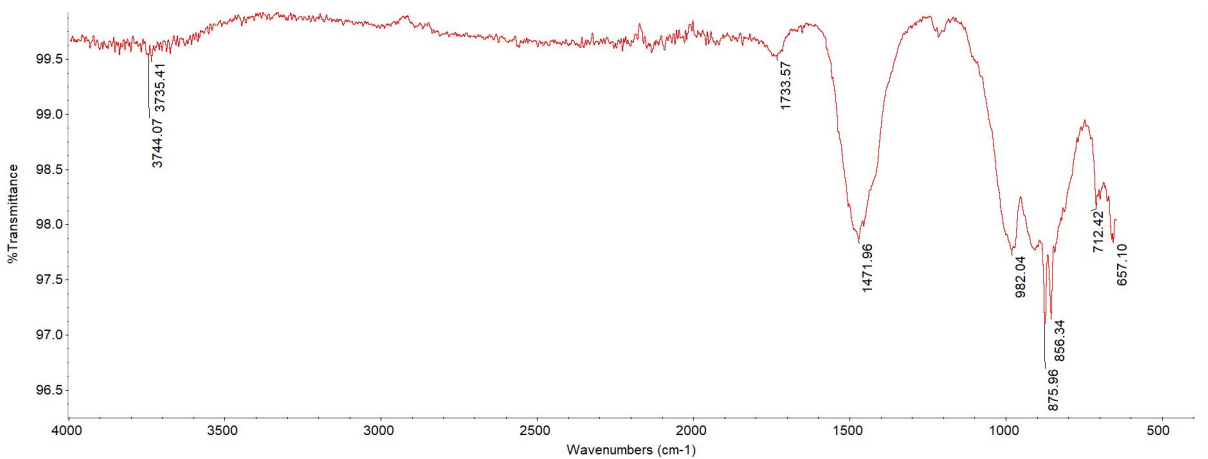


Figure B. 30: FTIR spectra of Lanolin functionalised BOS slag (1:5)

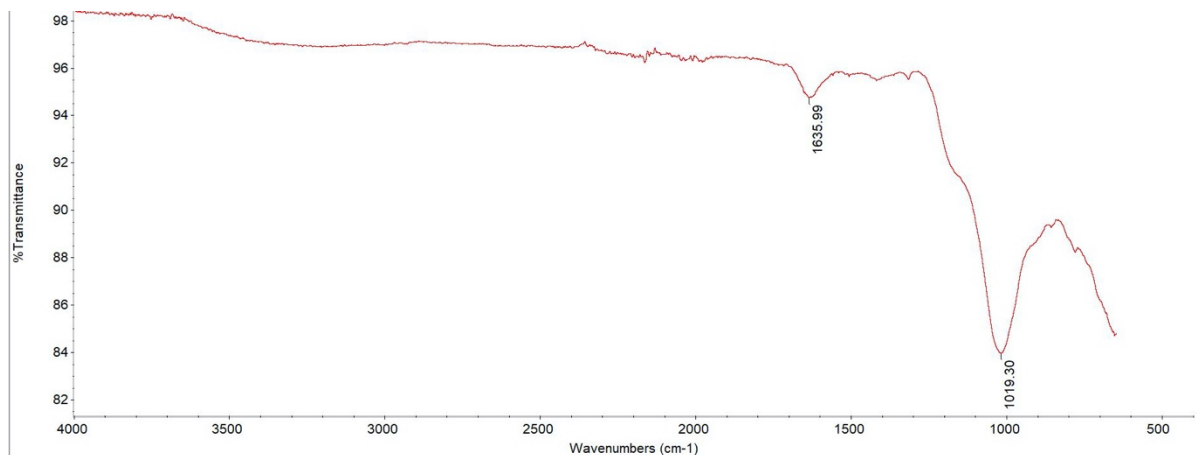


Figure B. 31: FTIR spectra of Cysteic acid functionalised BOS slag (1:1)

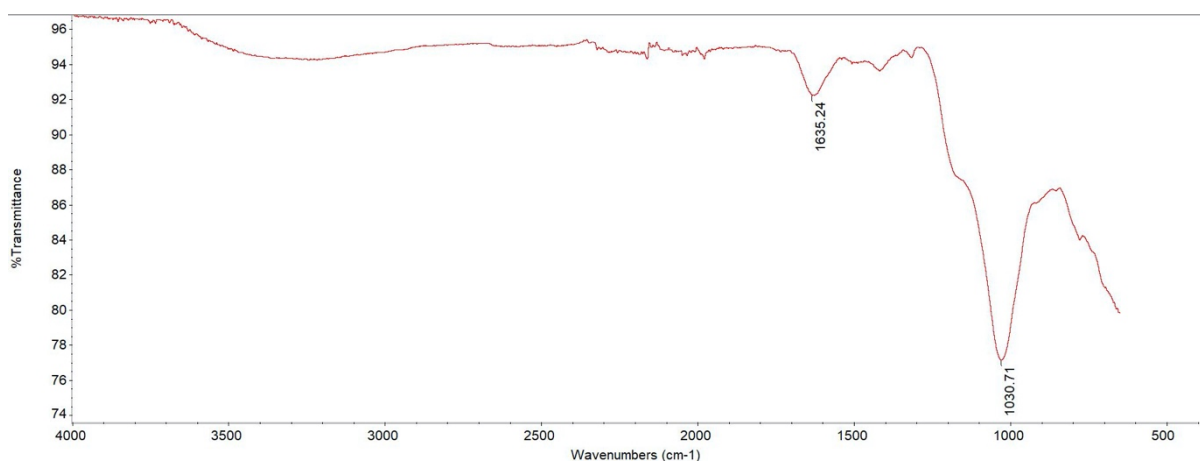


Figure B. 32: FTIR spectra of Cysteic acid functionalised BOS slag (1:1.25)

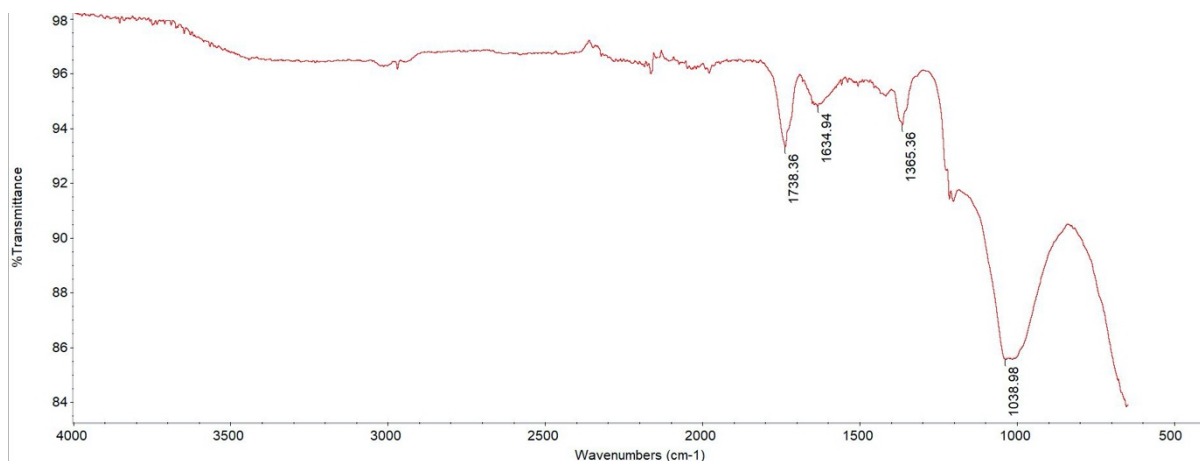


Figure B. 33: FTIR spectra of Cysteic acid functionalised BOS slag (1:1.5)

Bibliography

Abeywardena, M. R., Yashomala, M. A. D. H., Elkaduwe, R. K. W. H. M. K., Karunaratne, D. G. G. P., Pitawala, H. M. T. G. A., Rajapakse, R. M. G., Manipura, A., & Mantilaka, M. M. G. P. G. (2021). Fabrication of water-repellent polyester textile via dip-coating of in-situ surface-modified superhydrophobic calcium carbonate from dolomite. *Colloids and Surfaces A: Physicochemical and Engineering Aspects*, 629, 127397. <https://doi.org/10.1016/j.colsurfa.2021.127397>

Agilent. (2021). *Microwave Plasma Atomic Emission Spectroscopy (MP-AES) Application eHandbook*. https://www.agilent.com/cs/library/applications/5991-7282EN_MP-AES-eBook.pdf. Date accessed: 14/11/2022.

Alcock, N. W., Tracy, V. M., & Waddington, T. C. (1976). Acetates and acetate-complexes. Part 1. Preparation of acetato-complexes and conductimetric studies in the acetic anhydride solvent system. *Journal of the Chemical Society, Dalton Transactions*, 21, 2238. <https://doi.org/10.1039/dt9760002238>

Alexander, S., Eastoe, J., Lord, A. M., Guittard, F., & Barron, A. R. (2016). Branched Hydrocarbon Low Surface Energy Materials for Superhydrophobic Nanoparticle Derived Surfaces. *ACS Applied Materials and Interfaces*, 8(1), 660–666. <https://doi.org/10.1021/acsami.5b09784>

Alfaro, M. R., Ugarte, O. M., Lima, L. H. V., Silva, J. R., da Silva, F. B. V., da Silva Lins, S. A., & do Nascimento, C. W. A. (2021). Risk assessment of heavy metals in soils and edible parts of vegetables grown on sites contaminated by an abandoned steel plant in Havana. *Environmental Geochemistry and Health*. <https://doi.org/10.1007/s10653-021-01092-w>

Al-Shatty, W., Lord, A. M., Alexander, S., & Barron, A. R. (2017). Tunable Surface Properties of Aluminum Oxide Nanoparticles from Highly Hydrophobic to Highly Hydrophilic. *ACS Omega*, 2(6), 2507–2514. <https://doi.org/10.1021/acsomega.7b00279>

Andrade, H. D., de Carvalho, J. M. F., Costa, L. C. B., Elói, F. P. da F., e Silva, K. D. do C., & Peixoto, R. A. F. (2021). Mechanical performance and resistance to carbonation of steel slag reinforced concrete. *Construction and Building Materials*, 298.

<https://doi.org/10.1016/j.conbuildmat.2021.123910>

Annunziata Branca, T., Pistocchi, C., Colla, V., Ragolini, G., Amato, A., Tozzini, C., Mudersbach, D., Morillon, A., Rex, M., & Romaniello, L. (2014). Investigation of (BOF) Converter slag use for agriculture in Europe. *Metallurgical Research & Technology*, 111(3), 155–167. <https://doi.org/10.1051/metal/2014022>

Anton Paar. (2021). *BET Theory*. <https://wiki.anton-paar.com/se-en/bet-theory/#bet-equation>. Date Accessed: 20/11/2022.

Arbatan, T., Fang, X., & Shen, W. (2011). Superhydrophobic and oleophilic calcium carbonate powder as a selective oil sorbent with potential use in oil spill clean-ups. *Chemical Engineering Journal*, 166(2), 787–791. <https://doi.org/10.1016/j.cej.2010.11.015>

ASTM International. (2003). *D 1141-98 (Reapproved 2003) Standard Practice for the Preparation of Substitute Ocean Water 1*. www.astm.org

Athauda, T. J., Decker, D. S., & Ozer, R. R. (2012). Effect of surface metrology on the wettability of SiO₂ nanoparticle coating. *Materials Letters*, 67(1), 338–341. <https://doi.org/10.1016/j.matlet.2011.09.100>

Barka, N., Ouzaouit, K., Abdennouri, M., & Makhfouk, M. El. (2013). Dried prickly pear cactus (*Opuntia ficus indica*) cladodes as a low-cost and eco-friendly biosorbent for dyes removal from aqueous solutions. *Journal of the Taiwan Institute of Chemical Engineers*, 44(1), 52–60. <https://doi.org/10.1016/j.jtice.2012.09.007>

Bethley, C. E., Aitken, C. L., Harlan, C. J., Koide, Y., Bott, S. G., & Barron, A. R. (1997). Structural Characterization of Dialkylaluminum Carboxylates: Models for Carboxylate Alumoxanes. *Organometallics*, 16(3), 329–341. <https://doi.org/10.1021/om960576q>

Branca, T. A., Colla, V., Algermissen, D., Granbom, H., Martini, U., Morillon, A., Pietruck, R., & Rosendahl, S. (2020). Reuse and Recycling of By-Products in the Steel Sector: Recent Achievements Paving the Way to Circular Economy and Industrial Symbiosis in Europe. *Metals*, 10(3), 345. <https://doi.org/10.3390/met10030345>

Branca, T., Fornai, B., Colla, V., Pistocchi, C., & Ragolini, G. (2019). *APPLICATION OF BASIC OXYGEN FURNACE (BOFS) IN AGRICULTURE: A STUDY ON THE ECONOMIC VIABILITY AND EFFECTS ON THE SOIL* (Vol. 18, Issue 6).

<http://www.eemj.icpm.tuiasi.ro/>; <http://www.eemj.eu>

Brdar, M., Šćiban, M., Takači, A., & Došenović, T. (2012). Comparison of two and three parameters adsorption isotherm for Cr(VI) onto Kraft lignin. *Chemical Engineering Journal*, 183, 108–111. <https://doi.org/10.1016/j.cej.2011.12.036>

Breuer, F. R. (2021). *Improvement of the Utilization Versatility of High Chromium, Manganese and Phosphorus Basic Oxygen Furnace Slags by Carbo-thermal Reduction*. University of Leoben.

British Standards Institution. (2012). *PD CEN/TS 15862:2012 Characterisation of waste. Compliance leaching test. One stage batch leaching test for monoliths at fixed liquid to surface area ratio (L/A) for test portions with fixed minimum dimensions*.

Brunauer, S., Emmett, P. H., & Teller, E. (1938). Adsorption of Gases in Multimolecular Layers. *Journal of the American Chemical Society*, 60(2), 309–319. <https://doi.org/10.1021/ja01269a023>

Cao, L., Shen, W., Huang, J., Yang, Y., Zhang, D., Huang, X., Lv, Z., & Ji, X. (2019). Process to utilize crushed steel slag in cement industry directly: Multi-phased clinker sintering technology. *Journal of Cleaner Production*, 217, 520–529. <https://doi.org/10.1016/j.jclepro.2019.01.260>

Capodaglio, A. G., & Bolognesi, S. (2019). Ecofuel feedstocks and their prospects. In *Advances in Eco-Fuels for a Sustainable Environment* (pp. 15–51). Elsevier. <https://doi.org/10.1016/B978-0-08-102728-8.00002-4>

Chandru, P., Karthikeyan, J., & Natarajan, C. (2020). *Steel Slag—A Strong and Sustainable Substitute for Conventional Concreting Materials* (Vol. 11). https://doi.org/https://doi.org/10.1007/978-3-030-46800-2_2

Chang, E. E., Pan, S. Y., Chen, Y. H., Tan, C. S., & Chiang, P. C. (2012). Accelerated carbonation of steelmaking slags in a high-gravity rotating packed bed. *Journal of Hazardous Materials*, 227–228, 97–106. <https://doi.org/10.1016/j.jhazmat.2012.05.021>

Chen, C. Y., Zhuang, K. W., Chang, Y. H., Nagarajan, D., Huang, C. C., & Chang, J. S. (2021). Basic oxygen furnace slag as a support material for the cultivation of indigenous marine microalgae. *Bioresource Technology*, 342. <https://doi.org/10.1016/j.biortech.2021.125968>

Chen, Y. L., & Lin, C. T. (2020). Recycling of basic oxygen furnace slag as a raw material for autoclaved aerated concrete production. *Sustainability (Switzerland)*, 12(15). <https://doi.org/10.3390/SU12155896>

Cho, S. H., Oh, J. I., Jung, S., Park, Y. K., Tsang, Y. F., Ok, Y. S., & Kwon, E. E. (2020). Catalytic pyrolytic platform for scrap tires using CO₂ and steel slag. *Applied Energy*, 259. <https://doi.org/10.1016/j.apenergy.2019.114164>

Cui, P., Wu, S., Xiao, Y., Liu, Q., & Wang, F. (2021). Hazardous characteristics and variation in internal structure by hydrodynamic damage of BOF slag-based thin asphalt overlay. *Journal of Hazardous Materials*, 412. <https://doi.org/10.1016/j.jhazmat.2021.125344>

DEFRA. (2021). *DEFRA UKEAP: Precip-Net Rainwater Data for Ystradffyn*. https://uk-air.defra.gov.uk/data/non-auto-data?uka_id=UKA00505&view=data&network=ukeap&year=2021&pollutant=747#view. Date Accessed: 8/12/2021.

Doostdar, N., Manrique, C. J., Hamill, M. B., & Barron, A. R. (2011). Synthesis of calcium-silica composites: A route toward an in vitro model system for calcific band keratopathy precipitates. *Journal of Biomedical Materials Research Part A*, 99A(2), 173–183. <https://doi.org/10.1002/jbm.a.33172>

Dželetović, Ž. S., & Filipović, R. (1995). Grain characteristics of crops grown on power

plant ash and bottom slag deposit. *Resources, Conservation and Recycling*, 13(2), 105–113. [https://doi.org/10.1016/0921-3449\(94\)00040-C](https://doi.org/10.1016/0921-3449(94)00040-C)

Esmacili, M., Nouri, R., & Yousefian, K. (2017). Experimental comparison of the lateral resistance of tracks with steel slag ballast and limestone ballast materials. *Proceedings of the Institution of Mechanical Engineers, Part F: Journal of Rail and Rapid Transit*, 231(2), 175–184. <https://doi.org/10.1177/0954409715623577>

Falayi, T. (2020). A comparison between fly ash- and basic oxygen furnace slag-modified gold mine tailings geopolymers. *International Journal of Energy and Environmental Engineering*, 11(2), 207–217. <https://doi.org/10.1007/s40095-019-00328-x>

Fisher, L. V. (2018). *The Use of Steelmaking Slags in Marine Applications*. Swansea University .

Fisher, L. V., & Barron, A. R. (2019). The recycling and reuse of steelmaking slags — A review. In *Resources, Conservation and Recycling* (Vol. 146, pp. 244–255). Elsevier B.V. <https://doi.org/10.1016/j.resconrec.2019.03.010>

Fisher, L. V., & Barron, A. R. (2021). Suitability of Steel Making Slag as a Construction Material Resource. *Recent Progress in Materials*, 03(03), 1–1. <https://doi.org/10.21926/rpm.2103028>

Fisher, L. V., & Barron, A. R. (2022). Effect of functionalized and unfunctionalized basic oxygen steelmaking slag on the growth of cereal wheat (*Triticum aestivum*). *Resources, Conservation & Recycling Advances*, 15, 200092. <https://doi.org/10.1016/j.rcradv.2022.200092>

Fisher, L. V., & Barron, A. R. (2023). Functionalization of Basic Oxygen Steelmaking Slag. *AIP Conference Proceedings* 2643, 060014–060014. <https://doi.org/10.1063/5.0110355>

Foekema, E. M., Tamis, J. E., Blanco, A., van der Weide, B., Sonneveld, C., Kleissen, F., & van den Heuvel-Greve, M. J. (2021). Leaching of Metals from Steel Slag and Their Ecological Effects on a Marine Ecosystem: Validating Field Data with Mesocosm

Observations. *Environmental Toxicology and Chemistry*, 40(9), 2499–2509. <https://doi.org/10.1002/etc.5132>

Franco, L. C., Mendes, J. C., Costa, L. C. B., Pira, R. R., & Peixoto, R. A. F. (2019). Design and thermal evaluation of a social housing model conceived with bioclimatic principles and recycled aggregates. *Sustainable Cities and Society*, 51. <https://doi.org/10.1016/j.scs.2019.101725>

Freundlich, H. (1907). Über die Adsorption in Lösungen. *Zeitschrift Für Physikalische Chemie*, 57U(1), 385–470. <https://doi.org/10.1515/zpch-1907-5723>

Gao, D., Wang, F. P., Wang, Y. T., & Zeng, Y. N. (2020). Sustainable utilization of steel slag from traditional industry and agriculture to catalysis. In *Sustainability (Switzerland)* (Vol. 12, Issue 21, pp. 1–9). MDPI AG. <https://doi.org/10.3390/su12219295>

Gao, T., Dai, T., Shen, L., & Jiang, L. (2021). Benefits of using steel slag in cement clinker production for environmental conservation and economic revenue generation. *Journal of Cleaner Production*, 282. <https://doi.org/10.1016/j.jclepro.2020.124538>

Gautier, M., Poirier, J., Bodéan, F., Franceschini, G., & Véron, E. (2013). Basic oxygen furnace (BOF) slag cooling: Laboratory characteristics and prediction calculations. *International Journal of Mineral Processing*, 123, 94–101. <https://doi.org/10.1016/j.minpro.2013.05.002>

Gencil, O., Karadag, O., Oren, O. H., & Bilir, T. (2021). Steel slag and its applications in cement and concrete technology: A review. In *Construction and Building Materials* (Vol. 283). Elsevier Ltd. <https://doi.org/10.1016/j.conbuildmat.2021.122783>

Ghobadi, M., Zaarei, D., Naderi, R., Asadi, N., Seyedi, S. R., & Ravan Avar, M. (2021). Improvement the protection performance of lanolin based temporary coating using benzotriazole and cerium (III) nitrate: Combined experimental and computational analysis. *Progress in Organic Coatings*, 151, 106085. <https://doi.org/10.1016/j.porgcoat.2020.106085>

Gómez-Nubla, L., Aramendia, J., Fdez-Ortiz de Vallejuelo, S., & Madariaga, J. M. (2018). Metallurgical residues reused as filler after 35 years and their natural weathering implications in a mountain area. *Science of the Total Environment*, 618, 39–47. <https://doi.org/10.1016/j.scitotenv.2017.11.026>

Guo, F., Zhao, X., Peng, K., Liang, S., Jia, X., & Qian, L. (2019). Catalytic reforming of biomass primary tar from pyrolysis over waste steel slag based catalysts. *International Journal of Hydrogen Energy*, 44(31), 16224–16233. <https://doi.org/10.1016/j.ijhydene.2019.04.190>

Gwon, H. S., Khan, M. I., Alam, M. A., Das, S., & Kim, P. J. (2018). Environmental risk assessment of steel-making slags and the potential use of LD slag in mitigating methane emissions and the grain arsenic level in rice (*Oryza sativa* L.). *Journal of Hazardous Materials*, 353, 236–243. <https://doi.org/10.1016/j.jhazmat.2018.04.023>

Hansel, C. M., Fendorf, S., Sutton, S., & Newville, M. (2001). Characterization of Fe plaque and associated metals on the roots of mine-waste impacted aquatic plants. *Environmental Science and Technology*, 35(19), 3863–3868. <https://doi.org/10.1021/es0105459>

He, J., Li, R., Sun, X., Wang, W., Hu, J., Xie, H., & Yin, H. (2018). Effects of calcium alginate submicroparticles on seed germination and seedling growth of wheat (*Triticum aestivum* L.). *Polymers*, 10(10). <https://doi.org/10.3390/polym10101154>

Hepler, P. K. (2005). Calcium: A Central Regulator of Plant Growth and Development. *The Plant Cell*, 17(8), 2142–2155. <https://doi.org/10.1105/tpc.105.032508>

Hill, D., Barron, A. R., & Alexander, S. (2019). Comparison of hydrophobicity and durability of functionalized aluminium oxide nanoparticle coatings with magnetite nanoparticles—links between morphology and wettability. *Journal of Colloid and Interface Science*, 555, 323–330. <https://doi.org/10.1016/j.jcis.2019.07.080>

Hill, D., Barron, A. R., & Alexander, S. (2020). Controlling the wettability of plastic by thermally embedding coated aluminium oxide nanoparticles into the surface. *Journal of*

- Colloid and Interface Science*, 567, 45–53. <https://doi.org/10.1016/j.jcis.2020.01.116>
- Howell, T. A. (2005). LYSIMETRY. In *Encyclopedia of Soils in the Environment* (pp. 379–386). Elsevier. <https://doi.org/10.1016/B0-12-348530-4/00391-X>
- Hu, L., Wang, S., & Zhang, Q. (2021). Evaluation of Long-term Skid Resistance of Asphalt Mixture with Multi-content Basic Oxygen Furnace (BOF) Steel Slag Using the Circular Vehicle Simulator (CVS). *E3S Web of Conferences*, 248. <https://doi.org/10.1051/e3sconf/202124801044>
- Hu, R., Zhou, X., Wu, S., Yang, C., Xie, J., Yang, D., & Ye, Q. (2020). Bonding behavior and its affecting factors between basic oxygen furnace slag and asphalt. *Construction and Building Materials*, 253. <https://doi.org/10.1016/j.conbuildmat.2020.119153>
- Huong Nguyen, L., Dung Nguyen, T., Viet Nga Tran, T., Luong Nguyen, D., Son Tran, H., Lien Nguyen, T., Huong Nguyen, T., Giang Nguyen, H., Phong Nguyen Ho Chi, T., & Tuan Nguyen JFE Steel Corporation Japan Tomoo Isawa JFE Steel Cooperation Japan Yasutaka Ta JFE Steel Corporation Japan Ryoichi Sato, N. (2021). *Steel slag quality control for road construction aggregates and its environmental impact: Case study of Vietnamese steel industry-Leaching of heavy metals from steel making slag*. <https://doi.org/10.21203/rs.3.rs-342976/v1>
- Imashuku, S., & Wagatsuma, K. (2020). Determination of Area Fraction of Free Lime in Steelmaking Slag Using Cathodoluminescence and X-ray Excited Optical Luminescence. *Metallurgical and Materials Transactions B: Process Metallurgy and Materials Processing Science*, 51(5), 2003–2011. <https://doi.org/10.1007/s11663-020-01927-4>
- Islam, M., & Patel, R. (2011). Thermal activation of basic oxygen furnace slag and evaluation of its fluoride removal efficiency. *Chemical Engineering Journal*, 169(1–3), 68–77. <https://doi.org/10.1016/j.cej.2011.02.054>
- Jalull, G., & Ganjian, E. (2019). The Effect of Using Basic Oxygen Slag with By-Product and Non-Hazard Waste Materials to Produce Paving Blocks. In M. Limbachiya, P. Claisse, M. Bagheri, & E. Ganjian (Eds.), *Fifth International Conference on Sustainable Construction Materials and Technologies (SCMT5)* (pp. 441–454). International

Committee of the SCMT conferences. <http://www.claisse.info/Proceedings.htm>

Jexembayeva, A., Salem, T., Jiao, P., Hou, B., & Niyazbekova, R. (2020). Blended cement mixed with basic oxygen steelmaking slag (BOF) as an alternative green building material. *Materials*, 13(14). <https://doi.org/10.3390/ma13143062>

Jia, W., Markine, V. L., & Jing, G. (2021). Analysis of furnace slag in railway sub-ballast based on experimental tests and DEM simulations. *Construction and Building Materials*, 288. <https://doi.org/10.1016/j.conbuildmat.2021.123114>

Jiang, J., Zheng, Q., Yan, Y., Guo, D., Wang, F., Wu, S., & Sun, W. (2018). Design of a novel nanocomposite with C-S-H@LA for thermal energy storage: A theoretical and experimental study. *Applied Energy*, 220, 395–407. <https://doi.org/10.1016/j.apenergy.2018.03.134>

Karunakaran, R. G., Lu, C. H., Zhang, Z., & Yang, S. (2011). Highly transparent superhydrophobic surfaces from the coassembly of nanoparticles (≤ 100 nm). *Langmuir*, 27(8), 4594–4602. <https://doi.org/10.1021/la104067c>

Kashiwaya, Y., Tauchi, S., Nomura, T., & Akiyama, T. (2020). Kinetic analysis considering particle size distribution on Ca elution from slags in CaO-SiO₂-MgO-Al₂O₃-Fe₂O₃ system. *ISIJ International*, 60(12), 2859–2869. <https://doi.org/10.2355/isijinternational.ISIJINT-2020-265>

Kato, T., Kusui, T., Kosugi, C., & Fukushima, T. (2020). Environmental Impact Evaluation of Steelmaking Slag Applied to Coastal Area Development. *Tetsu-to-Hagane*, 106(1), 50–57. <https://doi.org/10.2355/tetsutohagane.tetsu-2019-026>

Kaufmann, J., & Schering, A. (2014). Analysis of Variance ANOVA. In *Wiley StatsRef: Statistics Reference Online*. Wiley. <https://doi.org/10.1002/9781118445112.stat06938>

Kaur, H., Kaur, H., & Kaur, R. (2014). Removal of Rhodamine-B dye from aqueous solution onto Pigeon Dropping: Adsorption, kinetic, equilibrium and thermodynamic studies. *J. Mater. Environ. Sci*, 5(6), 1830–1838.

<https://www.researchgate.net/publication/287564782>

Kehagia, F. (2009). Skid resistance performance of asphalt wearing courses with electric arc furnace slag aggregates. *Waste Management and Research*, 27(3), 288–294. <https://doi.org/10.1177/0734242X08092025>

Kim, J., & Azimi, G. (2021). Valorization of electric arc furnace slag via carbothermic reduction followed by acid baking – water leaching. *Resources, Conservation and Recycling*, 173. <https://doi.org/10.1016/j.resconrec.2021.105710>

Kim, S. H., Chung, H., Jeong, S., & Nam, K. (2021). Identification of pH-dependent removal mechanisms of lead and arsenic by basic oxygen furnace slag: Relative contribution of precipitation and adsorption. *Journal of Cleaner Production*, 279. <https://doi.org/10.1016/j.jclepro.2020.123451>

Kim, S., kim, Y., Usman, M., Park, C., & Hanif, A. (2021). Durability of slag waste incorporated steel fiber-reinforced concrete in marine environment. *Journal of Building Engineering*, 33. <https://doi.org/10.1016/j.jobbe.2020.101641>

Koide, Y., & Barron, A. R. (1995). [Al₅(tBu)₅(μ₃-O)₂(μ₃-OH)₂(μ₂-OH)₂(μ₂-O₂CPh)₂]: A Model for the Interaction of Carboxylic Acids with Boehmite. *Organometallics*, 14(8), 4026–4029. <https://doi.org/10.1021/om00008a060>

Laurén, S. (2021). Contact angle – What is it and how do you measure it? In *Biolin Scientific White Paper* . <https://www.biolinchina.com/wp-content/uploads/2021/03/WP-Contact-angle-What-is-it-and-how-do-you-measure-it.pdf>. Date Accessed: 19/11/2022.

Lee, S., Kim, S. H., Jung, S., Park, Y. K., Tsang, Y. F., & Kwon, E. E. (2020). Use of steel slag as a catalyst in CO₂-cofeeding pyrolysis of pine sawdust. *Journal of Hazardous Materials*, 392. <https://doi.org/10.1016/j.jhazmat.2020.122275>

Lee, S. M., Raja, P. M. V., Esquenazi, G. L., & Barron, A. R. (2018). Effect of raw and purified carbon nanotubes and iron oxide nanoparticles on the growth of wheatgrass prepared from the cotyledons of common wheat (: *Triticum aestivum*). *Environmental*

Science: Nano, 5(1), 103–114. <https://doi.org/10.1039/c7en00680b>

Lerman, C. (2017, August 14). *Hydrophobic vs Hydrophilic: Polyurethanes*. <https://info.alchemy-spetec.com/blog/hydrophobic-vs-hydrophilic-polyurethanes>. Date Accessed:19/11/2022.

Li, P., Guo, H., Gao, J., Min, J., Yan, B., Chen, D., & Seetharaman, S. (2020). Novel concept of steam modification towards energy and iron recovery from steel slag: Oxidation mechanism and process evaluation. *Journal of Cleaner Production*, 254. <https://doi.org/10.1016/j.jclepro.2019.119952>

Li, Y. F., Yang, P. A., Wu, C. H., Cheng, T. W., & Huang, C. H. (2021). A study on radiation cooling effect on asphalt concrete pavement using basic oxygen furnace slag to replace partial aggregates. *Sustainability (Switzerland)*, 13(7). <https://doi.org/10.3390/su13073708>

Li, Y., Ni, W., Gao, W., Zhang, Y., Yan, Q., & Zhang, S. (2019). Corrosion evaluation of steel slag based on a leaching solution test. *Energy Sources, Part A: Recovery, Utilization and Environmental Effects*, 41(7), 790–801. <https://doi.org/10.1080/15567036.2018.1520359>

Li, Y., Qi, X., Li, G., & Wang, H. (2021). Efficient removal of arsenic from copper smelting wastewater via a synergy of steel-making slag and KMnO₄. *Journal of Cleaner Production*, 287. <https://doi.org/10.1016/j.jclepro.2020.125578>

Li, Z. T., Lin, B., Jiang, L. W., Lin, E. C., Chen, J., Zhang, S. J., Tang, Y. W., He, F. A., & Li, D. H. (2018). Effective preparation of magnetic superhydrophobic Fe₃O₄/PU sponge for oil-water separation. *Applied Surface Science*, 427, 56–64. <https://doi.org/10.1016/j.apsusc.2017.08.183>

Lim, Y. C., Chen, C. F., Chen, C. W., & Dong, C. Di. (2021). Application of Basic Oxygen Furnace Slag in Increased Utilization of Dredged Harbor Sediment. *Journal of Sustainable Metallurgy*, 7(2), 704–717. <https://doi.org/10.1007/s40831-021-00379-7>

Lin, W. T., Tsai, C. J., Chen, J., & Liu, W. (2019). Feasibility and characterization mortar blended with high-amount basic oxygen furnace slag. *Materials*, *12*(6). <https://doi.org/10.3390/ma12010006>

Lin, Y., Yan, B., Shu, Q., & Fabritius, T. (2021). Synergetic valorization of basic oxygen furnace slag and stone coal: Metal recovery and preparation of glass-ceramics. *Waste Management*, *135*, 158–166. <https://doi.org/10.1016/j.wasman.2021.08.044>

Liu, C., Guo, M., Pandelaers, L., Blanpain, B., & Huang, S. (2016). Stabilization of Free Lime in BOF Slag by Melting and Solidification in Air. *Metallurgical and Materials Transactions B: Process Metallurgy and Materials Processing Science*, *47*(6), 3237–3240. <https://doi.org/10.1007/s11663-016-0809-4>

Liu, H., Zhu, B., Wei, H., Chai, C., & Chen, Y. (2019). Laboratory evaluation on the performance of porous asphalt mixture with steel slag for seasonal frozen regions. *Sustainability (Switzerland)*, *11*(24). <https://doi.org/10.3390/su11246924>

Liu, T., Wang, Y., Zeng, Y., Li, J., Yu, Q., Wang, X., Gao, D., Wang, F., & Cai, S. (2021). Effects from fe, p, ca, mg, zn and cu in steel slag on growth and metabolite accumulation of microalgae: A review. In *Applied Sciences (Switzerland)* (Vol. 11, Issue 14). MDPI AG. <https://doi.org/10.3390/app11146589>

Lupu, C., Jackson, K. L., Bard, S., & Barron, A. R. (2007). Water, acid, and calcium carbonate pretreatment of fly ash: The effect on setting of cement-fly ash mixtures. *Industrial and Engineering Chemistry Research*, *46*(24), 8018–8025. <https://doi.org/10.1021/ie0709279>

Lupu, C., Jackson, K. L., Bard, S., Rusakova, I., & Borrón, A. R. (2006). Control over cement setting through the use of chemically modified fly ash. *Advanced Engineering Materials*, *8*(6), 576–580. <https://doi.org/10.1002/adem.200500280>

Lv, J., Chen, Y. Q., Ding, A. M., Lei, B., Yu, J., Gao, X. M., Dai, C. B., & Sun, Y. H. (2021). Control of axillary bud growth in tobacco through toxin gene expression system. *Scientific Reports*, *11*(1). <https://doi.org/10.1038/s41598-021-96976-3>

Maguire-Boyle, S. J., & Barron, A. R. (2011). A new functionalization strategy for oil/water separation membranes. *Journal of Membrane Science*, 382(1–2), 107–115. <https://doi.org/10.1016/j.memsci.2011.07.046>

Maguire-Boyle, S. J., Huseman, J. E., Ainscough, T. J., Oatley-Radcliffe, D. L., Alabdulkarem, A. A., Al-Mojil, S. F., & Barron, A. R. (2017). Superhydrophilic Functionalization of Microfiltration Ceramic Membranes Enables Separation of Hydrocarbons from Frac and Produced Water. *Scientific Reports*, 7(1). <https://doi.org/10.1038/s41598-017-12499-w>

Maguire-Boyle, S. J., Liga, M. V., Li, Q., & Barron, A. R. (2012). Alumoxane/ferroxane nanoparticles for the removal of viral pathogens: The importance of surface functionality to nanoparticle activity. *Nanoscale*, 4(18), 5627–5632. <https://doi.org/10.1039/c2nr31117h>

Mallick, P. K. (2018). 2.18 Particulate Filled and Short Fiber Reinforced Polymer Composites. In *Comprehensive Composite Materials II* (pp. 360–400). Elsevier. <https://doi.org/10.1016/B978-0-12-803581-8.03837-6>

Manso, J. M., Polanco, J. A., Losañez, M., & González, J. J. (2006). Durability of concrete made with EAF slag as aggregate. *Cement and Concrete Composites*, 28(6), 528–534. <https://doi.org/10.1016/j.cemconcomp.2006.02.008>

Martins, A. C. P., Franco de Carvalho, J. M., Costa, L. C. B., Andrade, H. D., de Melo, T. V., Ribeiro, J. C. L., Pedroti, L. G., & Peixoto, R. A. F. (2021). Steel slags in cement-based composites: An ultimate review on characterization, applications and performance. In *Construction and Building Materials* (Vol. 291). Elsevier Ltd. <https://doi.org/10.1016/j.conbuildmat.2021.123265>

Mata, T. M., Martins, A. A., & Caetano, N. S. (2010). Microalgae for biodiesel production and other applications: A review. In *Renewable and Sustainable Energy Reviews* (Vol. 14, Issue 1, pp. 217–232). <https://doi.org/10.1016/j.rser.2009.07.020>

Merck. (2022). *What is FTIR Spectroscopy?* <https://www.sigmaaldrich.com/GB/en/technical-documents/technical-article/analytical->

[chemistry/photometry-and-reflectometry/fir-spectroscopy](#). Date Accessed: 20/11/2022.

Motz, H., & Geiseler, J. (2001). Products of steel slags an opportunity to save natural resources. *Waste Management*, 21, 285–293. www.elsevier.nl/locate/wasman

Natural Resources Wales. (2012). *Permit with Introductory Note for Tata Steel UK Limited*. <https://naturalresourceswales.gov.uk/media/2467/port-talbot-steelworks-permit.pdf>. Date Accessed: 9/9/2018.

Neves, R. D., & Fernandes de Almeida, J. C. O. (2004). Compressive behaviour of steel fibre reinforced concrete. *Structural Concrete*, 6(1), 1–8.

Nordtest. (1999). *NT BUILD 492 CONCRETE, MORTAR AND CEMENT-BASED REPAIR MATERIALS: CHLORIDE MIGRATION COEFFICIENT FROM NON-STEADY-STATE MIGRATION EXPERIMENTS*. <http://www.nordtest.info/wp/1999/11/21/concrete-mortar-and-cement-based-repair-materials-chloride-migration-coefficient-from-non-steady-state-migration-experiments-nt-build-492/> Date Accessed: 5/9/22.

Ouda, A. S. (2019). Evaluation of Superplasticized Mortars Containing High Volume Basic-Oxygen Slag Fine Aggregate Replacing Sand against Sea Water Attack. *Journal of Advanced Research in Applied Mechanics Journal Homepage*, 61, 1–12. www.akademiabaru.com/aram.html

Pan, Z., Zhou, J., Jiang, X., Xu, Y., Jin, R., Ma, J., Zhuang, Y., Diao, Z., Zhang, S., Si, Q., & Chen, W. (2019). Investigating the effects of steel slag powder on the properties of self-compacting concrete with recycled aggregates. *Construction and Building Materials*, 200, 570–577. <https://doi.org/10.1016/j.conbuildmat.2018.12.150>

Pathak, S., Choudhary, R., & Kumar, A. (2020). Investigation of Moisture Damage in Open Graded Asphalt Friction Course Mixtures with Basic Oxygen Furnace Steel Slag as Coarse Aggregate under Acidic and Neutral pH Environments. *Transportation Research Record*, 2674(8), 887–901. <https://doi.org/10.1177/0361198120925459>

Perkin Elmer. (2015). *Thermogravimetric Analysis (TGA) TGA 8000 TGA 4000 STA 6000*

/ STA 8000 The Thermogravimetric Instrument Family.
https://resources.perkinelmer.com/lab-solutions/resources/docs/faq_beginners-guide-to-thermogravimetric-analysis_009380c_01.pdf. Date Accessed:19/11/2022.

Piatak, N. M. (2018). Environmental Characteristics and Utilization Potential of Metallurgical Slag. In *Environmental Geochemistry: Site Characterization, Data Analysis and Case Histories* (pp. 487–519). Elsevier. <https://doi.org/10.1016/B978-0-444-63763-5.00020-3>

Pistocchi, C., Ragaglini, G., Colla, V., Branca, T. A., Tozzini, C., & Romaniello, L. (2017). Exchangeable Sodium Percentage decrease in saline sodic soil after Basic Oxygen Furnace Slag application in a lysimeter trial. *Journal of Environmental Management*, 203, 896–906. <https://doi.org/10.1016/j.jenvman.2017.05.007>

Polettini, A., Pomi, R., & Stramazzo, A. (2016). CO₂ sequestration through aqueous accelerated carbonation of BOF slag: A factorial study of parameters effects. *Journal of Environmental Management*, 167, 185–195. <https://doi.org/10.1016/j.jenvman.2015.11.042>

Reddy, K. R., Chetri, J. K., Kumar, G., & Grubb, D. G. (2019). Effect of basic oxygen furnace slag type on carbon dioxide sequestration from landfill gas emissions. *Waste Management*, 85, 425–436. <https://doi.org/10.1016/j.wasman.2019.01.013>

Redemann, C. T., Wittwer, S. H., & Sell, H. M. (1950). Precautions in the Use of Lanolin as an Assay Diluent for Plant Growth Substances. *Plant Physiology*, 25(2), 356–358.

Riley, A. L., MacDonald, J. M., Burke, I. T., Renforth, P., Jarvis, A. P., Hudson-Edwards, K. A., McKie, J., & Mayes, W. M. (2020). Legacy iron and steel wastes in the UK: Extent, resource potential, and management futures. *Journal of Geochemical Exploration*, 219, 106630. <https://doi.org/10.1016/j.gexplo.2020.106630>

Rodushkin, I., Ruth, T., & Sa Huhtasaari, A. Ê. (1999). Comparison of two digestion methods for elemental determinations in plant material by ICP techniques. *Analytica Chimica Acta*, 378, 199–200.

Rosenzweig, C., Solecki, W., Parshall, L., Gaffin, S., Lynn, B., Goldberg, R., Cox, J., & Hodges, S. (2006). *MITIGATING NEW YORK CITY'S HEAT ISLAND WITH URBAN FORESTRY, LIVING ROOFS, AND LIGHT SURFACES*. www.ucar.edu/mm5overview.

Rout, G. R., & Sahoo, S. (2015). Role of Iron in Plant Growth and Metabolism . *Reviews in Agricultural Science*, 3(0), 1–24. <https://doi.org/10.7831/ras.3.1>

Roychand, R., Kumar Pramanik, B., Zhang, G., & Setunge, S. (2020). Recycling steel slag from municipal wastewater treatment plants into concrete applications – A step towards circular economy. *Resources, Conservation and Recycling*, 152. <https://doi.org/10.1016/j.resconrec.2019.104533>

Sagiri, S. S., Behera, B., Pal, K., & Basak, P. (2013). Lanolin-based organogels as a matrix for topical drug delivery. *Journal of Applied Polymer Science*, 128(6), 3831–3839. <https://doi.org/10.1002/app.38590>

Saha, S., Sarkar, S., & Sinha, A. (2019). Use of Basic Oxygen Furnace (BOF) Steel Slag for Acid Mine Drainage Treatment: A Laboratory Study. *Mine Water and the Environment*, 38(3), 517–527. <https://doi.org/10.1007/s10230-019-00615-3>

Sakurai, Y., Yang, X., Hisaka, Y., & Tsukihashi, F. (2020). Nutrient Supply to Seawater from Steelmaking Slag: The Coupled Effect of Gluconic Acid Usage and Slag Carbonation. *Metallurgical and Materials Transactions B: Process Metallurgy and Materials Processing Science*, 51(3), 1039–1047. <https://doi.org/10.1007/s11663-020-01805-z>

Sandanayake, M., Bouras, Y., Haigh, R., & Vrcelj, Z. (2020). Current sustainable trends of using waste materials in concrete—a decade review. In *Sustainability (Switzerland)* (Vol. 12, Issue 22, pp. 1–38). MDPI AG. <https://doi.org/10.3390/su12229622>

Sarperi, L., Surbrenat, A., Kerihuel, A., & Chazarenc, F. (2014). The use of an industrial by-product as a sorbent to remove CO₂ and H₂S from biogas. *Journal of Environmental Chemical Engineering*, 2(2), 1207–1213. <https://doi.org/10.1016/j.jece.2014.05.002>

Shaul, O. (2002). Magnesium Transport and Function In Plants: The Tip of the Iceberg .

BioMetals, 15(3), 307–321. <https://doi.org/10.1023/A:1016091118585>

Shen, H., & Forssberg, E. (2003). An overview of recovery of metals from slags. *Waste Management*, 23(10), 933–949. [https://doi.org/10.1016/S0956-053X\(02\)00164-2](https://doi.org/10.1016/S0956-053X(02)00164-2)

Shi, D., Yao, Y., Ye, J., & Zhang, W. (2019). Effects of seawater on mechanical properties, mineralogy and microstructure of calcium silicate slag-based alkali-activated materials. *Construction and Building Materials*, 212, 569–577. <https://doi.org/10.1016/j.conbuildmat.2019.03.288>

Si, X., Jiang, L., Wang, X., Ding, Y., & Luo, L. (2015). Determination of isoniazid content via cysteic acid/graphene modified glassy carbon electrode. *Analytical Methods*, 7(2), 793–798. <https://doi.org/10.1039/C4AY02013H>

Siedlecka, E. (2020). Comprehensive use of products generated during acid leaching of basic oxygen furnace sludge. *Journal of Cleaner Production*, 264. <https://doi.org/10.1016/j.jclepro.2020.121543>

Silva, J., & Uchida R. (2000). Chapter 3: Essential Nutrients for Plant Growth: Nutrient Functions and Deficiency Symptoms. In *Plant Nutrient Management in Hawaii's Soils, Approaches for Tropical and Subtropical Agriculture* (pp. 31–55). University of Hawaii at Manoa, College of Agriculture & Tropical Resources.

Sipilä, J., Teir, S., & Zevenhoven, R. (2008). *Carbon dioxide sequestration by mineral carbonation Literature review update 2005-2007*. <https://remineralize.org/wp-content/uploads/2015/10/LITR1.pdf>

Sithole, N. T., Ntuli, F., & Okonta, F. (2020). Fixed bed column studies for decontamination of acidic mineral effluent using porous fly ash-basic oxygen furnace slag based geopolymers. *Minerals Engineering*, 154. <https://doi.org/10.1016/j.mineng.2020.106397>

Suzuta, K., Watanabe, K., Maeda, T., & Ito, L. (2016). Evaluation of Cysteic Acid in Bleached Hair Using Infrared Spectroscopy. *Journal of Fiber Science and Technology*,

72(1), 1–8. <https://doi.org/10.2115/fiberst.2016-0004>

Tahwia, A. M., Abd El Raheem, A. H., & Elalfy, A. K. (2020). Use of Steel Slag in Eco-Friendly Rigid Pavement. *Mansoura Engineering Journal*, 45(1). <https://doi.org/10.21608/bfemu.2020.89166>

Technical Committee. (2002). *BS EN 12457-1:Characterisation of waste-Leaching-Compliance test for leaching of granular waste materials and sludges-Part 1: One stage batch test at a liquid to solid ratio of 2 l/kg for materials with high solid content and with particle size below 4 mm (without or with size reduction)*.

Todeschini, G. (2017). Review of Tidal Lagoon Technology and Opportunities for Integration within the UK Energy System. *Inventions*, 2(3), 14. <https://doi.org/10.3390/inventions2030014>

Vessal, A. (2019). Removal of sulphates from aluminium powder coating effluent using basic oxygen furnace slag and granulated blast furnace slag. *IOP Conference Series: Earth and Environmental Science*, 227(5). <https://doi.org/10.1088/1755-1315/227/5/052008>

Wang, C., Sheng, Y., Hari-Bala, Zhao, X., Zhao, J., Ma, X., & Wang, Z. (2007). A novel aqueous-phase route to synthesize hydrophobic CaCO₃ particles in situ. *Materials Science and Engineering C*, 27(1), 42–45. <https://doi.org/10.1016/j.msec.2006.01.003>

Wang, C., Sheng, Y., Zhao, X., Pan, Y., Hari-Bala, & Wang, Z. (2006). Synthesis of hydrophobic CaCO₃ nanoparticles. *Materials Letters*, 60(6), 854–857. <https://doi.org/10.1016/j.matlet.2005.10.035>

Wang, F. P., Liu, T. J., Cai, S., Gao, D., Yu, Q., Wang, X. M., Wang, Y. T., Zeng, Y. N., & Li, J. G. (2021). A review of modified steel slag application in catalytic pyrolysis, organic degradation, electrocatalysis, photocatalysis, transesterification and carbon capture and storage. In *Applied Sciences (Switzerland)* (Vol. 11, Issue 10). MDPI AG. <https://doi.org/10.3390/app11104539>

Wang, H. Y., Wang, W. C., Wang, J. C., & Chen, Y. W. (2021). Evaluation of the

engineering properties and durability of mortar produced using ground granulated blast-furnace slag and stainless steel reduced slag. *Construction and Building Materials*, 280. <https://doi.org/10.1016/j.conbuildmat.2021.122498>

Wen, T., Yang, L., Dang, C., Miki, T., Bai, H., & Nagasaka, T. (2020). Effect of basic oxygen furnace slag on succession of the bacterial community and immobilization of various metal ions in acidic contaminated mine soil. *Journal of Hazardous Materials*, 388. <https://doi.org/10.1016/j.jhazmat.2019.121784>

Wen, T., Yang, L., Dang, C., Yang, M., Miki, T., Bai, H., & Nagasaka, T. (2020). Effect of modified basic oxygen furnace slag on the controlled release of nitrate nitrogen and the functional microbial community in soil. *Journal of Environmental Management*, 261. <https://doi.org/10.1016/j.jenvman.2020.110191>

White, P. J., & Broadley, M. R. (2003). Calcium in plants. In *Annals of Botany* (Vol. 92, Issue 4, pp. 487–511). <https://doi.org/10.1093/aob/mcg164>

World Steel Association. (2021). *Climate change and the production of iron and steel*. <https://worldsteel.org/wp-content/uploads/Climate-policy-paper-2021-1.pdf>. Date Accessed: 28/8/2023.

World Steel Association. (2023, January 31). *December 2022 crude steel production and 2022 global crude steel production totals*. <https://worldsteel.org/media-centre/press-releases/2023/december-2022-crude-steel-production-and-2022-global-totals/>. Date Accessed: 28/8/2023.

Wu, C. H., Huang, C. H., Li, Y. F., Lee, W. H., & Cheng, T. W. (2020). Utilization of basic oxygen furnace slag in geopolymeric coating for passive radiative cooling application. *Sustainability (Switzerland)*, 12(10). <https://doi.org/10.3390/SU12103967>

Wu, T., Liu, H. T., Zhao, G. P., Song, J. X., Wang, X. L., Yang, C. Q., Zhai, R., Wang, Z. G., Ma, F. W., & Xu, L. F. (2020). Jasmonate and ethylene-regulated ethylene response factor 22 promotes lanolin-induced anthocyanin biosynthesis in ‘zaosu’ pear (*Pyrus bretschneideri* rehd.) fruit. *Biomolecules*, 10(2). <https://doi.org/10.3390/biom10020278>

Xie, J., Wang, Z., Wang, F., Wu, S., Chen, Z., & Yang, C. (2021). The life cycle energy consumption and emissions of asphalt pavement incorporating basic oxygen furnace slag by comparative study. *Sustainability (Switzerland)*, *13*(8). <https://doi.org/10.3390/su13084540>

Xie, J., Yang, C., Zhang, L., Zhou, X., Wu, S., & Ye, Q. (2020). Investigation of the physico-chemical properties and toxic potential of Basic Oxygen Furnace Slag (BOF) in asphalt pavement constructed after 15 years. *Construction and Building Materials*, *238*. <https://doi.org/10.1016/j.conbuildmat.2019.117630>

Xue, Y. J., Hu, Z. H., & Niu, Y. Y. (2020). Single and coadsorption of copper, cadmium, lead and zinc onto basic oxygen furnace slag. *Desalination and Water Treatment*, *179*, 242–251. <https://doi.org/10.5004/dwt.2020.24868>

Yang, L., Yang, M., Xu, P., Zhao, X., Bai, H., & Li, H. (2017). Characteristics of nitrate removal from aqueous solution by modified steel slag. *Water (Switzerland)*, *9*(10). <https://doi.org/10.3390/w9100757>

Yi, H., Xu, G., Cheng, H., Wang, J., Wan, Y., & Chen, H. (2012). An Overview of Utilization of Steel Slag. *Procedia Environmental Sciences*, *16*, 791–801. <https://doi.org/10.1016/j.proenv.2012.10.108>

Yilmaz, D., Lassabatere, L., Deneele, D., Angulo-Jaramillo, R., & Legret, M. (2013). Influence of Carbonation on the Microstructure and Hydraulic Properties of a Basic Oxygen Furnace Slag. *Vadose Zone Journal*, *12*(2), vzj2012.0121. <https://doi.org/10.2136/vzj2012.0121>

Yu, Q., Liu, T. J., Cai, S., Wang, F. P., Gao, D., Wang, X. M., Wang, Y. T., & Zeng, Y. N. (2021). A review on the effect from steel slag on the growth of microalgae. In *Processes* (Vol. 9, Issue 5). MDPI AG. <https://doi.org/10.3390/pr9050769>

Zareei, S. A., Ameri, F., Bahrami, N., Shoaee, P., Moosaei, H. R., & Salemi, N. (2019). Performance of sustainable high strength concrete with basic oxygen steel-making

(BOS)slag and nano-silica. *Journal of Building Engineering*, 25. <https://doi.org/10.1016/j.jobe.2019.100791>

Zhang, L., Wang, N., Yang, M., Ding, K., Wang, Y. Z., Huo, D., & Hou, C. (2019). Lipid accumulation and biodiesel quality of *Chlorella pyrenoidosa* under oxidative stress induced by nutrient regimes. *Renewable Energy*, 143, 1782–1790. <https://doi.org/10.1016/j.renene.2019.05.081>

Zhang, W., Zhang, T., Li, T., Lv, G., & Cao, X. (2021). Basic research on the leaching behavior of vanadium-bearing steel slag with titanium white waste acid. *Journal of Environmental Chemical Engineering*, 9(1). <https://doi.org/10.1016/j.jece.2020.104897>

Zhang, Y., Zhang, J., Li, X., & Wu, X. (2019). Preparation of hydrophobic lauric acid/SiO₂ shape-stabilized phase change materials for thermal energy storage. *Journal of Energy Storage*, 21, 611–617. <https://doi.org/10.1016/j.est.2018.12.022>

Zhang, Z., Feng, Y., Liu, N., Zhao, Y., Wang, X., Yang, S., Long, Y., & Qiu, L. (2020). Preparation of Sn/Mn loaded steel slag zeolite particle electrode and its removal effect on rhodamine B(RhB). *Journal of Water Process Engineering*, 37. <https://doi.org/10.1016/j.jwpe.2020.101417>